Understanding and control of the effect of potential induced degradation in p-type crystalline silicon solar cells

p 型結晶シリコン太陽電池における電圧誘起劣化（PID）の影響の理解と制御

July 2020

NGUYEN CHUNG DONG

Division of Materials Science

Nara Institute of Science and Technology

To my loved ones!

Abstract

Solar cell's performance degradation leads to a reduction in the performance of photovoltaic (PV) power generation systems over time. Recently, potential induced degradation (PID) has been an exciting topic for PV experts due to its significant impact on the performance deterioration of solar modules. Notably, the severe power loss level due to PID has been dominantly observed in crystalline silicon (c-Si) solar modules. On the other hand, micro-cracks could cause inactive regions in solar cells, leading to the degradation of their electrical performance and mechanical stability. Currently, the PID effect and its mechanism were found in intact solar modules after conventional PID stress tests under three main conditions composed of high voltage, temperature, and humidity. However, the actual PID effect occurring in outdoor installed modules is affected by not only the above conditions but also UV light radiation. Besides, outdoor installed modules also can simultaneously suffer from PID stress and mechanical stress, such as micro-cracks. Therefore, a more precise understanding of the PID phenomenon has to be investigated for such issues. This study progresses three crucial points as follows: Understanding and proposing a model of PID mechanism related to micro-cracks, Presenting and discussing recovery possibility and method for PID-affected micro-cracked solar cells, Clarifying the effect of UV light for solar cells within PID stress tests and utilizing it to control PID behavior.

In chapter 2, the PID effect was observed at micro-cracked regions as a hot spot phenomenon through electroluminescence (EL), lock-in thermal (LIT) images. The deterioration of maximum power (P_{max}) contributed by fill factor (FF), open-circuit voltage (V_{oc}), and short-circuit current density (J_{sc}) of PID-affected micro-cracked solar cells was monitored by current density-voltage (J–V) characteristics before and after PID stresses. The PID level due to micro-cracks depends not only on the length but also on other factors such as width and depth of

micro-cracks in solar cells. The PID shunting phenomenon introduced the performance deterioration at micro-cracked regions. Under a high potential, Na^+ ions drift from the front cover glass to the active cell surface and penetrate to the p–n junction at the micro-cracked regions where they accumulate and decorate the whole cross-section site of micro-cracks. It is assumed that the Na-decorated micro-cracked areas act as local defects. When the local defect concentration is high enough, the local defects form shunting paths across the p-n junction, leading to the reduction of shunt resistance (R_{sh}) as well as FF and V_{oc}. The model of the PID mechanism due to micro-cracks was confirmed by energy-dispersive X-ray (EDX) spectroscopy mapping, secondary-ion mass spectrometry (SIMS), and scanning electron microscope (SEM) images.

In chapter 3, the author reveals that the PID shunting path due to the decoration of Na^+ ions at micro-cracked areas acts as the primary PID mechanism causing the losses of V_{oc} and FF for p-type c-Si solar modules. Besides, micro-cracks also serve as the additional recombination center, which reduces J_{sc}, V_{oc}, and effective carrier's lifetime (τ_{eff}) of solar modules after PID stress processes. This hypothesis is confirmed by an external quantum efficiency (EQE) response, and microwave photo-conductance decay (μ-PCD) method at the micro-cracked regions before and after PID stresses. This work shows a challenge of the PID recovery process for un-laminated solar cells with or without micro-cracks. In contrast, the PID recovery has been made significantly but incompletely for both laminated intact and micro-cracked solar cells by the electrical PID recovery method (biasing a reverse high voltage). The incomplete power recovery behavior of PID-affected solar cells is attributed to be due to the partial recovery of R_{sh} and FF. In this work, the author supposes that the degradation and regeneration of the τ_{eff} value are a function of the PID stress and recovery processes. The μ-PCD response also plays a critical role in indicating the PID effect due to micro-cracks of solar cells. Besides, the author discusses the decreasing tendency of the loss of electrical characteristics due to the

PID stress process after PID degradation/recovery cycles (cyclic PID test). Possibility, the cyclic PID test with suitable conditions becomes a promising method to control the PID effect.

Chapter 4 shows that irradiating UV light in the 300–390 nm wavelength range on p-type c-Si solar cells during the PID stresses can slow down the PID effect. The silicon nitride (SiN_x) layer absorbs the UV light to generate electrons and holes, resulting in increasing of SiN_x conductivity and reducing the electrical field applied in SiN_x, which prevents or minimizes Na^+ ions penetration into the c-Si solar cell. Therefore, the increased SiN_x conductivity under UV light in the 300–390 nm wavelength range is the key mechanism to delay the power loss rate due to PID. Also, the τ_{eff} values, rapid (τ_1), and slow (τ_2) decay time constants were important indicators to observe the PID behavior in this study. Under the effect of the UV light during the PID stress, the values of τ_{eff}, τ_1, and τ_2 could be slowed down because fewer Na ions penetration into crystal defects of the active cell layer, the lower formation of deep-level states owing to the penetration of Na ions into the active Si layer, and less number of defects acting as traps, respectively.

In the final chapter, the author elucidates the PID mechanism and the PID recovery possibility for micro-cracked solar cells and demonstrates the PID delay effect of UV light in the 300–390 nm wavelength range. The achieved PID behavior in this work is more realistic and accurate for solar modules in the field. Also, UV light should be considered as an essential factor for both outdoor and indoor PID tests.

Acknowledgments

I would like to express my gratitude and gratefulness to my supervisors Prof. Yukiharu Uraoka, and Assoc. Prof. Yasuaki Ishikawa of the Information Device Science Laboratory, Division of Materials Science, Nara Institute of Science and Technology, for giving me this excellent opportunity to work on photovoltaic quality and reliability studies.

I also would like to extend many thanks to Prof. Yukiharu Uraoka and Assoc. Prof. Yasuaki Ishikawa for providing helpful guidance, valuable advice, and enthusiastic support during the duration of my studies. And, I wish to thank Prof. Hisao Yanagi and Assoc. Prof. Hiroaki Benten for their useful suggestions as well as their insightful comments and questions that improved my studies.

I sincerely acknowledge Dr. Volker Naumann at Fraunhofer Center for Silicon Photovoltaics CSP, Germany, for collaboration work and giving me the chance of oversea study in his Laboratory. Besides, I wish to express my sincerest thanks to Prof. Atsushi Masuda at Niigata University, Prof. Kyotaro Nakamura, at Toyota Technological Institute, Assoc. Prof. Sachiko Jonai at Niigata University and Dr. Mohammad Aminul Islam at University of Malaya, Malaysia, for collaboration work, their helpful discussions, and advice.

I also wish to thank Assoc. Prof. Mutsunori Uenuma, Asst. Prof. Mami N. Fujii, Asst. Prof. Juan Paolo S. Bermundo, Asst. Prof. Michael Paul A. Jallorina, for their help, support throughout my research, and for their advice in improving the study. I would also wish to thank Mr. Kobe Takashi, Mr. Akio Watakabe, and Mr. Hirotoshi Kawahira for their help and support in checking and maintaining the equipment that is used in the experiments as well as for their companionship and support. I would also like to thank Ms. Yukiko Morita for her invaluable help in coordinating various administrative requests and procedures, which made my stay during the duration of the research more comfortable.

I would wish to thank the former and current members of the PV group: Dr. Mohammad Aminul Islam, Dr. Itaru Raifuku, Dr. Uchiyama Shunsuke, Dr. Hashima Yuki, Ms. Nakai Yuya, Ms. Oshima Takuya, Ms. Kobayashi Daisuke, Ms. Sato Ryosuke, Ms. Sasakawa Go, Ms. Asashita Naoki, and Ms. Iwasaki Megumi for their valuable discussions during the weekly meetings. I would also wish to thank the former and current members of the Information device science laboratory for their useful suggestions and comments in the multiple instances that my research could be improved: discussions, monthly seminars, preparations for conference presentations, and discussions in the office.

I would also wish to thank the former and current dean of the graduate school of materials science: Prof. Kiyomi Kakiuchi and Prof. Jun Ohta for also providing me the opportunity to study in NAIST. I also wish to thank the administrative staff from the graduate school of materials science and the staff from the international affairs division for their help and support during my stay.

I wish to thank my parents Nguyen Van Nghia, Dao Thi Toan, for the never-ending love and support. Finally, I would want to thank my wife Pham Thi Hong and my son Nguyen Quang Lam for their patience, understanding, and love without which all of this would not be possible.

Nara, July 2020

Nguyen Chung Dong

List of Abbreviations

Abbreviation	Description
ARC	Anti-reflective Coating
a-Si	Amorphous Silicon
Cat-CVD	Catalytic Chemical Vapor Deposition
c-Si	Crystalline Silicon
DWS	Diamond Wire Sawing
EDX	Energy Dispersive X-ray
EL	Electroluminescence
EQE	External Quantum Efficiency
EVA	Ethylene-Vinyl Acetate
FF	Fill Factor
FWHM	Full Width at Half Maximum
IEC	International Electro-technical Commission
I_{sc}	Short-Circuit Current
I–V	Current-Voltage
J_{sc}	Short-Circuit Current Density
J–V	Current density-Voltage
LIT	Lock-in Thermal
LO	Liquid Oxidation

P_{max}	Maximum Power
PE-CVD	Plasma-Enhanced Chemical Vapor Deposition
PET	Polyethylene Terephthalate
PID	Potential Induced Degradation
PID-p	Potential Induced Degradation Polarization
PID-s	Potential Induced Degradation Shunting
PV	Photovoltaic
PVF	Polyvinyl Fluoride
R_s	Series Resistance
R_{sh}	Shunt Resistance
SEM	Scanning Electron Microscope
SIMS	Secondary Ion Mass Spectrometry
SiN_x	Silicon Nitride
SRH	Shockley Read Hall
SWS	Slurry Wire Sawing
UV	Ultraviolet
V_{dc}	Direct Current Voltage
V_{oc}	Open Circuit Voltage
μ-PCD	Microwave Photo-conductance Decay
τ_1	Rapid decay time constant

τ_2	Slow decay time constant
τ_{bulk}	Bulk Lifetime
τ_{diff}	Diffusion Lifetime
τ_{eff}	Effective lifetime
τ_{surf}	Surface Lifetime

Table of contents

Chapter 1 | Introduction

1.1. Photovoltaic (PV) reliability

Solar energy is radiant light and heat from the Sun applied to technologies such as solar heating, PVs, solar thermal energy, solar architecture. Currently, solar energy is one of the primary renewable energy sources which could address many of the challenges for the world. It would become a significant contributor to the world's energy mix up to 2050, as shown in Figure 1. 1 [1].

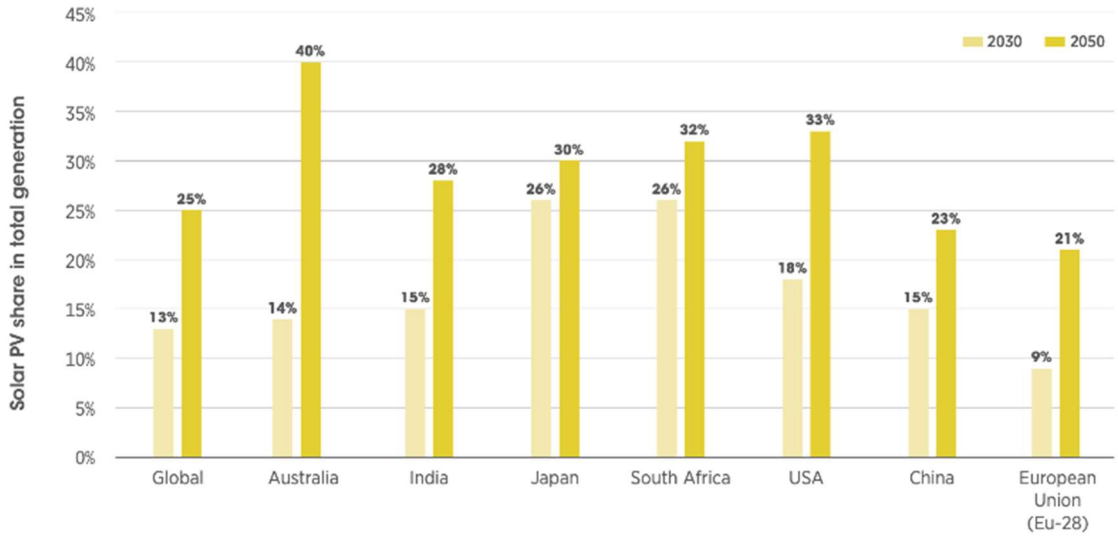

Figure 1. 1. Higher penetration of solar power in electricity grids is foreseen in various countries by 2030 and 2050 [1].

A solar cell is an electric device that converts solar energy into electrical power based on the PV effect, which was discovered by Becquerel in 1839 [2]. A variety of PV cell technologies are developed based on PV materials such as mono-crystalline, poly-crystalline, and amorphous silicon (a-Si), as well as dye sensitizer, organic-inorganic lead halide, etc. The production share of c-Si solar cells dominates the global solar market with more than a share of 95% in 2017, as shown in Figure 1. 2 [3].

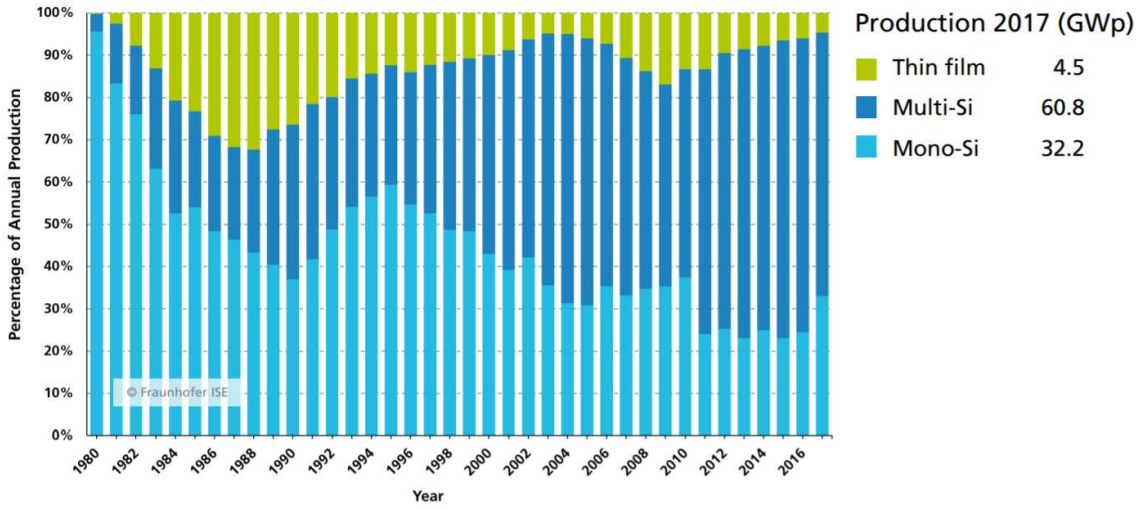

Figure 1. 2. Percentage of global annual production [3].

Solar cells need solar energy to generate electricity, so they need to be installed outdoors. However, severe environmental factors such as high temperature and humidity, irradiation, dirt, and soil adversely affect the performance and reliability of solar cells. To protect the solar cells from unfavorable environmental factors, a solar module as an encapsulated construction of a solar cell is made by adding several packaging materials, such as glass, encapsulant, and back-sheet. For conventional crystalline silicon (c-Si) solar modules, an aluminum frame is set up around the edge of connected cell series to mount and protect them. To optimize the solar cell performance, a large number of solar modules connected in series or parallel form a PV system.

PV reliability is one of the critical parameters which distribute the reduction of the cost and simultaneously the enhancement of the performance of the PV system. So far, although the price of a PV system is higher than the rate for traditional energy sources [4], solar energy would be more cost-effective by increasing reliability, simultaneously leading to a longer lifespan of the PV system in the future. Therefore, PV reliability, which becomes one of the most urgent issues for PV technology, attracts more attention from researchers, industries, and policymakers. The PV reliability problem is not only for solar cells but also for materials of

solar modules composed of glass, encapsulation materials as ethylene-vinyl acetate (EVA), and back-sheet. Because these materials are in close contact with the solar cells, their characteristics directly affect the ultimate reliability of PV systems.

The solar module performance can be degraded by several factors, such as heat, humidity, UV light irradiation, and mechanical shock [5][6][7]. Each one of these various mentioned factors may induce one or more typical types of degradation for c-Si solar modules such as corrosion, delamination, deterioration caused by UV light irradiation (discoloration, acetic acid), breakage, micro-cracks, potential induced degradation (PID). Degradations caused by corrosion, delamination, and breakage are briefly presented in this Section. Degradations caused by UV light irradiation, micro-cracks, PID are shown and discussed in the next Sections in detail.

1.1.1. Corrosion degradation

Corrosion is caused by moisture ingression to the module edge of the sheet material, leading to an increase of the electrical conductivity of the material and leakage currents. The corrosion at the metal frame causes deterioration of the solar modules, as shown in Figure 1. 3. Therein, the dislocation of the metal structure also induces adverse problems such as electrical hazards and corrosion. Kemp showed that the moisture in the solar module is correlated with the rate of degradation, especially in damp-heat geographic locations [8]. Also, Wohlgemuth and Kurtz found out that corrosion appeared after 1000 h of exposure of PV module under 85ºC and 85% of relative humidity [9]. Carlson et al. demonstrated that the sodium contained in the glass is reactive with moisture, causing the corrosion of solar module edges [10]. The ingress of the moisture into the solar modules remains significant during their lifetime due to the relatively fast water diffusion in the EVA layer, leading to more rapid and considerable corrosion

degradation. The method to prevent moisture ingress is to seal the solar modules by low diffusive gaskets with a large quantity of desiccant [8].

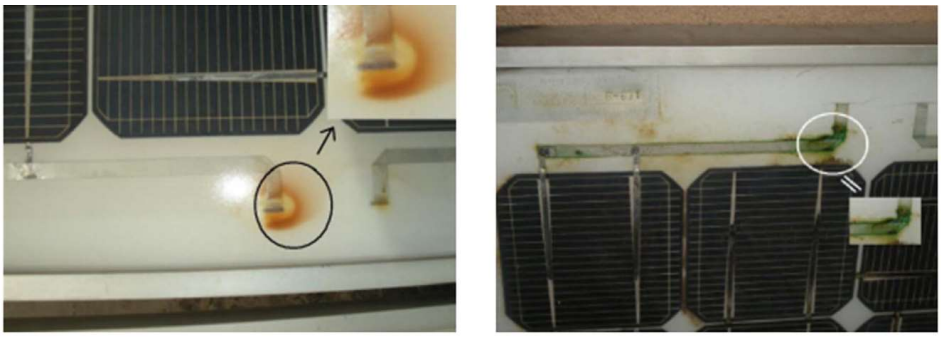

Figure 1. 3. Corrosion of metallic contact [11].

1.1.2. Delamination degradation

Delamination, which occurs between the encapsulating polymer and the cells or between cells and the front glass, causes the increase of the light reflection and water penetration into the solar module structure [7]. Skoczek et al. investigated the delamination degradation for the solar modules from tests based on the IEC 61215 standard [12].

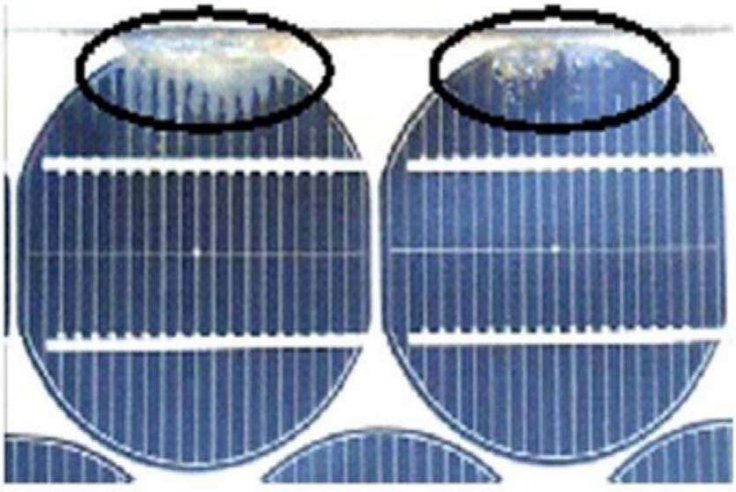

Figure 1. 4. Delamination in a PV module [13].

Delamination becomes more significant at the edges of the solar modules, as shown in Figure 1. 4, because of electrical risks for the entire installation. When solar modules operate

in damp-heat climates, delamination causes moisture penetration in the solar modules, resulting in various chemical and physical degradations such as metal corrosion of the module structure. Jansen and Delahoy demonstrated that salt accumulation and moisture penetration into the solar modules might be a cause of the delamination. Also, etched interfacial connections by hydrofluoric acid in the solar modules lead to delamination [14].

1.1.3. Degradation caused by breakage

Figure 1. 5. A solar module with a broken glass [13].

One of the significant adverse degradation factors for solar modules is glass breakage, which commonly occurs in several cases such as installation, maintenance, and the transportation of modules on the installation sites. For example, a crystalline solar module was broken during operation for five years, as shown in Figure 1. 5. The performance degradation of solar modules caused by the breakage becomes more significant under damp-heat conditions due to moisture ingress. Other degradation types, such as corrosion, discoloration, and delamination, also may result in the breakages of solar modules [15]. To reduce the fabrication costs of solar cells and enhance the solar cell performance, the thickness and the surface of cells decreased from 300 µm to 200 µm to even less than 100 µm while the cell size increased to 210 mm × 210 mm. Therefore, solar cells become more fragile and sensitive to breakages.

1.2. Degradation due to ultraviolet (UV) light

The encapsulating layer of solar modules made from polymeric materials is utilized as an electrical insulator to protect solar modules from harsh conditions of temperature, humidity, electrical and mechanical stresses, thermal cycling, and UV light radiation. However, the polymeric materials of solar modules are gradually deteriorated during the operating lifetime of solar cells. UV light radiation existing in sunlight from the Sun in the form of UVA (320–400 nm) and UVB (280–320 nm) is responsible for this deterioration [16]. Besides, the UV light exposure on solar cells is also considered as the primary cause of the aging of solar cells, leading to the degradation of solar modules.

1.2.1. Discoloration degradation

Discoloration degradation often occurs in the encapsulant of solar modules, EVA, and adhesive materials between the glass and the solar cells. Discoloration, which is a change in the color of the material from white to yellow or brown, modifies light transmittance through solar cells, leading to reduced performance in solar modules. The primary causes of EVA discoloration degradation are UV light irradiation combined with damp-heat conditions of more than 50 ^{o}C [17]. This degradation may also happen in various regions of solar modules due to the different characteristics of encapsulating polymers. Discolored solar cells are shown in Figure 1. 6.

Kojima and Yanagisawa showed that radiation of 4000 W/m^2 of the UV light in the 280-380 nm wavelength range could cause the rapid discoloration degradation for solar cells after 400 h exposure. Meanwhile, no change occurred under a 1000 W/m^2 radiation in the same wavelength range even after 500 h of exposure [18]. Wohlgemuth and Kurtz found that the discoloration of the encapsulant occurs at a temperature of 60 ^{o}C under global UV irradiation of 15 kWh/m^2 where the UV power intensity in the 280-385 nm wavelength range is not more than 250 W/m^2 [9]. Most reports highlighted the degradation of c-Si solar modules caused by

EVA discoloration degradation related to UV irradiation exposure in the long term [9][19][20][21]. Mainly, Realini found out the correlation between the electrical characteristics of the module and the discoloration of its encapsulant [22]. Discoloration reduces the short-circuit current (I_{sc}) of the solar modules from 10% to 13% for complete discoloration, leading to the significant degradation of maximum power (P_{max})of solar modules.

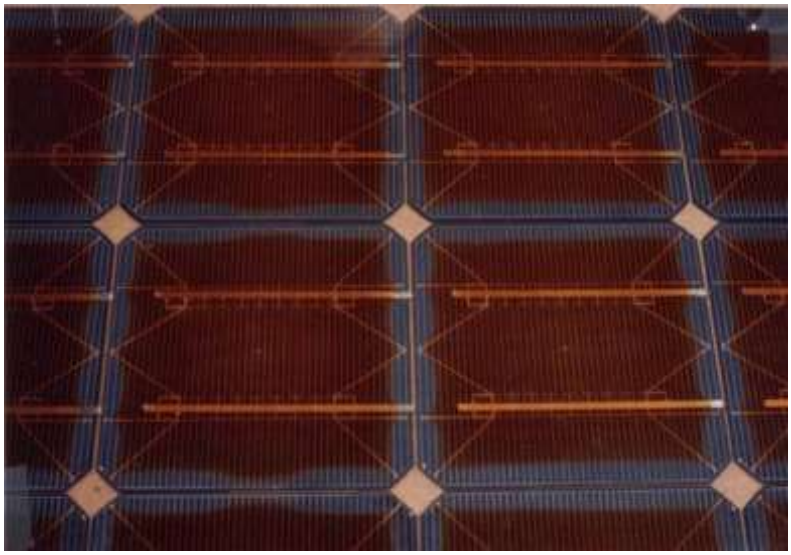

Figure 1. 6. Discoloration of the encapsulant due to UV light and heat [23].

1.2.2. Degradation by acetic acid

UV light irradiation combined with moisture and high temperature on solar modules contributed to accelerating the PV power degradation [24]. In this case, the PV deterioration is induced by acetic acid, which is generated in EVA under UV light irradiation based on the photochemical reaction [20][25] and under the damp-heat conditions due to the hydrolysis reaction [20][26][27]. In combined acceleration tests for the degradation of solar modules, T. Ngo et al. reported that the combination of UV light irradiation and damp-heat conditions could generate a higher acetic acid concentration in the EVA layer [24]. They proposed that the acetic acid made in the solar modules produces the chemical reactions with electrode materials, leading to the corrosion effect on Ag electrodes. This effect causes some characteristic changes

of Ag electrodes such as the increase in contact resistance as well as the decrease in adhesion strength, resulting in the power loss of solar modules. Herein, UV light irradiation plays a critical role in the acetic acid generation, which causes the power degradation of solar modules.

1.3. Degradation caused by micro-cracks

1.3.1. Classification of cracks

Cracks with various shapes and sizes in c-Si solar cells can be classified by their size, shape, position, direction [28], and severity [29]. For example, line-shaped cracks are formed by scratches due to wafer sawing or laser cutting [30]. Star-shaped cracks are composed of several line cracks with a tendency to cross each other. Based on the size of cracks, they are divided into two main categories: macro-cracks and micro-cracks. A crack with a width of less than 100 μm is considered as a micro-crack [26]. Based on the position of cracks, there are visible cracks (edge cracks) on the wafer surface, interior cracks below the wafer surface.

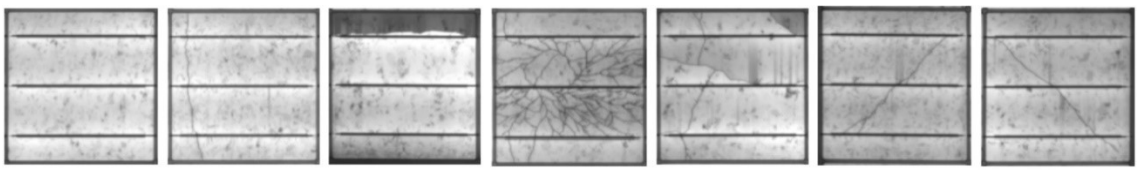

Figure 1. 7. Crack types of solar cells (from left to right): no crack, perpendicular, parallel, dendritic, multiple directions, +45º, -45º [31].

In terms of the crack direction, various crack types are composed of diagonal, parallel to busbars, perpendicular to busbars, +45º, -45º, and multiple directions cracks, as shown in Figure 1. 7. For the crack severity, cracks of solar cells consist of modes of A, B, and C, as shown in Figure 1. 8. Mode-A cracks cause insignificant performance degradation because of no connection to the cell area. Meanwhile, mode-B and C cracks result in partially and wholly broken solar cells, respectively, leading to severe power loss and forming hot spots [32].

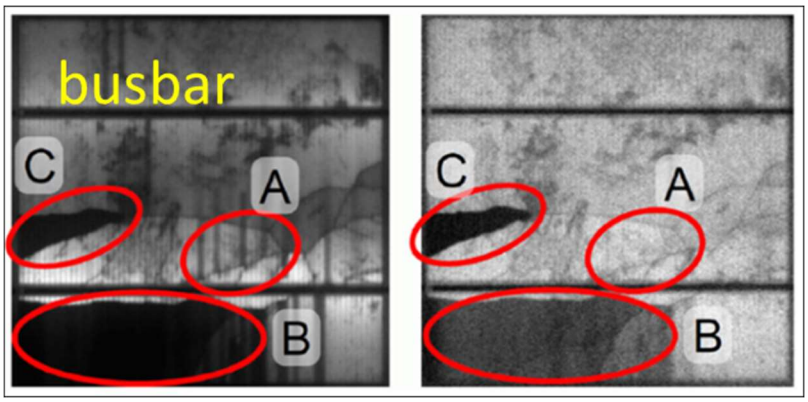

Figure 1. 8. Electroluminescence (EL) images of the same solar cell with crack modes A, B, and C [29].

1.3.2. Origin of micro-cracks

Micro-cracks can be formed in some processes of cutting Si ingots, manufacturing cells, transportation, installation. Besides, they also can be induced by environmental factors during the operation period of cells, such as snow, wind, storm, etc. Sawing Si ingots is the first step resulting in micro-cracks in the surface or subsurface of the Si wafers. Two Si wafer sawing technologies are widely utilized based on the diamond wire (DWS) and the conventional slurry wire (SWS). Micro-cracks with the typical crack depths of about 2-13 µm appear periodically along the direction of sawing due to DWS [33]. However, micro-cracks with an average depth between 10 and 20 µm were found out with random distribution in the case of SWS [34]. Several vital processing steps during the production of solar cells composed of the firing process, the soldering process induce the residual stress, the thermo-mechanical stress, respectively, which can cause micro-cracks. The laminating (encapsulation) process shows high residual stresses in solar modules, tending to form micro-cracks. This process causes the maximum strains close to the edge of the copper interconnector, thus micro-cracks commonly occur in this area.

Furthermore, micro-cracks due to lamination are typical of the ±45° orientation [35]. Packaging and transportation of solar modules also cause micro-cracks, causing a power loss lower than 1% based on simulation tests [36]. Also, harsh outdoor conditions, such as deep thermal cycles, high wind speeds, snow loading, and hail impacts may cause micro-cracks, leading to performance degradation and reduced reliability of solar modules during their lifetime. Although it is difficult to avoid the formation of micro-cracks during both the manufacturing process and the operating process of solar modules, mitigating the formation and propagation of micro-cracks is essential. EL, LIT images, and current-voltage (*I–V*) measurements are conventional methods to detect and determine the electrical and mechanical characteristics of micro-cracks.

1.3.3. Impact of micro-cracks on solar module performance

The current generated by a solar cell is proportional to the active area of the cell. The active area becomes the inactive area when the current collection from the finger to the busbars is blocked by micro-cracks, leading to the degradation of the electrical performance, and the mechanical integrity of the cell. Grunow et al. reported that micro-cracking occurs in parallel and is centered between the busbars, resulting in a power loss of up to 4%. The micro-cracking was parallel on both sides of both busbars, causing the highest power loss of 60% [37].

As mentioned above, there are three (A, B, and C) modes of cell micro-cracks in Figure 1. 8. Kontges et al. presented the dependence of the power degradation of a solar module on the number of mode-A micro-cracks, as shown in Figure 1. 9a. Mode-A micro-cracks cause little power loss for the solar module since they do not generate inactive cell areas. If there are some solar cells with mode-A micro-cracks, the power loss is negligible. The power loss of a 60-cell solar module is from 1 to 2.5 % when the number of micro-cracks increases. The power loss due to micro-cracks becomes higher after the mechanical load, and accelerated aging by 200

humidity freeze cycles is a function of the number of micro-cracked cells, as shown in Figure 1. 9b. The highest power loss is less than 9.6 % in this case. After the solar module aging process, some cell micro-cracks changed from mode A to mode B, or mode C, leading to more significant power loss [29].

Khatri et al. investigated the long-term reliability of PV modules and the power loss using accelerated aging tests and revealed that the increase of the series resistance (R_s) (about 7 %) in the cell due to micro-cracks could cause a power loss of 4% and a FF reduction of 3% [38]. Micro-cracks could be critical for the long-term reliability of solar modules and thus should be suppressed as much as possible.

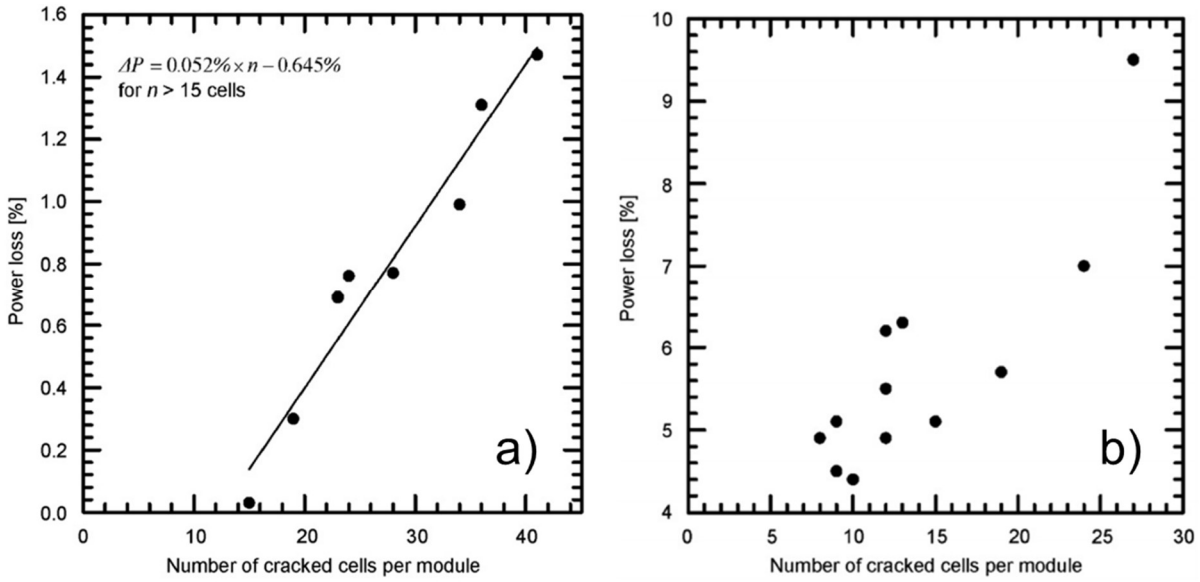

Figure 1. 9. a) The power loss for a 60-cell solar module with a cell size of 15.6 × 15.6 cm^2 caused by mode-A micro-cracks, b) the power loss after the mechanical load and 200 humidity freeze cycles versus the number of micro-cracked cells [29].

1.4. Potential induced degradation

To meet the large power requirements around the world, solar modules are connected in a series and parallel to generate the maximum PV system voltage up to 1000 V_{dc}. When a solar module

frame is grounded for safety reasons, the solar modules in these systems are subjected to high voltage stress, leading to their performance degradation. The Jet Propulsion Laboratory found out the high voltage stress for both c-Si modules and a-Si thin-film modules in the 1980s [39]. Then, National Research Energy Laboratory, Florida Solar Energy Center, investigated the high voltage stress on various types of solar modules in the early 2000s [10][40][41]. Recently, the high voltage stress was observed in rear-junction n-type c-Si PV modules at an outdoor test array of SunPower company in Germany [42] in 2005.

The term PID was first introduced by Pingel et al. in 2010 [43]. PID is a high voltage stress type wherein the electric potential difference between the solar cells and the module frame causes leakage currents, leading to the drift and diffusion of alkali metal ions (Na^+) within the module between the cell-active layer and other elements of the module (e.g., glass, mount, and frame). In standard p-type c-Si solar modules, leakage currents can flow from the module frame to the solar cells through six different pathways, as illustrated in Figure 1. 10 [44] [43][45]. Therein, the path one is the most detrimental because solar modules often operate outdoor under harsh environmental conditions, such as rain and high humidity conditions, resulting in significantly increased surface conductivity of the front glass [44][46]. Besides, the relative importance of different leakage current pathways depends on various range of factors, such as temperature, humidity, dew condensation, and encapsulation materials.

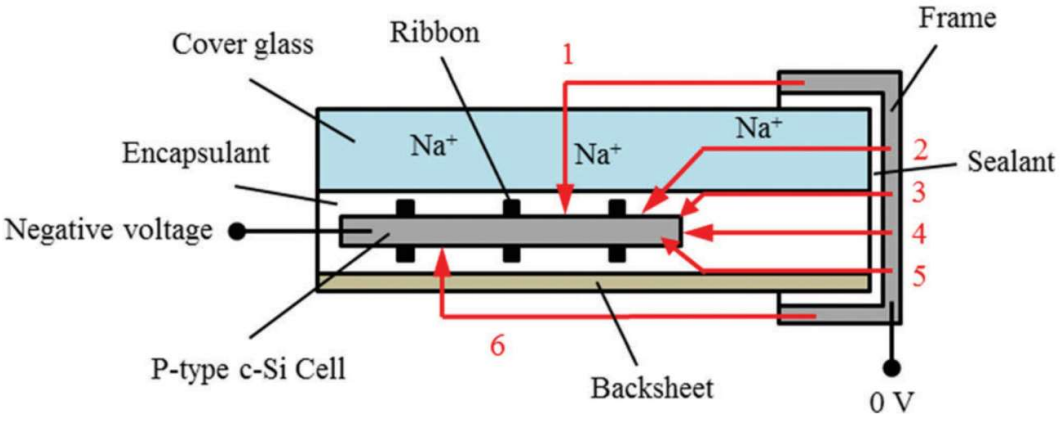

Figure 1. 10. The possible pathways of leakage currents [44].

1.4.1. Main factors influencing the PID behavior

The PID effect is affected by many factors, such as the properties of the anti-reflective (AR) coating layer, encapsulation materials, module construction, system topologies, grounding conditions of the glass surface, and UV/light radiation. Mainly, three crucial factors influence and accelerate the PID effect composed of temperature, humidity, and applied voltage.

1.4.1.1. Temperature factor

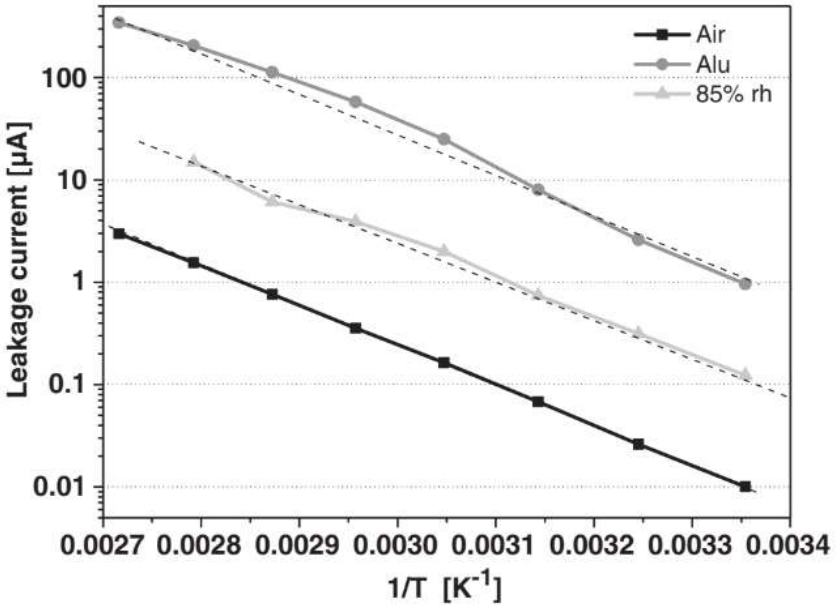

Figure 1. 11. Arrhenius plot of the leakage current at 1000 V negative bias at 85% relative humidity [46].

Temperature accelerates PID progression by activating the processes of the drift and diffusion of alkali metal ions, which form the Arrhenius-type relation, as shown in Figure 1. 11 [46] [47]. It is noted that the relationship is valid at fixed humidity levels because the activation energy increases versus humidity [40][42]. Also, the relationship differs for different types of solar modules. Generally, the activation energy is in the range of 0.7 to 0.9 eV for standard p-type c-Si solar modules at high relative humidity levels [46][48][49].

1.4.1.2. Humidity factor

In addition to temperature, humidity is another important environmental factor affecting PID progression. Firstly, humidity influences on the dominant leakage current paths in the solar module. Leakage currents mainly occur at the module edges under dry conditions. In contrast, the surface conductivity of the front cover glass is relatively high under high humidity or wet conditions, so the leakage current path is dominant through the surface and bulk of the front glass [41]. Secondly, leakage current increases with an increased humidity level. At a given temperature, the magnitude of the leakage current at a high relative humidity is more significant than that at a low relative humidity [39][46].

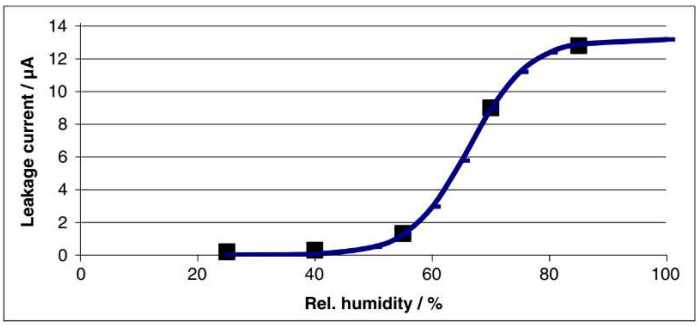

Figure 1. 12. Leakage current as a function of the relative humidity at 85 °C at 300 V negative bias [46].

Hoffmann et al. reported that the leakage current is higher than usual on rainy days during the early morning [50][44][46]. However, on rainy days, solar radiation causes increased module temperature, resulting in the decreased humidity within the solar modules. Under high temperature combined with low humidity within the solar modules, the surface conductivity is small, and the leakage current paths concentrate at the module edges [46][51]. Finally, humidity also influences PID in the long term due to moisture penetration into the solar modules causing the reduced bulk resistivity of the encapsulation materials [19][52]. A

sigmoidal growth function of the leakage current versus relative humidity was modeled by Hoffmann et al. [46], as shown in Figure 1. 12.

1.4.1.3. Voltage factor

PID is dependent on both the polarity and magnitude of the applied voltage. For standard p-type c-Si solar modules, PID is caused by negative voltage bias, whereas it is not affected by positive voltage bias. Positive ions (Na^+) drift through the anti-reflective coating (ARC) layer to the interface of the active cell layer due to the negative voltage bias, leading to a solar power loss [43][45]. Still, the positive ions move away from the active cell. As shown in Figure 1. 13, Xiong et al. revealed that positive bias caused slight PID effects, whereas negative bias caused severe power degradation for the standard p-type c-Si PV modules [53][54]. However, the opposite is valid for the back-contact n-type solar module.

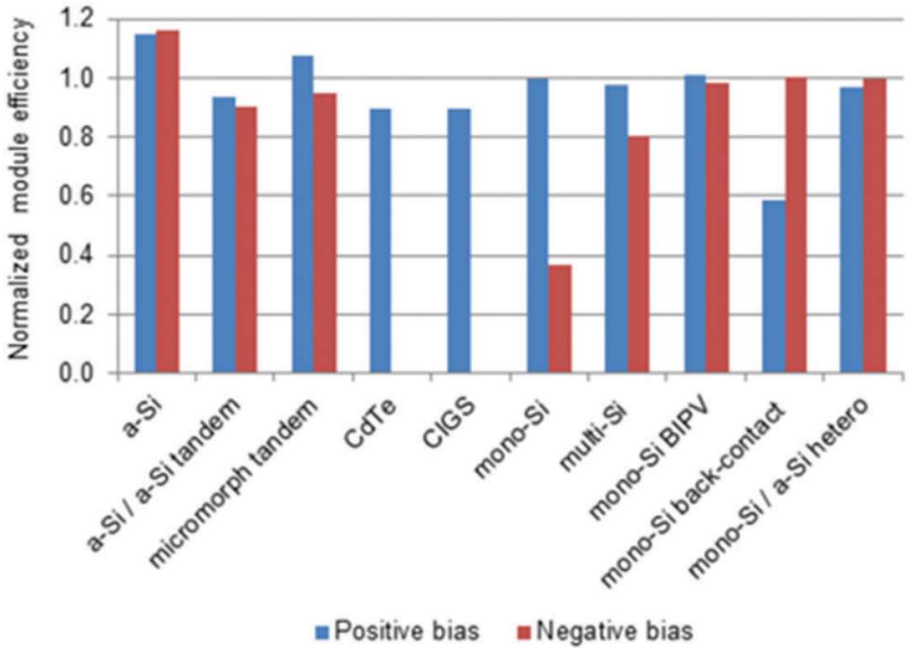

Figure 1. 13. Normalized solar module efficiencies after the positive or negative voltage bias during damp-heat conditions [53].

Hattendorf et al. reported that the severity of PID is non-linear proportional to the magnitude of the applied voltage (-250 V to -750 V) under the same climatic conditions for the same test

period [55]. However, further investigations are necessary to evaluate the potential risks for grid-connected systems with 1500 V_{dc} voltage in the future.

1.4.2. PID test methods

Solar panels are usually tested indoors under harsh conditions to ensure that they can operate 20 to 25 years under field conditions. Different indoor test methods, combined with varying parameters of stress, were developed to test PID susceptibility for solar modules. The test methods can induce the damage severity for the solar modules. Furthermore, the indoor PID tests are relatively different from the outdoor PID tests, but their relationship is still not clear. The development of the different PID test methods is essential to assess the PID stability for solar modules. Herein, the author outlines laboratory PID test methods at both the module level and the cell level.

1.4.2.1. PID tests in a climatic chamber for the module level

This method allows conducting PID tests by applying a high voltage to solar modules under high temperature and relative humidity in a climatic chamber [56][50][57], as shown in Figure 1. 14. Humidity and temperature can be controlled carefully to guarantee repeatability in each specific case. The negative and positive electrodes of the high voltage power source are connected to the two shortened leads and the grounded frame of the solar module, respectively. An additional apparatus is utilized to monitor the leakage current during PID tests. Besides, some other individual climatic chambers allow determining the module performance *in situ* without removing the modules from the chambers [58].

The primary procedure of this test method is based on the IEC 62804-1 standard for solar modules in a climatic chamber, including a temperature of 60 ^{o}C, relative humidity of 85%, and an applied specific voltage (typically -1000 V) for a test duration of 96 h [59]. The selective values of the PID test parameters are dependent on the purpose of the work. According to

experiments of Koentopp et al., if temperature and humidity in the climatic chamber cannot be controlled stably, the results of the PID tests will be invalid [60]. Based on IEC 62804-1 standard, the temperature and the relative humidity of solar modules should be stabilized in turn before the application of voltage bias.

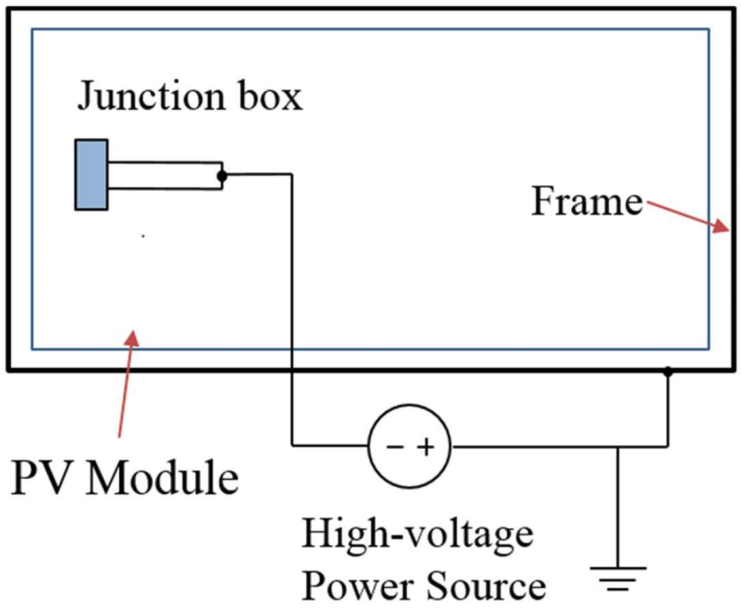

Figure 1. 14. Schematic diagram of the PID test setup in a climate chamber [61].

Besides, PID tests could be performed by employing a conductive layer on the top of the solar modules instead of the module frame [50]. According to IEC 62804-1, the conductive layer, such as aluminum (Al) or copper (Cu) foil, covers the front surface of the solar modules. However, Al foil is commonly utilized in most cases. Moreover, the pressure is also put on the Al foil to ensure uniform contact between the Al foil and the glass surface.

1.4.2.2. PID tests at the cell level

a. PID tests with a corona discharge assembly

Testing PID at the solar cell level is more convenient for researchers to investigate the root cause of PID than that at the module level because it is easy to get the damaged cell to do microscopic investigations after PID tests. The corona discharge technique with the schematic

diagram shown in Figure 1. 15 is employed to cause the PID effect directly to solar cells [62][63]. Positive ions, which are generated and deposited onto the front surface of the test cell by the tip of a thin wire due to a high applied potential, resulting in an electrical field across the test cell. However, the nature of the deposited charges is different from Na ions and not representative of their transport in solar modules. It is noted that Na ions in the method exist on the cell surface before PID and might be variable later. The positive ions in the corona discharge cause damages for the SiN_x film and change its characteristics over time, making the method less valid. Furthermore, the approach ignores the strong influence of the encapsulation material and the glass sheet on the electric field distribution, leading to changes in realistic PID behavior.

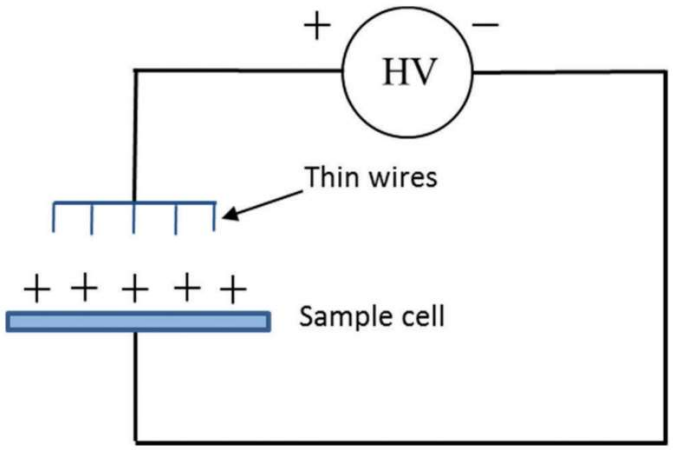

Figure 1. 15. Schematic diagram of a corona-discharge assembly for PID tests [61].

b. Cell-level PID tests with module-like layer stacks

As mentioned above, PID tests with a corona discharge assembly provide a various range of advantages, but they also have obvious drawbacks. Another cell-level PID test method considering the impacts of the packaging materials needs to be developed to overcome the disadvantages of the corona discharge PID test method [52][64]. Recently, Fraunhofer Center for Silicon PVs has developed a cell-level PID test method based on the module-level PID test methodology, as shown in Figure 1. 16 [64].

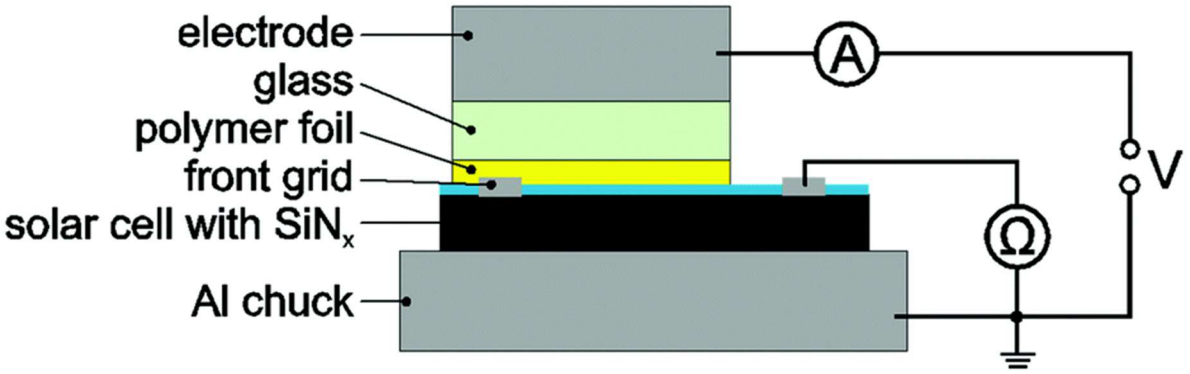

Figure 1. 16. A cell-level PID test method with a module-like structure [64].

The solar cell is put on a temperature-controlled Al chuck to achieve a uniform temperature distribution. Then, an encapsulating layer and a glass plate are placed in turn on the top of the test cell. A high voltage applied between the metal block and the Al chuck to induce the potential difference across the stacked layers. The PID-affected solar cells in this method can be easily removed from the encapsulation material and the glass sheet without contamination for the microscopic investigations. Furthermore, this method allows monitoring *in-situ* R_{sh} as well as the PID progression in the test cell during the PID test period.

1.4.3. PID mechanisms in c-Si solar modules

1.4.3.1. PID-shunting in p-type c-Si solar modules

PID-shunting (PID-s) is the primary PID type in conventional p-type c-Si solar modules. PID-s is closely related to a reduction of the R_{sh} [43][45][60] and the increased dark saturation current due to recombination in the space-charge region (J_{02}) and the ideality factor (n_2) of the second diode term [64][65]. Here, Na^+ ions are supposed to be a dominant cause in the PID-s progression of PID-s [50][48]. It has been suggested that Na contamination originates from the soda-lime glass sheet, even exists on the Si substrate surface before PID. Na^+ ions migrate towards the interface between the Si substrate and the ARC layer due to the negative voltage bias, and ingress into crystal defects, such as stacking faults, throughout the p-n junction,

leading to significant ohmic and non-linear shunting of the cells and their performance deterioration [50][66][67][68][69]. The stacking faults with the length of about a few micrometers extend from the SiN_x/Si interface across the p-n junction into the Si wafer bulk. Stacking faults are supposed to be formed and grown during phosphorus pre-deposition [70]. Naumann et al. reported that stacking faults are created and developed through the penetration of Na ions [71].

As illustrated in Figure 1. 17a, Na^+ ions penetrating the stacking faults are neutralized by free electrons in the n^+ emitter, leading to continuous ingression of Na^+ ions into the stacking faults. The Na decoration of the stacking faults induces a band of defect states within the original bandgap, as sketched in Figure 1. 17b. Therein, shunting paths, as marked in process 1, might be formed across the p-n junction when the concentration level of local defects in the PID-affected regions is sufficiently high. In contrast, if the concentration level of local defects in the PID-affected areas is not high enough, these defects act as Shockley-Read-Hall (SRH) recombination centers in the depletion region, as marked in process 2 [64][69]. The bulk area is not affected by the PID effect because the depth of the stacking faults across the p-n junction is shallow about a few micrometers.

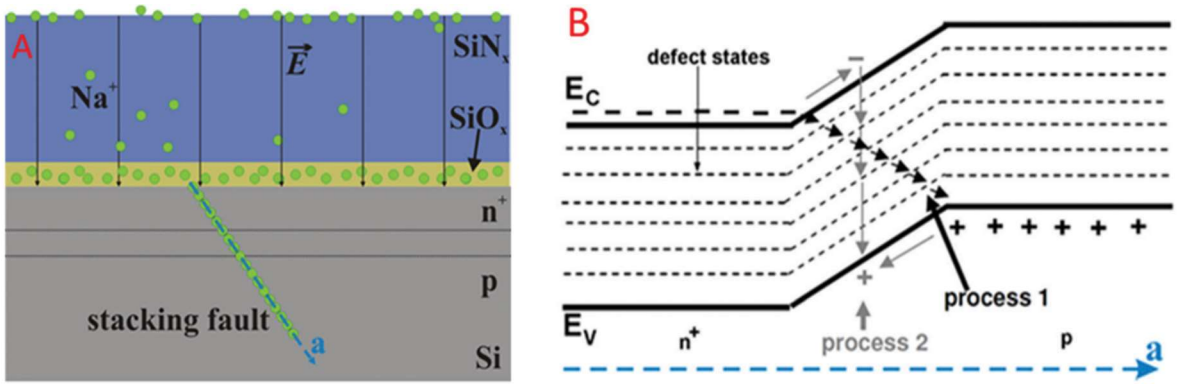

Figure 1. 17. a) Schematic drawing of Na^+ ion diffusion into the stacking faults, b) the proposed band structure along a Na decorated stacking fault [69].

1.4.3.2. PID-polarization in n-type c-Si solar modules

The surface polarization effect occurs in n-type high-efficiency back-contact c-Si cells with silicon dioxide (SiO_2) for surface passivation [42]. Therein, current leaks from the active cell through the EVA layer and the glass plate to the grounded frame due to high positive potential leads to the accumulation of negative charges on the surface of the ARC layer, as illustrated in Figure 1. 18a [42]. The electrons (negative charges), which are trapped within the SiN_x layer due to the high resistivity of the SiO_2 and/or SiN_x film, attract the photon-generated holes (positive charges) in the front region of the cell to the front surface of the cell. Therefore, the recombination of electrons and holes occurs on the front surface of the cells, resulting in an increase of the surface recombination and the decrease of the photon-generated current and voltage [42]. Besides, the mismatch between the cells in the module also causes significant FF and efficiency losses.

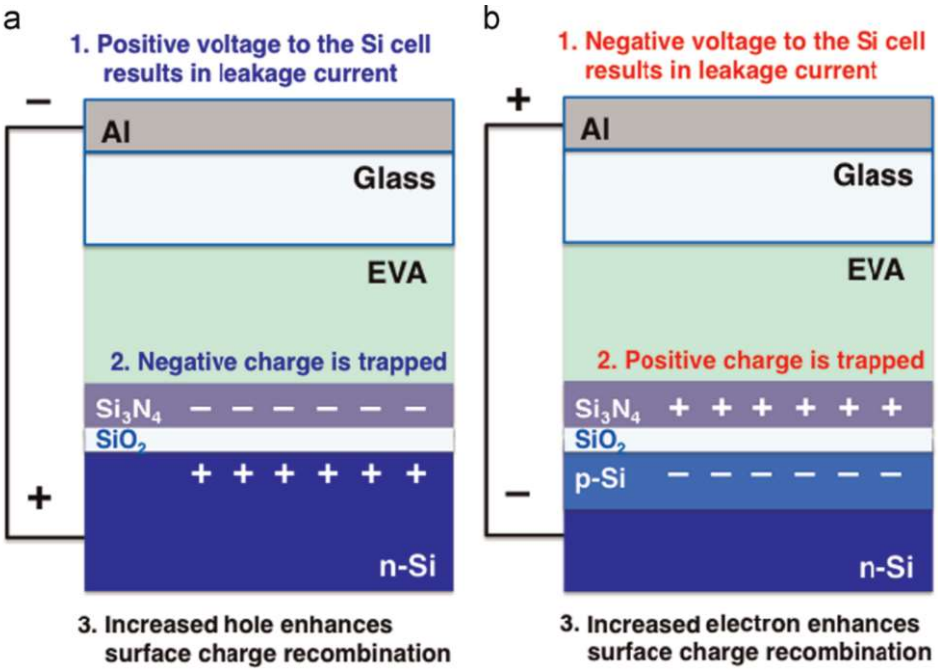

Figure 1. 18. The schematic diagram for the proposed PID mechanism in n-type c-Si solar modules: (a) n-type high-efficiency back-contact c-Si cells [42] *and (b) a n-type high-efficiency front-junction c-Si cells [72].*

Furthermore, the surface polarization effect also occurs in n-type high-efficiency front-junction c-Si cells, as illustrated in Figure 1. 18b [72]. However, different from the n-type high-efficiency back-contact c-Si cells, the performance degradation of the high-efficiency n-type front-junction c-Si cells was caused by the increased surface recombination due to the accumulation of positive charges in the passivation [42][72].

Apart from the surface polarization effect in n-type c-Si solar modules, Na contamination in Si under the negative voltage bias is considered as another candidate causing additional SRH recombination centers, leading to increased surface recombination [70][71]. Nevertheless, further research needs to be performed to clarify this hypothesis.

1.4.4. PID recovery in standard p-type c-Si solar cells

Thermal methods, electrical methods, and their combination can also be utilized for PID recovery. However, all of these PID recovery methods cannot completely recover the efficiency of c-Si solar modules. So far, there is still no complete recovery method developed.

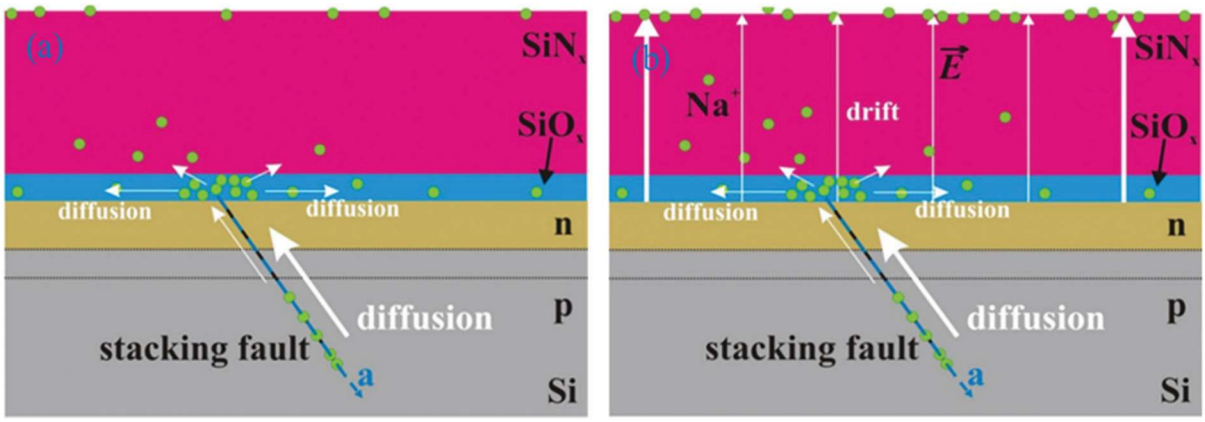

Figure 1. 19. Schematic diagram of the PID recovery process: a) by thermal method (250 °C), b) by the electrical approach (+ 600 V) [73].

Thermal recovery is temperature-activated regeneration of the power lost due to the PID-s effect. The rate of the regeneration process is proportional to the increase of module

temperature compliant with the Arrhenius relation [74]. Under the thermal process, Na^+ ions diffuse out of the PID-affected areas due to the concentration difference, leading to the performance generation of the PID-affected solar cells, as illustrate in Figure 1. 19a [73]. Thus, a higher temperature results in a faster generation rate [47]. Also, the regeneration process is affected by the extent of the PID pre-damage and dependent on the PID-damaged level [74].

The electrical recovery method is used by applying a reserve voltage (commonly +1000 V) to the PID-affected solar cells. The methodology of this method is based on the out-diffusion model, as shown in Figure 1. 19b. Therein, Na^+ ions diffuse out of from the interface under an applied reverse voltage bias, leading to a higher concentration gradient of Na^+ ions between the Na-decorated stacking faults and the interface [73].

Apart from the methods mentioned above, PID recovery can also be conducted by storing the PID-damaged modules in darkness at room temperature. However, it spends about several hundred days for the degraded performance to be recovered by this method [75].

1.5. Motivation

As mentioned in the previous sections, a various range of reliability issues has been found out in c-Si solar cells/modules. So far, after a long time in research, theoretical and experimental scientists all over the world have investigated and developed a lot of solutions to overcome some of the reliability issues significantly. One of the degradations, as mentioned above types, is called PID, which has been discussed and paid attention from many PV specialists because PID causes a severe failure of the solar modules under outdoor conditions.

The PID effect dominantly occurs in solar modules based on the c-Si technology, which dominates the global solar energy share. So, the PID effect needs to be overcome for the c-Si technology in three levels of cell, module, and system. To date, PV experts have investigated, developed, and employed many methods for preventing or minimizing PID in both the

laboratory and industry. However, the commonly utilized methods for PID mitigation are to establish new PID-free c-Si technologies in the cell, module, and system levels. Thus, that is not enough to overcome PID for the existing c-Si technologies.

As presented in the above subsection, UV light is a detrimental factor to PV reliability and stability. Generally, the UV light mainly leads to the acceleration of PV performance deterioration during the damp-heat (DH) tests because it causes the aging degradation of PV modules such as chemical corrosion degradation, discoloration degradation, acetic acid. The actual PID effect occurring in outdoor installed modules should be affected by not only high temperature, humidity, and high voltage but also the UV light radiation. However, so far, the UV light irradiation has not been utilized in the conventional indoor PID tests combined with the DH tests because of the limited apparatus and cost. Therefore, the PID effect, combined with the impact of UV light irradiation on PV performance, has not yet been investigated. Also, the mechanism of PID-s observed in outdoor (indoor PID tests together with UV light irradiation) has not been discussed and compared with the indoor PID mechanism.

Besides, it is well-known that the stacking fault contaminated by Na ions is the primary mechanism of the PID-s behavior in p-type c-Si solar cells. However, we have not known whether other candidates cause the PID-s effect. Indeed, outdoor installed modules may be subjected to mechanical stress, such as micro-crack, which results in the PV performance deterioration dependent on micro-cracking types. In particular, the PV performance degradation due to micro-cracks becomes more severe under aging processes. However, the power loss behavior due to micro-cracks combined with the PID stress process has not been considered and examined. The PID mechanism related to micro-cracks has not been understood clearly. So a more precise understanding of the PID phenomenon should be investigated comprehensively.

1.6. Dissertation outline

The first chapter briefly outlined the relevant issues of PV reliability, including degradation types composed of aging degradation, mechanical degradation, and high voltage stress degradation. Also, the effects of UV light irradiation and micro-cracks on the degradation of solar modules were discussed in detail. Notably, this chapter presented the background, the status of current research, and development for PID. Also, this chapter highlighted limited issues for PID investigation, leading to perform this study.

Chapter 2 shows the PID shunts at micro-cracked regions observed by EL, LIT images, external quantum efficiency (EQE) responses, current density-voltage (*J–V)* curves, and microstructure analysis. Also, this chapter proposes the decoration of sodium (Na) ions in micro-cracks as the primary mechanism resulting in PID for p-type c-Si solar cells.

Chapter 3 demonstrates that apart from acting as shunting defects as mentioned in chapter 2, micro-cracks also serve as the additional recombination center, leading to the deterioration of J_{sc}, and τ_{eff} in PID-affected solar cells. This chapter presents the PID recovery method by applying a reverse bias voltage for PID-affected solar cells related to micro-cracks. The performance of PID-affected solar cells at micro-cracked regions was regenerated significantly, albeit incompletely. Furthermore, this chapter also assesses and models the dependence of the PID behavior after degradation/regeneration cycles on the duration of PID stress and recovery processes.

Chapter 4 suggests that irradiating UV light in the 300–390 nm wavelength range on p-type c-Si solar cells during the PID test can delay the degradation of the solar cell performance caused by PID. Also, in this chapter, the author proposes a mechanism of the PID delay effect by UV light irradiation during the PID test in p-type c-Si solar cells.

The final chapter summarizes the work, including the elucidation of the PID mechanism related to micro-cracks, the PID recovery for solar cells with micro-cracks, and the finding of the PID delay method by using the UV light irradiation. This chapter also discusses further research directions for PID in c-Si solar cells/modules in the future.

Chapter 2 | PID mechanism related to micro-cracks

2.1. Introduction

PID results in significant performance degradation, as well as reduced durability in levels of solar cells, modules, and systems. Understanding the PID mechanisms will enable researchers and manufacturers to remedy the defects present in common types of solar cells, as well as manufacture robust next-generation cells that can prevent and limit the effects of PID. There are many types of commercial solar cells, and each type has a unique degradation mechanism. PID mechanisms for these different kinds of cells have been published such as conventional p-type c-Si [48][45][43], front-emitter n-type c-Si [72][76][77][78], rear-emitter n-type c-Si [79][80], n-type back-contact c-Si [42][81], a-Si thin-film [40][82], c-Si/a-Si heterojunction [83], cadmium telluride thin-film [84][85], and copper indium gallium selenide thin-film [84][86][87] solar modules. The major cause of PID defects for p-type Si solar cells is sodium (Na) ion migration from the soda-lime glass through the encapsulation layer into the solar cell. For conventional p-type c-Si solar modules, the PID shunt defect is the most common type of PID mechanism as it is closely associated with the degradation of the R_{sh}.

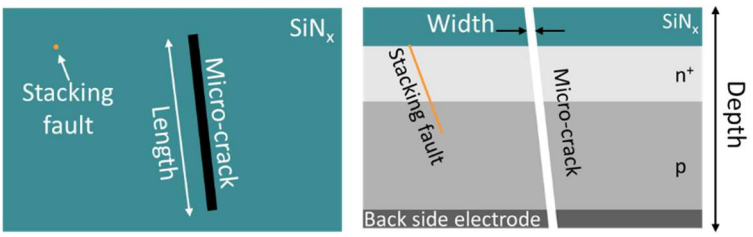

a) The top view *b) The cross-sectional view*

Figure 2. 1. Shape comparison between stacking fault and micro-crack in a solar cell.

Crystal defects are considered as the root cause of PID behavior. To date, stacking fault (intrinsic crystal defect) plays a dominant role causing the PID effect for p-type c-Si solar cells. Also, micro-crack (extrinsic crystal defect) could be another critical candidate that might lead

to a severe PID effect for c-Si solar cells. However, no investigation has reported on the influence of micro-crack on PID behavior as well as its mechanism. Figure 2. 1 shows the difference in terms of shape between stacking fault and micro-crack. Micro-crack, which has a width below 100 μm [88] with unlimited length, could extend from the SiN_x surface to the back-side electrode of solar cells. Meanwhile, the stacking fault (depth of a few μm) has a tiny dimension compared with micro-crack. Micro-cracks result from processes such as manufacturing, storage, transportation, installation, etc. It is noted that if micro-cracks cause inactive regions in the cells, they degrade the electrical performance as well as the mechanical stability of these cells themselves, resulting in cell damages and the solar module performance deterioration. the PID phenomenon could occur in both intact and micro-cracked solar cells installed in the field.

This chapter focuses on the effect of micro-cracks on the PID phenomenon and presents the influence of Na ion decorated micro-cracks on the evolution of PID in p-type c-Si solar cells as well as proposing a degradation mechanism. Regions of the solar cells with PID shunts were detected by EL and lock-in-thermal (LIT) images. The local *J–V* curve characteristics in micro-cracked areas of the solar cells, which were measured before and after PID stress tests indicated the presence of micro-crack related PID shunts. Analyzes and evaluations from SEM images, energy dispersive X-ray (EDX) spectroscopy mapping, and secondary-ion mass spectrometry (SIMS) were also conducted to show the Na ion decoration in micro-cracked regions as the critical cause of PID defects.

2.2. Experimental procedure

2.2.1. Crystalline Si cell-based modules

To examine the role of Na ion decorated micro-cracks on the evolution of PID for Si solar cells, commercial p-type based c-Si solar cells with a size of 156 mm × 156 mm and the thickness of

200 µm were utilized. First, micro-cracks were formed in the solar cells by the mechanical method. Then, solar modules were done based on the micro-cracked Si solar cells. The structure of solar modules similar to the standard solar modules consists of the following: two soda-lime glasses with the size of 200 mm × 200 mm and the thickness of 3.2 mm to cover the front and rear sides of solar modules, two commercial encapsulation EVA films with the thickness of 0.45 mm, and one Si solar cell between two EVA films. However, it is essential to note that these solar modules were un-laminated during the experimental processes. Herein, an un-laminated solar module is a stacked structure of glass/EVA/c-Si cell/EVA/glass without a laminating process, as shown in Figure 2. 2a. The advantage of un-laminated solar modules is that it is easy to separate layers of solar modules without containing the residue of the EVA films on the solar cell surface after the PID stress tests. The structure of un-laminated solar modules was also demonstrated in the work of V. Naumann et al. [69]. The structure mentioned above facilitates the analysis of other microstructural characteristics to clearly understand the PID mechanism related to Na ion decorated micro-cracked regions of the solar cells.

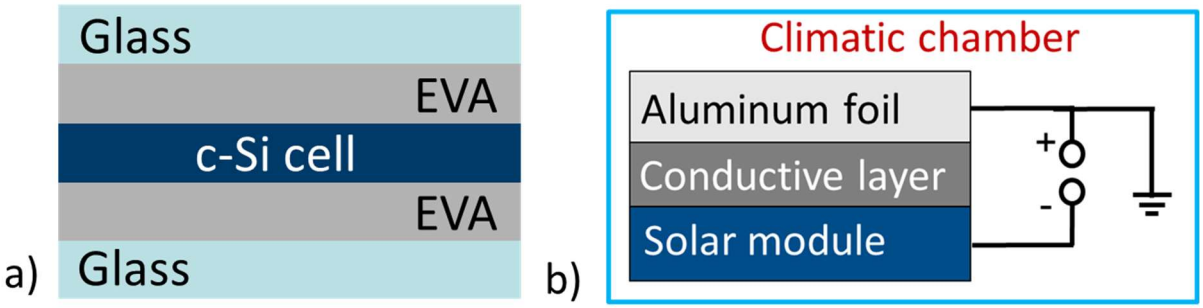

Figure 2. 2. a) un-laminated solar module, b) PID setup in a climatic chamber.

2.2.2. PID stress tests

In this chapter, PID stress tests were performed following the common PID stress test procedure for the module-level PID stress tests. An aluminum plate with a thickness of 0.5 cm and a conductive rubber layer were put in front of the soda-lime glass were connected with the

positive high voltage of a power supply (Kikusui, PID insulation Tester, TOS721OS). This was done to cover the whole front side of the solar module to homogeneously apply a voltage to the surface of the Si solar module [72][89][90][91]. Meanwhile, negative and positive electrodes of the solar modules were short-circuited and connected with the negative high voltage of the power supply. PID stress tests were performed by applying a high voltage of 1000 V in a climatic chamber (LH-113, Espec Corp.), as illustrated in Figure 2. 2b, with the following conditions: temperature of 65 ºC, relative humidity of 85%, for 50 h and 100 h.

2.2.3. Electrical characteristics of the solar modules

Characteristics of solar modules such as one sun-illuminated *J–V* curves, EL, and LIT images were characterized before and after forming micro-cracks and PID stress tests. Electrical characteristics such as P_{max}, V_{oc}, J_{sc}, FF, and R_{sh} in these micro-cracked regions of the solar cells were extracted from one sun-illuminated *J–V* curves measured by using CEP-2000RP system (Bunkokeiki Co., Ltd.). Besides, this system was used to characterize EQE responses. To make a more precise measurement of the electrical characteristics in the micro-cracked regions, a shadow mask with a slot of 1 cm × 1 cm in size was used in all measurements. Each data point in each area was calculated by the mean value of three measurements received in each region and at the same time. It is noted that the illuminated *J–V* characteristics, which were locally measured in micro-cracked areas, could be not really accurate but with the aid of the shadow mask during measurements. Thus, the normalized local characteristics showed that the tendency of degradation behavior caused by micro-cracks after PID stress tests was acceptable.

Meanwhile, EL and LIT images of solar modules were characterized by a THEMOS-1100L (Hamamatsu Photonics Inc.) measurement system. EL and LIT images of this work were taken by InGaAs camera cooled around minus 70ºC, applied current density of 20 mA/cm^2 (applied

maximum current density of 40 mA/cm^2), exposure time of 200 ms, and the use of InSb camera, respectively. Because the THEMOS-1100L system has no function to measure the exact temperature, the color bar was not shown in all of the LIT images. All these measurements were directly performed for the bare solar cell without having the glass and the EVA films.

The regions of micro-crack related PID shunt were observed from EL and LIT images. Pieces of the PID shunt regions that were cut by a laser scribing system were further investigated by employing electron microscopy methods. A low vacuum scanning electron microscopy (SEM, Hitachi SU 6600) system integrated EDX spectroscopy measurement was used to find the regions of micro-crack related PID shunt. Characterizations of these PID regions were performed with acceleration voltages of 5 kV for SEM measurement, and 15 kV for EDX measurement.

2.2.4. Background of EL and LIT methods

a) Principle of the EL method

EL imaging is utilized as a diagnostic tool for determining the optical and electrical characteristics of photovoltaic modules [92][93]. It could detect defects such as PID-shunting, micro-cracks, macro-cracks, cell fractures, etc. Figure 2. 3 shows the configuration of the EL imaging system. EL images could be taken when radiative recombination of charge carriers (electrons and holes) due to an applied forward voltage causes a light emission. So, EL intensity is proportional to the applied forward voltage, the number of minority charge carriers, and parasitic resistances R_s, R_{sh} of solar cells. Also, EL intensity depends on the presence of crystal defects which restrict the radiative recombination processes. That means EL intensity at defected locations is relatively low.

The R_{sh} reduction can cause a decrease in the local voltage of PID-affected locations of solar cells, leading to a decrease in their EL intensity. Therefore, the EL image of the PID-affected

solar cell has a weaker signal compared with a PID-free solar cell, i.e. the EL image of the PID-affected cell is darker. Furthermore, there is also an increase in non-radiative recombination in the p-n junction of more severe PID-affected cells. So, these solar cells will have a very weak EL intensity regardless of the number of injected carriers.

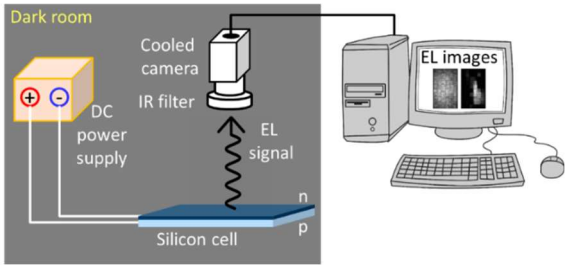

Figure 2. 3. The configuration of an EL imaging system.

b) Principle of the LIT method

LIT method is considered as a useful characterization tool widely used in solar cell research. The principle of lock-in thermography is based on the application of a periodic input energy wave to the surface of the object which is examined and analyzing the local temperatures on the surface of the object. The LIT principle consists of three basic steps, as shown in Figure 2. 4. Firstly, periodic excitation sources such as voltage, current, light sources are introduced into a solar cell. Secondly, a cooled infrared camera with a certain frame rate can capture a stream of temperature images of the solar cell. Finally, all captured images are transferred to a computer, in which they could be evaluated and averaged based on the lock-in principle [47]. The final resulting images could be considered as a map of heat generation.

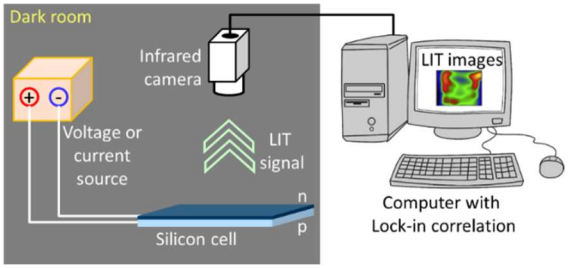

Figure 2. 4. The configuration of a LIT imaging system.

The LIT technique can detect the periodic local surface temperature variation in local shunting areas by biasing a pulsed voltage to the cell in the dark [47]. This technique may not only capture the shunting position with an accuracy of 5 mm but also determine shunting types (linear or non-linear) [94].

2.3. Results and discussions

2.3.1. Micro-crack related PID shunt regions via LIT and EL images

Figure 2. 5a showed EL and LIT images for the whole solar cell (sample #1) before and after forming micro-cracks, and after the PID stress tests for 50 h, 100 h. Three main micro-cracked regions are generated by the mechanical method in sample #1. After being formed by the mechanical method, micro-cracks cannot be seen with the naked eye but can be observed through EL images of Figure 2. 5b. The dark regions in Figure 2. 5c and d. can be seen in the micro-cracked areas after the PID stress test for 50 h and 100 h. The images also reveal that the PID formed shunts were related to micro-cracks. In particular, it is clear from EL images that these regions become darker and broader over the PID stress test duration. The three main hot spots in the LIT images were the corresponding micro-cracked regions in the EL images. The hot spots observed in the LIT image of Figure 2. 5b arise from the micro-cracked areas in sample #1. Research has shown that because the I_{sc} of the micro-cracked region is lower than the operating current of the whole solar cell, which gives rise to reverse biasing[95][96]. Thus, dissipating the generated power into energy in the form of heat, which is an indication of performance degradation in the micro-cracked regions. The hot spots were continuously observed in the LIT image of Figure 2. 5c, while the rest regions of Figure 2. 5c became much cooler than that of Figure 2. 5b. It is proposed that the performance degradation of sample #1 in the micro-cracked regions became more severe. Notably, the dark areas of the EL images and the hot regions of LIT images in the micro-cracked regions are the evidence of PID by

junction leakage due to the R_{sh} decrease. In this case, there is no evidence to reveal that the R_s resistance increase can cause PID.

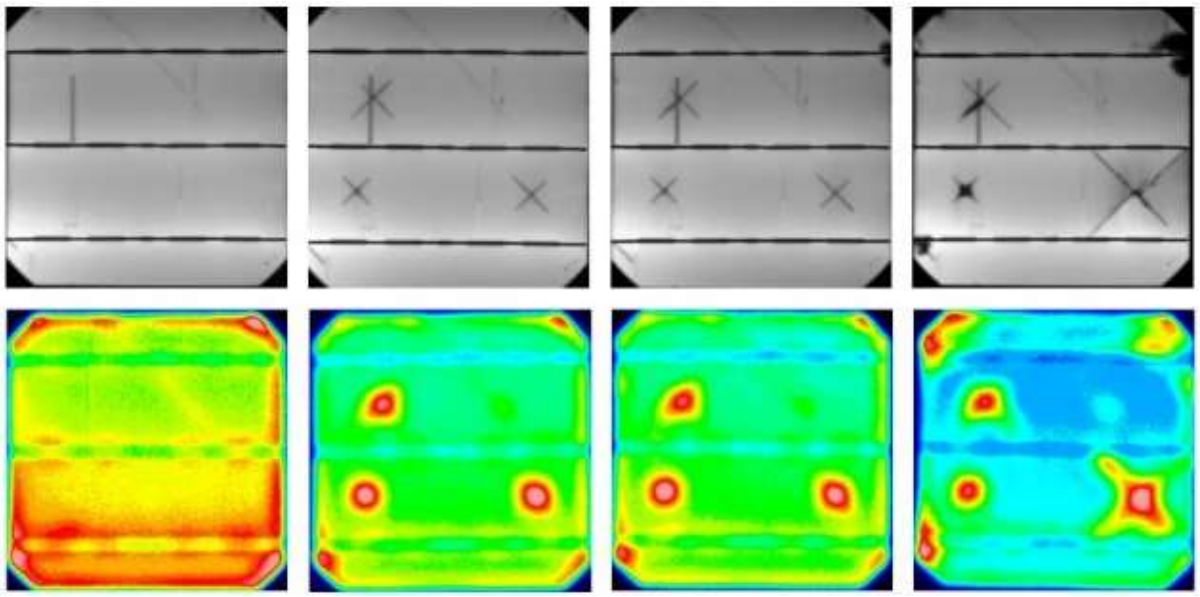

Figure 2. 5. EL (the top row) and LIT (the bottom row) images of PID shunt related to micro-cracks of sample #1; a) fresh, b) after forming the micro-cracks, c) after the PID stress test for 50 h; d) after the PID stress test for 100 h.

2.3.2. Electrical characteristics of micro-crack related PID shunt regions

To confirm the repeatability of the micro-crack related PID and the influence of geometric properties and types of micro-cracks on the performance degradation of PID, PID stress tests were performed in another solar cell (sample #2) with the same PID conditions as for the previous solar cell. A portion of sample #2 with micro-cracks indicated in Figure 2. 6 was selected to measure and analyze electrical characteristics of micro-crack related PID shunt regions in this section. Electrical characteristics were characterized in four regions marked by the red squares in Figure 2. 6, which consist of three micro-cracked regions and one intact region to compare the influence of micro-cracks with that of the intact region on PID shunts.

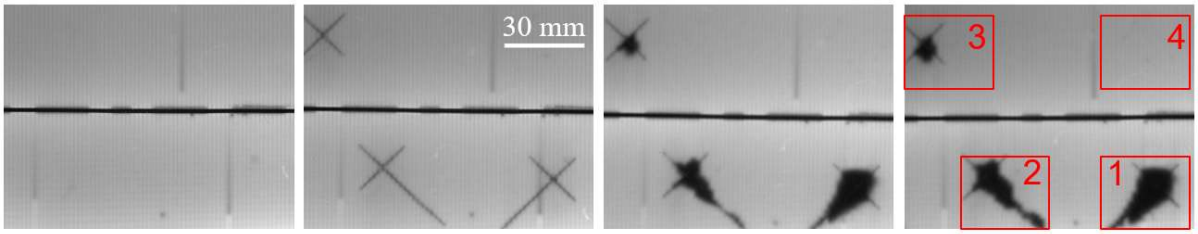

Figure 2. 6. EL images of PID shunt related to micro-cracks of sample #2; a) fresh, b) after forming the micro-cracks, c) after testing PID for 50 h; d) after testing PID for 100 h.

Figure 2. 7 clearly indicates the dependence of normalized local electrical characteristics such as P_{max}, V_{oc}, J_{sc}, FF, and R_{sh} in micro-crack related PID shunt regions on PID stress test durations and on geometric properties of micro-cracks. The local electrical characteristics in the micro-cracked regions of sample #2 degraded significantly after PID stress tests. It seems that FF was degraded as much as V_{oc}, which is uncharacteristic of the PID shunting mechanism. This might be due to using the shadow mask in the one sun-illuminated *J–V* measurements. However, important information can still be obtained from the degradation behavior.

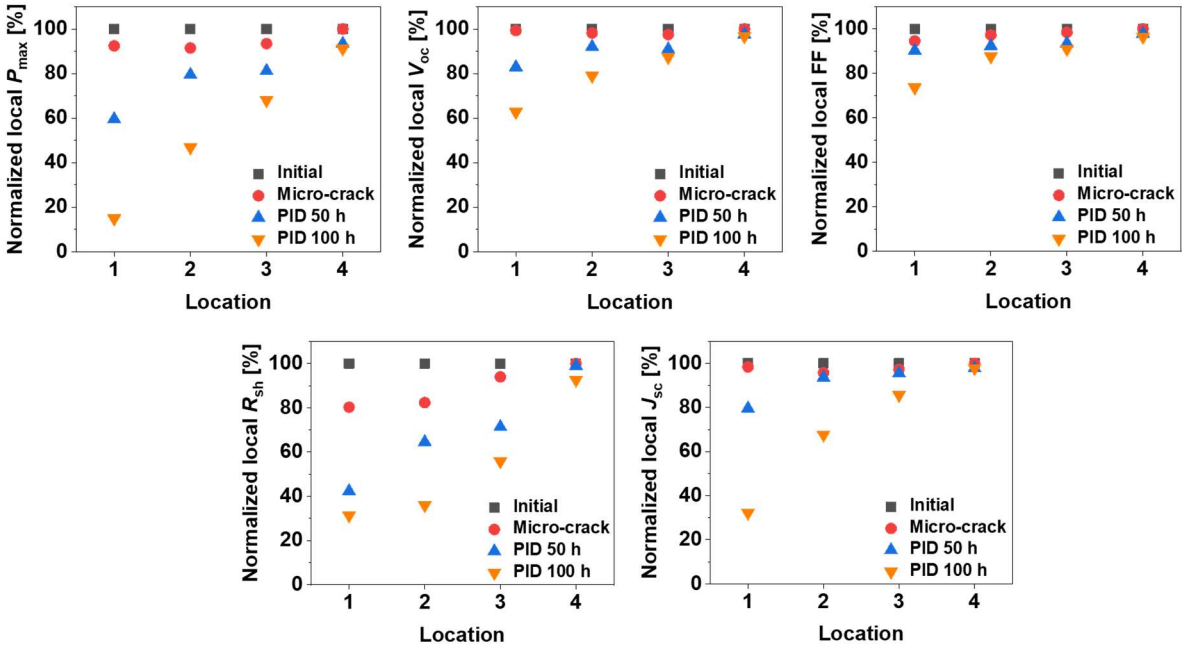

Figure 2. 7. The dependence of normalized J_{oc}, V_{oc}, P_{max}, FF, and R_{sh} via PID durations on micro-crack related PID shunt regions.

The length of the micro-crack line in Si solar cells causes an effect on the PID shunt behavior, as demonstrated in the work of J. Käsewieter et al. [97]. Though the length of a micro-crack line in region 2 is slightly longer than that in regions 1 and 3, the micro-crack related PID shunt area in region 1, which is larger than that in regions 2 and 3, can be clearly seen via EL images in Figure 2. 6 after the PID stress test for 50 h. It can be observed that the electrical characteristics, which significantly degraded in the micro-cracked regions 1, 2, and 3 after the PID stress tests, are proportional to their own PID shunt affected areas. Meanwhile, it can be seen from the data that the PID shunt was not observed in region 4 of Figure 2. 6, and electrical characteristics in Figure 2. 7 of this region reduced insignificantly. It is assumed that the micro-crack related shunt area depends not only on the length but also on other factors such as width and depth of micro-cracks in solar cells. The electrical characteristics of these regions are in good agreement with the EL intensity of the corresponding regions. This means that the higher the intensity and areas of dark regions are, the larger the degradation level of electrical characteristics in corresponding regions.

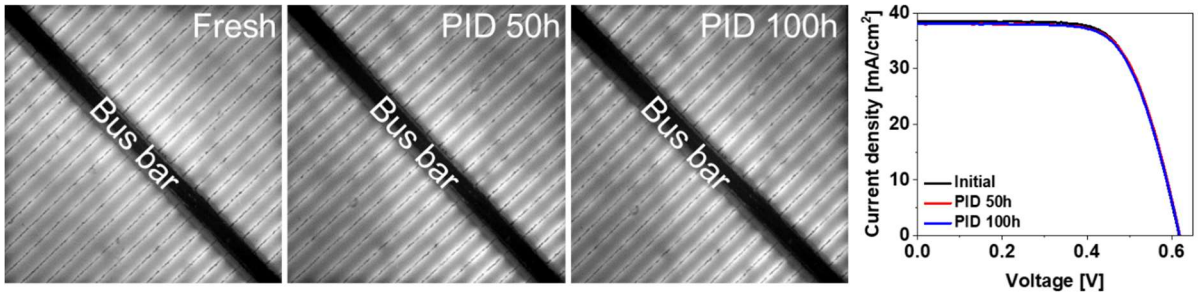

Figure 2. 8. EL images (left) and J–V curves (right) of sample #3 before and after PID stress tests of 50 h and 100 h.

Sample #3, an intact mini solar cell (30 mm × 30 mm) was subjected to PID stress tests for 50 h and 100 h to confirm if micro-cracked regions are related to PID. EL images and one sun-illuminated *J–V* curves were shown in Figure 2. 8, and electrical characteristics were indicated in Table 2. 1. It is clearly observed that the performance degradation of sample #3 is negligible

after PID stress tests. Thus, this indicates that the PID defect might not occur in the intact regions of Si cells but occur in micro-cracked regions.

Table 2. 1. Electrical characteristics of sample #3 before and after PID stress tests.

	P_{max} (mW)	V_{oc} (V)	FF	J_{sc} (mA/cm^2)	R_{sh} (Ω)
Fresh	16.2	0.619	0.682	38.51	572.6
After PID 50 h	16.1	0.617	0.679	38.10	546.9
After PID 100 h	16.0	0.612	0.671	38.22	535.9
Degradation after PID 100h	1.48%	1.13%	1.61%	0.75%	6.41%

The larger the width and the depth of micro-cracks are, the higher the resistance across the micro-cracks becomes [98]. These high resistances block the generated charge carrier transportations to the fingers and then to bus bars of the solar cell. Hence, the carrier collecting probability strongly reduces in these regions. Blocked carriers at the edges of the micro-cracks are rapidly recombined. As such, these regions become high recombination centers, which results in strongly degrading their EQE responses. Consequently, the larger the width and depth of the micro-crack region are, the more strongly the EQE responses and electrical characteristics degrade in the micro-cracked region.

Figure 2. 9 showed EQE responses of 4 regions of sample #2 marked in Figure 2. 6 after forming micro-cracks and after PID stress test for 100 h. After micro-cracked regions were formed in sample #2, EQE responses of regions 1, 2, 3 started to reduce from region 3 to region 1 slightly. This indicates that micro-crack related PID regions were most severely affected from region 3 to region 1 under high temperature, high humidity, and high voltage [29][99] (the micro-crack related PID mechanism discussed in Section 2.3.4 in detail). This resulted in severely deteriorated electrical characteristics from region 3 to region 1.

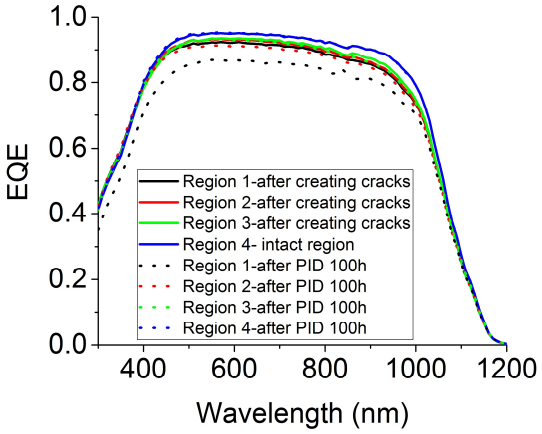

Figure 2. 9. EQE of 4 regions of the solar cell marked in Figure 2. 6.

2.3.3. SEM and EDX mapping analysis

To understand the micro-crack related PID mechanism of crystalline solar cells in detail, SEM and EDX measurements were performed. The micro-cracked regions in which PID shunts were observed through EL and LIT images were cut into smaller pieces of solar cells to facilitate SEM images and EDX mapping analysis. A laser scribing system was used to avoid making another crack caused by micro-cracks, thus preserving the initial nature of PID shunts. Cracks at the edges of pieces of solar cells after laser beam cutting are not observed in EL images (not shown here). Figure 2. 10 shows an SEM image of the micro-cracked region with high PID shunt density. The width of micro-cracks is in the range of 15−40 µm, which satisfies the standard of micro-cracks [19].

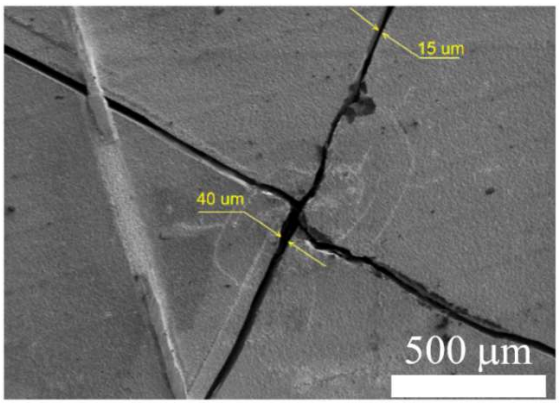

Figure 2. 10. SEM image of a micro-cracked region.

Figure 2. 11a illustrated the EDX mapping on the surface of an intact region before PID stress tests. Meanwhile, the EDX mapping on the surface of the micro-cracked region affected by PID is shown in Figure 2. 11b. Also, EDX mapping on the cross-section site of the micro-cracked region was indicated in Figure 2. 11c. Elemental composition information was obtained by EDX mappings in scanning SEM mode.

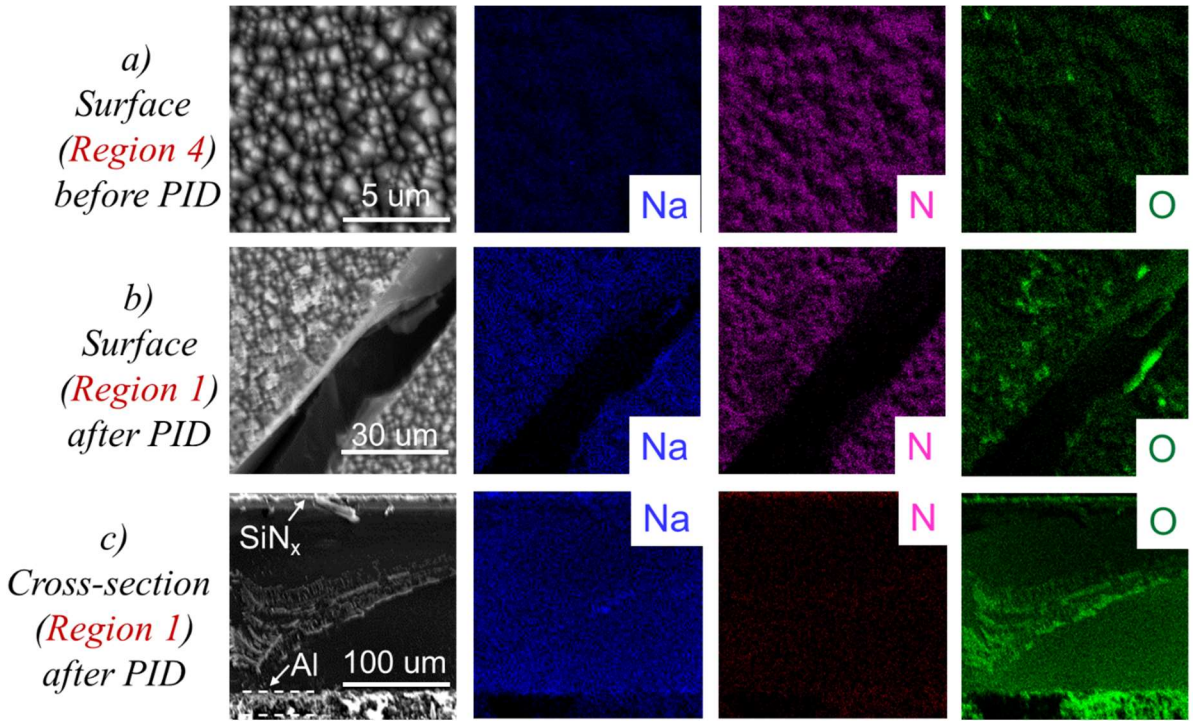

Figure 2. 11. EDX mappings: a) on the surface of an intact region before PID stress tests; b) on the surface of the micro-cracked region affected by PID; c) on the cross-section site corresponding to the micro-cracked region.

The corresponding EDX mappings on the surface as well as on the cross-section site of micro-cracked regions indicated the elemental distribution of Na, O, N (Si is not mentioned as it is the primary component). A high EDX signal of N can be clearly observed in Figure 2. 11a and b but almost not observed in Figure 2. 11c which shows the SiN_x layer of the solar cell. Especially, before the PID stress tests, the concentration of Na ions is very low on the surface of the solar cell, as shown in Figure 2. 11a, because Na is one of the common impurities of

solar cells. However, the Na ion concentration increases significantly after PID stress tests on not only the surface but also the cross-section site of the solar cell, which will be explained in Section 2.3.4 in detail. A SIMS (secondary-ion mass spectrometry) profile was characterized and employed to confirm the increase of the Na ion concentration on the surface of the active cell layer after the PID test, as presented in Figure 2. 12. On the solar cell surface, the Na ion concentration is closed to 10^{18} atom/cc before the PID test, while it is up to around 10^{20} atom/cc after PID of 300 h. Evidently, the Na ion concentration may not increase to such the value after PID of 100 h (in this work), but this implied that the Na ion concentration also enhances significantly after the PID process.

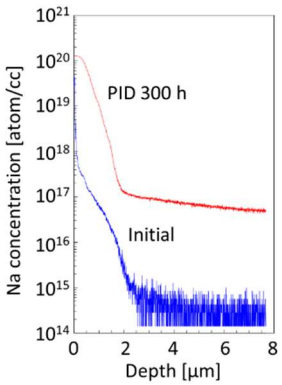

Figure 2. 12. Na concentration on the surface of a solar cell before/after a PID test.

Besides, the concentration of the O element in Figure 2. 11b and c is higher than that in Figure 2. 11a. That means the O elemental concentration increases on the cell surface and the cross-section of micro-cracks in the solar cell after the PID test. This is because H_2O and O_2 penetrated easily into the active Si cell layer through the gaps between the cell layer and EVA layers of the un-laminated solar module under damp-heat conditions. Therein, Na-O, Si-O species were formed on the cell surface even on the cross-section of the micro-cracks. No evidence reveals that oxygen can affect the PID effect at micro-cracked regions.

These findings of EDX mapping show that after PID stress tests, Na ions were located on the surface and the whole cross-section site from the surface to the interface between the Si base and the back-side electrode of the solar cell.

2.3.4. The PID shunting mechanism caused by Na decorated micro-cracks

As PID shunts of micro-cracked regions have been identified in the above samples, typical degradation of R_{sh} in the corresponding regions was observed after the same PID stress test, under conditions for the module based PID stress tests [66][68][67]. The above-presented results have shown that micro-cracks play an important role in the evolution of PID shunts. It is essential to note that micro-cracks with a thickness of 15−40 μm have extended from the Si surface through the p-n junction to the back-side electrode. The EDX mapping proves that Na ions were found in the entire cross-section site of the micro-cracks of the solar cells after the PID stress tests. Sodium ions drift into the Si surface from the soda-lime glass through the encapsulation EVA layer under the effect of the strong electric field, as demonstrated by PID shunt progresses in ref. [69][100][64][101]. In the micro-cracked regions, Na ions diffusing into p-n junction were neutralized by the free electrons of the n^+ emitter region, which helps other Na ions to continue migrating to the depth of the micro-cracked regions as illustrated in Figure 2. 13. Possibly, Na ions might not penetrate deeply into the Si cell from the surface in the intact vicinities where there is no sign of significant deterioration of the local electrical characteristics. Thus, the Na ion decorated micro-cracks of the solar cells are attributed to making PID shunts across the p-n junction after the PID stress tests.

Before the PID stress tests, the presence of micro-cracks blocked the transportation of electrons and holes towards the electrodes of solar cells, hence micro-cracked regions were inactive or low-active parts of solar cells observed through the degradation of electrical

characteristics in Figure 2. 7. After the PID stress tests, the Na ions at the edge of the micro-cracked regions capture the free electrons in both the n^+ emitter and p base layers. Consequently, the Na ion decorated micro-cracked region became recombination centers, which degraded the output power and the efficiency of solar cells. On the other hand, after the PID stress tests, the Na decorated micro-cracked regions act as local defects. Due to Na ions decorating the entire cross-section site of the micro-cracked regions from the Si surface to the back sheet of the solar cell, the local defect concentration in the PID shunt region is high enough to form shunting paths across the p-n junction, which leads to ohmic conductivity across the p-n junction. Shunting paths reduced the R_{sh} of solar cells, so the amount of current flowing through the solar cell junction and the voltage from the solar cell was decreased.

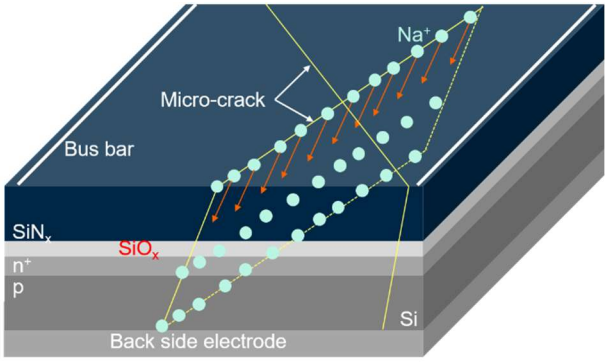

Figure 2. 13. The scheme of the PID mechanism at the micro-cracked regions of solar cells after the PID stress tests.

2.4. Conclusions

This chapter investigated the PID shunting type related to micro-cracks on solar cells. The degradation of typical R_{sh} is an important cause, which may lead to PID of p-type crystalline Si solar cells. Local PID shunts related to micro-cracks are revealed via EL images and LIT. We have shown the influence and mechanism of Na-ion-decorated micro-cracks on the evolution of PID through detailed analysis and evaluation from measurements of electrical characteristics, SEM images, and EDX mappings.

Chapter 3 | Recover possibilities of PID caused by the micro-cracked locations in solar cells

3.1. Introduction

Outdoor installed modules may be subjected to mechanical stresses, such as macro and micro-cracks, which results in the PV performance deterioration dependent on cracking types. Although the naked eye cannot see micro-cracks with a small width (< 100 μm), they still cause the degradation of the performance and reliability in solar cells. The influence level of micro-cracks on the degradation depends on the length, width, depth, and type of micro-cracks. The micro-crack induced deterioration becomes more significant after the aging process by humidity freeze cycles [98][29]. In particular, the PID phenomenon has been observed in micro-cracked areas of p-type c-Si solar cells, where the local electric characteristics of solar cells have deteriorated more severely [102]. The critical cause of the PID effect in micro-cracked regions is related to the decoration of the Na ions at the cross-sectional site of micro-cracks [102]. Herein, PID shunting (PID-s), which is the primary PID mechanism related to micro-cracks, causes the severe reduction of R_{sh} as well as the degradation of the performance and lifetime of the solar cells.

However, there is no research to overcome the performance deterioration owing to the PID effect related to micro-cracks. Therefore, a PID recovery process should be examined for the PID-affected micro-cracked solar cells. A PID recovery method by biasing a reversed voltage for PID-affected micro-cracked p-type c-Si solar cells with and without lamination was utilized in this work. PID stress/recovery cycles were also performed for micro-cracked solar cells. The electrical characteristics of the solar cells were measured and analyzed before and after PID stress and recovery processes. Furthermore, characterizations composed of EL, lock-in

thermography (LIT) images, dark and illumination current density–voltage (J–V) curves, EQE responses, and τ_{eff} were utilized to support analyses and conclusions of this work.

3.2. Experimental procedure

3.2.1. PID stress and recovery processes of solar modules

Two commercial p-type based c-Si solar cells with large size of 156 mm × 156 mm and a thickness of 200 µm were utilized in this work. The first large cell was cut into small pieces with a size of 15 mm × 15 mm by a micromachining system (Oxford Lasers Ltd.). Six similar small pieces called mini-cells were employed in this work as well. Three mini-cells had micro-cracks induced by the mechanical method, and the rest of the mini-cells were kept intact.

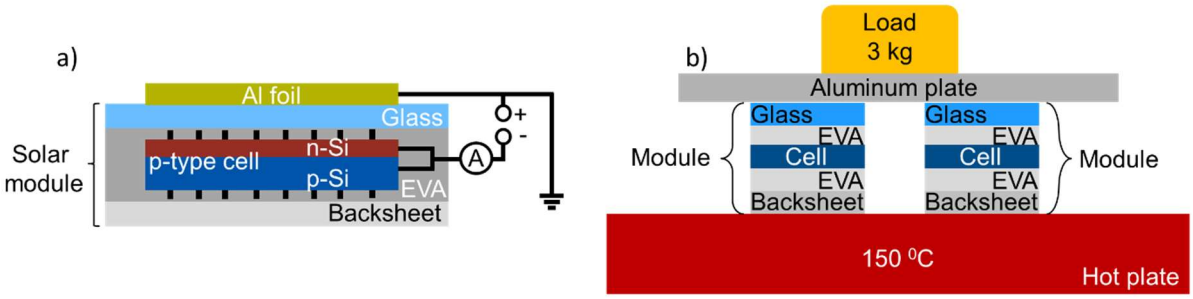

Figure 3. 1. a) The diagram of the PID stress setup and b) the diagram of a laminating process.

As shown in Figure 3. 1a, the structure of a mini solar module consists of one mini-cell between two commercial first-cure-type EVA films, one soda-lime glass plate on the top of EVA film, and one back-sheet below the bottom EVA film. The thickness of the EVA film and glass plate is 450 µm and 3.2 mm, respectively. The EVA film, the glass, and the back sheet has a size of 60 mm × 60 mm. The back-sheet is composed of polyvinyl fluoride (PVF) of 38 µm/polyethylene terephthalate (PET) of 250 µm/PVF of 38 µm. It is noted that six mini solar cells were laminated by heating and load (laminating process) for 1 h before all experimental tests, as illustrated in Figure 3. 1b.

On the other hand, we formed several micro-cracked areas in the other large cell by the same mechanical method and made one large module from the micro-cracked large cell. The structure of the large module is composed of one large micro-cracked cell located between two EVA films and two soda-lime glasses with a size of 200 mm × 200 mm covering both top and bottom EVA films. However, the micro-cracked large module was not laminated during the experimental processes. Such a structure of un-laminated solar modules was examined and utilized for both PID stress and recovery tests in the works of Naumann et al. [64][73]. This is to easily separate the active solar cell from the EVA films for the analysis of other microstructural characteristics in PID-affected solar cells [102].

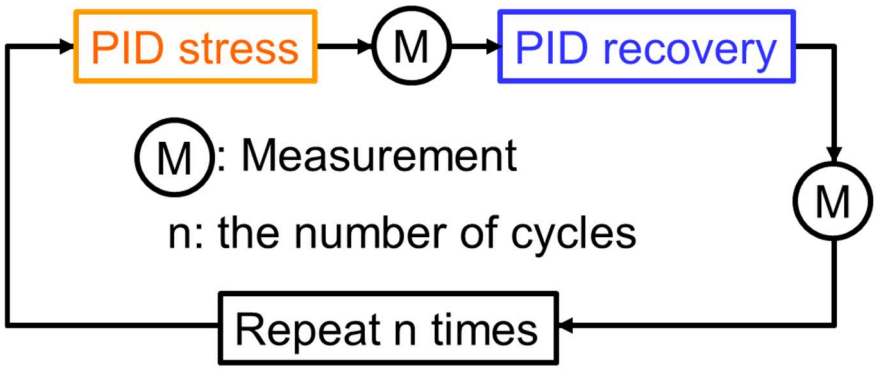

Figure 3. 2. The flow chart of the PID stress/recovery cycles.

A PID stress test of solar modules was carried out in a climatic chamber (LH-113, Espec Co.), as illustrated in Figure 3. 1a. Herein, an aluminum (Al) foil acts as the grounded frame of a solar module. The negative and positive terminals of the high voltage power source (PID insulation Tester, TOS721OS, Kikusui Electronics Co.) are connected to the two shortened leads and the grounded frame of a solar module, respectively. The mini-modules were subjected to PID stress tests with a duration of up to 96 h under a high voltage of 1000 V, a temperature of 85 ºC, a relative humidity (RH) of 85%. Meanwhile, the large module was subjected to a PID stress test with a duration of 150 h under a high voltage of 1000 V, a temperature of 65 ºC (<85 ºC to avoid the melting of EVA films), RH of 85%. PID recovery

tests were performed by biasing a reverse high voltage between a solar cell and the Al foil with a recovery duration of 72 h for mini-modules and 150 h for large solar modules. In this study, the cyclic PID stress tests with the same duration of 72 h for stress and recovery were also performed in eleven cycles for mini intact and micro-cracked solar modules, as shown in Figure 3. 2. It is noted that measurements were conducted immediately after cooling down to room temperature (25 ^{0}C).

3.2.2. The measurement of electrical characteristics of solar modules

EL and LIT images were taken by a THEsMOS-1100L (Hamamatsu Photonics K. K.) with the InGaAs camera before and after the PID stress and recovery processes with the applied current density of 10 mA/cm^2 at room temperature. Dark current–voltage (*I–V*) and illumination *J–V* curve characteristics of solar modules were measured by a solar simulator under standard test conditions (1 sun, AM 1.5, 25 °C). EQE responses were characterized by a CEP-2000RP (Bunkokeiki Co., Ltd.). Notably, to get acceptable measured results at local areas of the large micro-cracked solar module, measurements of the electrical characteristics and EQE responses at the micro-cracked region were made by using a shadow mask with a slot of 15 mm × 15 mm in size [102].

3.2.3. Microwave photo-conductance decay signal curves and carriers' effective lifetime

Microwave photo-conductance decay (μ-PCD) is a measurement method of the charge carrier's lifetime used in semiconductor. The measurement principle of the μ-PCD method is based on the temporal change of the microwave reflectivity, as illustrated in Figure 3. 3. A sample (semiconductor wafer) is irradiated by a laser (its energy over the energy bandgap of silicon), excess carriers in the sample are generated. Then, these excess carriers disappear by electron-

hole recombination within a time constant (carrier lifetime) which depends on the physical properties of the sample. The carrier lifetime is very sensitive to the presence of defects in the sample. A microwave antenna transmits an incident wavelength and receives a reflected microwave. In principle, μ-PCD uses the reflected microwave as a probe. The number of excess carriers increases by laser irradiation and then decreases due to recombination. This changes the conductivity of the sample, leading to the change of the microwave reflectivity. Herein, the microwave reflectivity of a sample is equivalent to the ratio between the reflected microwave intensity and the incident microwave intensity.

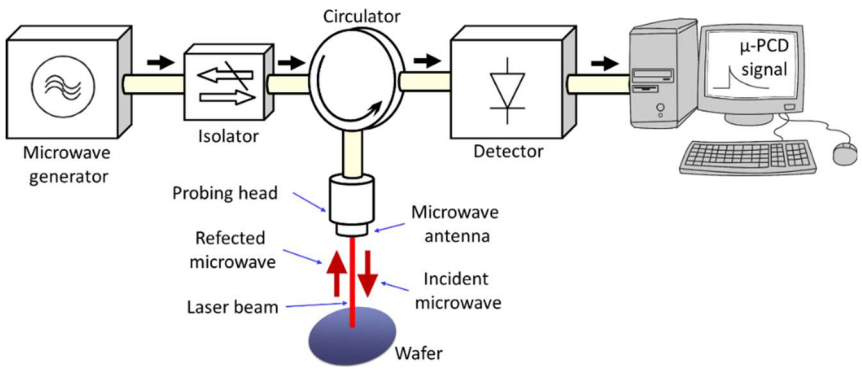

Figure 3. 3. A schematic diagram of the μ-PCD method.

In this work, the μ-PCD signal curves and τ_{eff} values of solar cells were directly measured by a commercially available μ-PCD measurement system (WT-1000B, Semilab Inc.). In the μ-PCD measurement system, excess carriers were generated by 200-ns-width pulsed light with the photon flux of 1.2×10^{13} $cm^{-2}s^{-1}$ from a 904 nm diode laser, and the penetration depth of the 904-nm-wavelength light is about 30 μm in Si. The microwave signal frequency within the range of 10 and 11 GHz depends on each sample to get the highest μ-PCD signal curves from the decayed minority carrier density. The μ-PCD measurement system could be used as a method that indicates the PID behavior of c-Si solar cells, as reported in some publications [103][104].

Generally, μ-PCD is utilized for wafer, but in this work, it was used for solar cells that have

an entirely different structure composed of a highly doped emitter, p-n junction, and bulk. The surface and bulk recombination coexist and affect each other in the measurement of the effective carrier's lifetime. The measured value of τ_{eff} with μ-PCD is contributed by the bulk lifetime (τ_{bulk}), the diffusion lifetime (τ_{diff}), and the lifetime of two surfaces (τ_{surf}). τ_{eff} values are estimated based on the μ-PCD signal curve, as illustrated in Figure 3. 4.

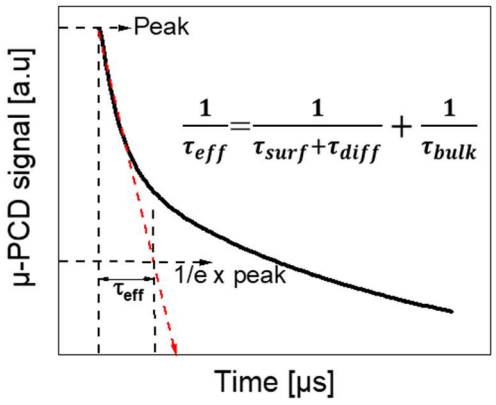

Figure 3. 4. An estimated effective lifetime based on the μ-PCD signal curve.

3.3. Results and discussion

3.3.1. The behavior of PID stress and recovery in micro-cracked large solar modules

Figure 3. 5 showed EL and LIT images of the micro-cracked large solar module before and after the PID stress for 150 h, and after the PID recovery for 75 h and 150 h. The micro-cracked large solar module is subjected to PID stress for 50 h, and 100 h had been reported in our previous work [102]. In this work, the PID-shunting defect extending at around the micro-cracked areas after PID duration of 150 h was also observed in the dark regions of EL images as well as the corresponding hot spots in LIT images. Notably, after PID recovery tests for 75 h and 150 h, PID recovery behavior was not seen in EL and LIT images. It seems that the risk of high voltage stress becomes more severe. Also, the dark areas in EL images appear at the

edges of the cell. Measurements of *J–V* characteristic curves and EQE responses were made at the micro-cracked region A marked by red-square in the EL images.

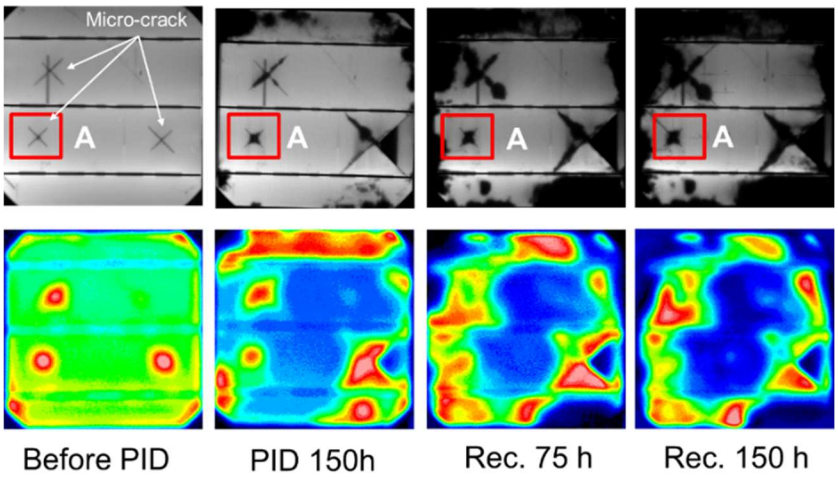

Figure 3. 5. EL (the top row) and LIT (the bottom row) images of large micro-cracked solar modules before and after PID stress and recovery processes.

Figure 3. 6a shows the relative losses of P_{max}, V_{oc}, FF, J_{sc}, and R_{sh} before and after PID stress and recovery processes. After a PID duration of 150 h, P_{max} degradation was 81.32% attributed to the losses of 47.71%, 58.15%, and 14.67% in V_{oc}, FF, and J_{sc}, respectively. Notably, the loss of electrical characteristics continued reducing even after the PID recovery process for 75 h and 150 h. The deterioration of P_{max}, V_{oc}, FF, and J_{sc} after the PID recovery process for 150 h was 86.66%, 56.77%, 61.06%, and 20.74%, respectively.

Furthermore, EQE response was lost in the full wavelength range of 400 nm to 1100 nm after a PID duration of 150 h, but it was not recovered after the PID recovery process for 75 h and 150 h, as shown in Figure 3. 6b. The PID effect occurring at micro-cracked areas is due to PID shunting caused by the decoration of sodium (Na^+) ions on the across-section site of micro-cracks [102]. It is the crucial PID effect related to micro-cracks in p-type c-Si solar cells, which mainly causes the degradation of V_{oc} and FF. This effect is confirmed by the R_{sh} reduction of 99.31% measured at the micro-cracked region A after a PID duration of 150 h. However, R_{sh}

is not recovered after the PID recovery process for 150 h. Also shown in Figure 3. 6c, R_s increased 56.96% after PID duration of 150 h and even continued increasing 158.23% after PID recovery duration of 150 h. The elevated humidity within the package of the un-laminated solar module associated with acetic acid formation from the encapsulation layer [105][25] under the high applied voltage bias causes electrolytic corrosion mainly at micro-cracked areas and the cell edge of the solar module [48][39]. Electrolytic corrosion causes the R_s increase, leading to the reduction of FF and J_{sc} at the micro-cracked region after both PID stress and recovery processes. This phenomenon also explains why dark areas appeared at the edges of the module in EL images. Furthermore, corrosion and dissolution of cell metallization due to electrochemical reactions at micro-cracked regions under the high voltage stress combined with damp-heat stress [20] are also considered as other causes for the performance degradation after the PID recovery process.

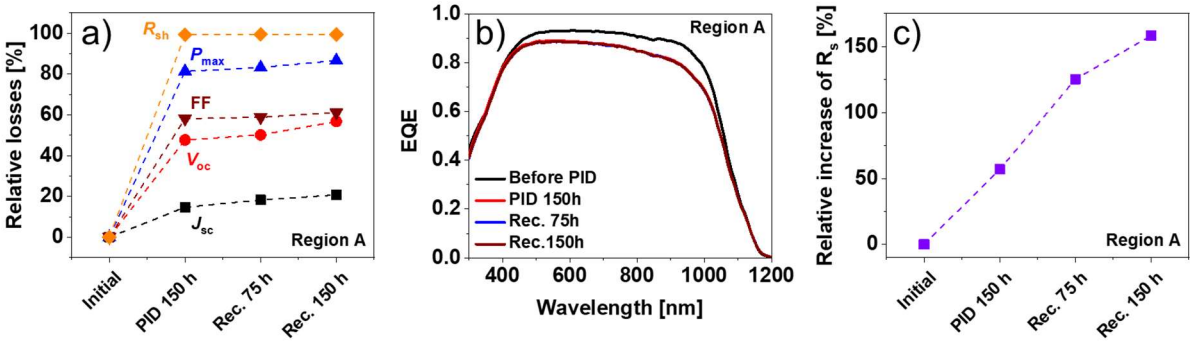

Figure 3. 6. a) Relative losses of electrical characteristics, b) EQE responses and c) relative increase of R_s at the micro-cracked region A shown in Fig. 2 before and after PID stress and recovery processes.

Likewise, we predicted that the elevated humidity at micro-cracked areas causes the increase of the surface conductivity on the cross-section site of micro-cracks. Under a high voltage bias combined with the high conductivity condition, Na^+ ions with high concentration could drift/diffuse into the deep inside of the micro-cracked areas. So, it is difficult for a reverse

voltage bias to push Na^+ ions out of micro-cracks during the PID recovery process. However, explicit evidence from further investigations should be essential to clarify this hypothesis. Thus, the PID recovery is a big problem for the PID-affected un-laminated solar module, especially, at micro-cracked areas and the edges. The un-laminated solar module is convenient for microscopic analysis but adverse for PID recovery tests.

3.3.2. The behavior of PID stress and recovery in intact and micro-cracked mini solar modules

The comparison of PID stress and recovery behavior between mini micro-cracked and intact solar modules was observed through EL images, as shown in Figure 3. 7. The dark region in the micro-cracked solar cell was found mainly at the micro-cracked position and expended to nearby locations after a PID duration of 48 h and 72 h, respectively. Meanwhile, the dark region in the intact solar cell slightly changed mainly in the vicinity of the bus-bar after PID duration of 48 h, and in the added corner area after 72 h.

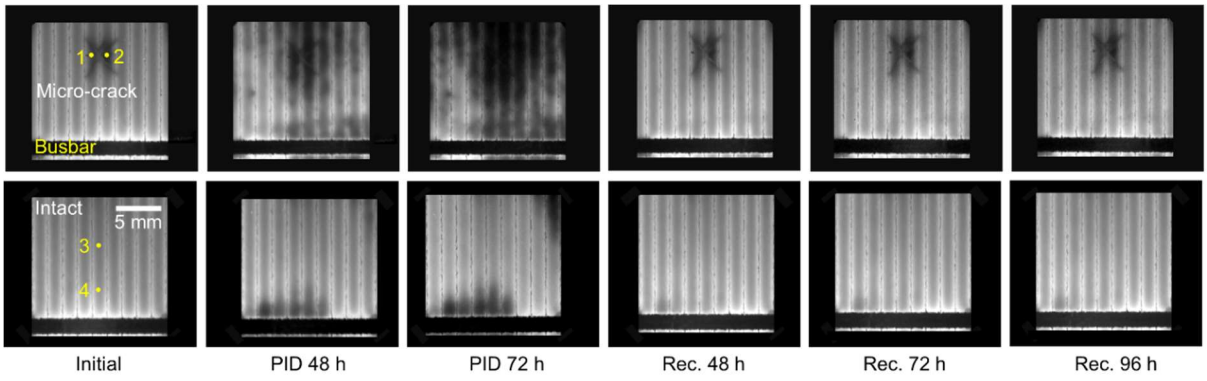

Figure 3. 7. EL images of mini intact and micro-cracked solar modules before and after PID stress and recovery processes. Note that points 1 and 2 (at the micro-cracked region) and points 3 and 4 (at the intact area) were marked for measurement of the effective carrier's lifetime.

So, it could be seen that PID behavior occurs more severely at micro-cracked locations. The

obtained results indicated that micro-cracks play a critical role in PID behavior, which is in good agreement with our previous work [102]. It is worth noting that the dark areas in the EL images of both mini solar cells disappeared after the PID recovery process. Thus, PID recovery could be performed well in both mini micro-cracked and intact modules.

Figure 3. 8 shows one-sun illumination *J–V* curves of six intact and micro-cracked solar modules before and after PID stress and recovery processes. It is observed that the deterioration level of electrical characteristics after the PID stress process in the micro-cracked modules was much more significant than that in the intact modules. The deterioration of electrical characteristics in the mini micro-cracked modules, which was contributed by the losses of not only V_{oc}, FF, but also J_{sc}, is similar to the PID behavior at the micro-cracked areas of the before-mentioned large module. This result is also in good agreement with the achieved results of our previous work [102]. Notably, electrical characteristics in the PID-affected intact and micro-cracked modules were recovered well.

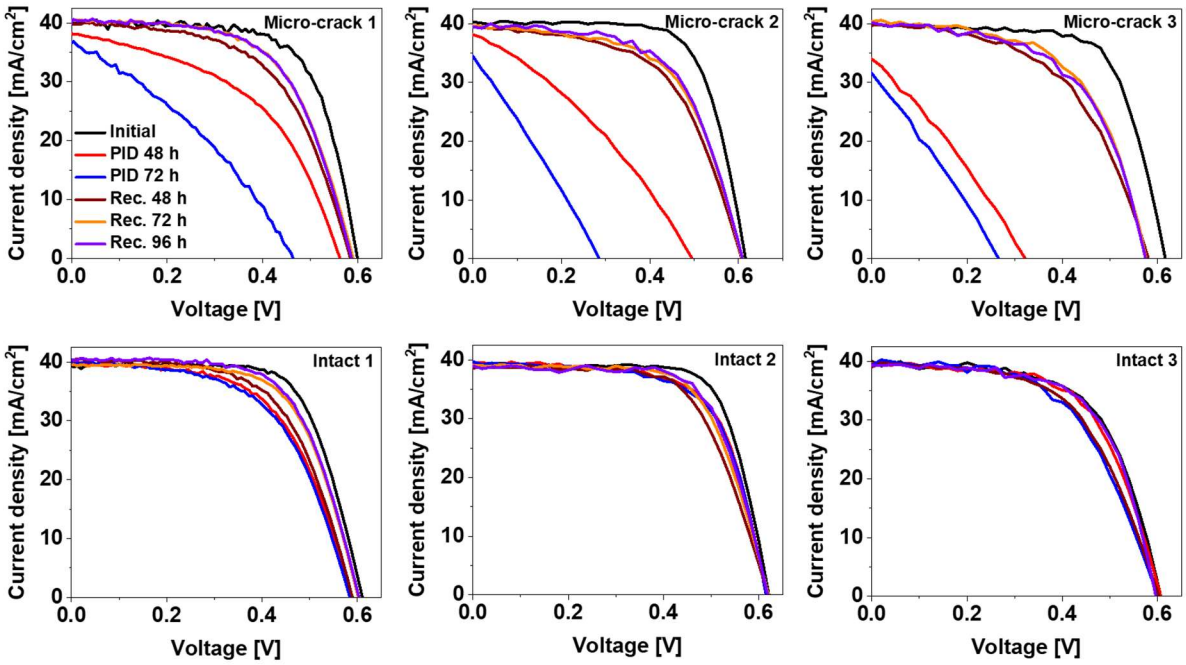

Figure 3. 8. One-sun illumination J–V curves of the intact and micro-cracked solar modules before and after PID stress and recovery processes.

Electrical characteristics of solar cells, including P_{max}, V_{oc}, FF, and J_{sc}, were extracted from the above one-sun illumination J–V curves and averaged in three samples in each case for intact and micro-cracked modules. Meanwhile, R_{sh} was estimated according to the equivalent circuit of the double diode model for the slope of the dark I–V curve at $V = 0$ [106] and also averaged in three corresponding samples. Figure 3. 9 compares the averaged relative losses of P_{max}, V_{oc}, FF, J_{sc}, and R_{sh} between the intact modules and the micro-cracked modules before and after PID tress and recovery processes.

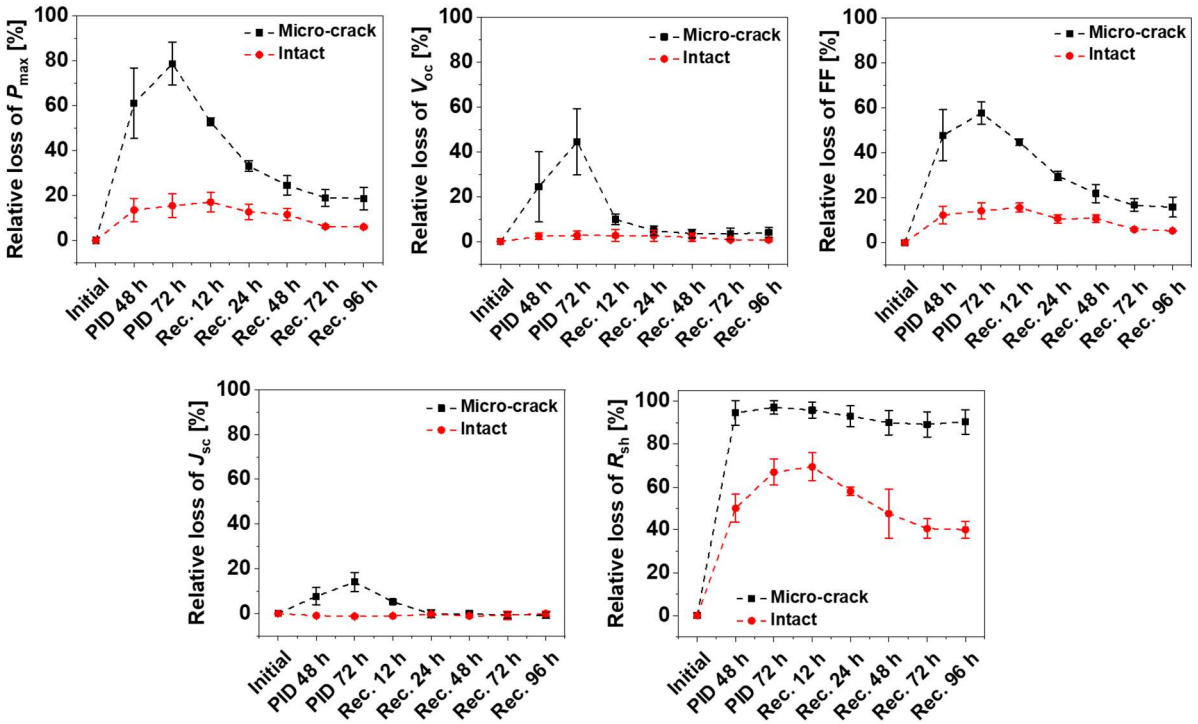

Figure 3. 9. Comparison of relative losses of P_{max}, V_{oc}, FF, J_{sc}, and R_{sh} in tested solar modules micro-cracks before and after PID stress and recovery processes.

In the micro-cracked modules, P_{max} severely deteriorates by 78.68 % after the PID stress duration of 72 h, which was attributed to a V_{oc} loss of 44.51 %, FF loss of 57.74 %, and J_{sc} loss of 14.08 %. All electrical characteristics regenerated significantly but incompletely by the PID recovery process of 72 h, which have relative losses of 18.97 %, 3.41 %, 16.67 %, and 0.64 % in P_{max}, V_{oc}, FF, and J_{sc}, respectively. The change of all electrical characteristics is negligible

even after the PID recovery process up to 96 h, with relative losses of 18.63 %, 4.03%, 15.81%, and 0.71% in P_{max}, V_{oc}, FF, and J_{sc}, respectively. Also shown in Figure 3. 9, PID recovery behavior occurs quickly at an early stage. The performances gradually improve by the time and eventually saturates regardless of the increasing PID recovery duration. In the intact modules, P_{max} reduces by 15.43 % contributed by degradations of 2.78 % and 14.15 % in V_{oc} and FF after PID stress duration of 72 h, respectively. The relative losses in P_{max}, V_{oc}, and FF are 6.15 %, 0.84 %, and 5.92 % after the PID recovery duration of 72 h, and 5.98 %, 0.72 %, and 5.28 % after the PID recovery duration of 96 h, respectively. Thus, the PID recovery was accomplished well but incompletely as well. After the PID stress process of 72 h, the R_{sh} relative loss of approximately 100% in the micro-cracked modules is more severe compared with the R_{sh} relative loss (66.94%) in the intact modules. After the PID recovery process of 72 h even 96 h, R_{sh} regenerated slightly (the R_{sh} relative loss of 90.41%) in the micro-cracked modules, while R_{sh} in the intact modules was recovered more significantly (the R_{sh} relative loss of 44.09%). This is because the decoration of Na ions in micro-cracks is more severe than that in other crystal defects (dominant stacking faults), so it is more difficult for Na ions to diffuse out of micro-cracks compared with other crystal defects. However, the incomplete regeneration of R_{sh} in micro-cracked even intact modules due to the PID recovery process is good agreement with the literature [73]. This observation revealed that the PID-affected level in the micro-cracked solar modules is more severe than that in the intact ones. Possibly, only a specific portion of Na^+ ions was diffused out of shunted regions such as stacking faults and micro-cracks after the PID recovery. Therefore, the R_{sh} regeneration in the intact and micro-cracked modules after the PID recovery is incomplete regardless of increasing the PID recovery duration, leading to their non-full PID recovery behavior.

Furthermore, the comparison of EQE responses before and after PID stress and recovery processes between intact module no. 1 (intact 1) and micro-cracked module no.1 (micro-crack

1) was indicated in Figure 3. 10. It is noted that the EQE response in the micro-cracked area of the mini micro-cracked solar module after PID stress of 72 h is noisy because of the EQE scaling error when measuring severely shunted cells, as demonstrated in the literature [75]. It could be seen that the EQE response in the intact module shows no change before and after PID stress and recovery processes. This observation indicates that only the electrical shunt path influences the performance degradation due to PID in p-type c-Si solar cells without micro-cracks, as investigated in works [50][66][67]. It is also important to mention that the EQE response in the micro-cracked modules dropped significantly after the PID stress process but was almost completely recovered. The loss of the EQE response after PID stress revealed that micro-cracked areas decorated by Na ions act as recombination centers. Possibly, the EQE regeneration caused by the PID recovery process is due to the Na-ion out-diffusion from micro-cracked areas under high applied reverse voltage. The decrease and increase of the EQE response cause degradation and regeneration of V_{oc} and J_{sc} after PID stress and recovery processes, respectively.

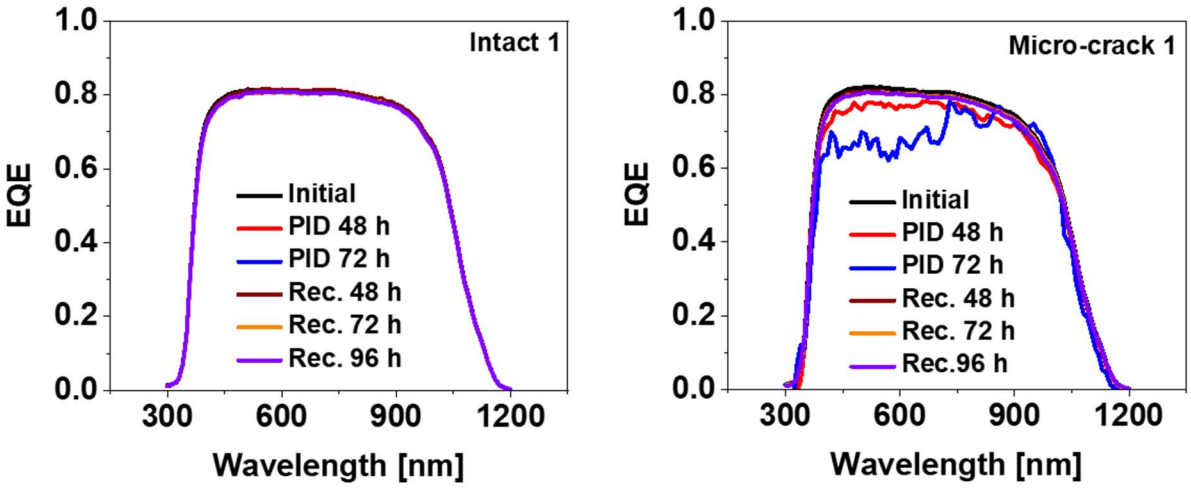

Figure 3. 10. EQE response behavior of intact and micro-cracked solar modules before and after PID stress and recovery processes.

The μ-PCD signal and the τ_{eff} value were measured at two points (1 & 2) for the micro-cracked region of each micro-cracked module, at two points (3 & 4) for the intact region of

each intact module. Herein, four points from 1 to 4 were marked in Figure 3. 7. Figure 3. 11a, and b show the μ-PCD signal for the intact module no.1 (intact 1) and the micro-cracked module no. 1 (micro-crack 1), respectively. It is observed that the μ-PCD signals, including rapid and slow time constant decay components, in both cases, presented faster decay profile after the PID stress process. However, the reduction level of the μ-PCD signal for the micro-cracked module is much more significant than that for the intact module after the PID stress process. Also, the μ-PCD signal due to the PID recovery process for the intact module was almost completely regenerated while that for the micro-cracked module was retrieved incompletely.

Table 3. 1. Average τ_{eff} values at the intact and micro-cracked positions before and after the PID stress and recovery processes.

	Averaged effective carrier's lifetime τ_{eff} [μs]	
	At the intact position	At the micro-cracked position
Initial	11.53 ± 0.47	12.10 ± 0.19
PID 48 h	11.04 ± 0.62	4.67 ± 1.27
PID 72 h	10.42 ± 0.47	2.91 ± 0.97
Rec. 48 h	11.07 ± 0.47	9.52 ± 0.62
Rec. 72 h	11.24 ± 0.43	10.15 ± 0.49
Rec. 96 h	11.35 ± 0.37	10.26 ± 0.46

In each case, the τ_{eff} values were averaged in three modules and listed in Table 3. 1. The average τ_{eff} relative losses at the intact and micro-cracked positions after the PID stress and recovery processes were presented in Figure 3. 11c. The average τ_{eff} reduction in the intact

modules is suspected to be influenced by the Na-decorated stacking faults, which act as shunting defects across the p-n junction. However, the τ_{eff} loss in the micro-cracked modules is thought to be due to both shunting defects and additional recombination centers at the micro-cracked areas. After the PID recovery process, the τ_{eff} value in both cases was regenerated effectively but did not reach the original value, in particular, for the micro-cracked modules. The out-diffusion of Na^+ ions from micro-cracked areas, resulting in the suppression of carrier recombination, could be considered a possibility which regenerates the τ_{eff} value. However, the minimizing of carrier recombination centers is not efficient enough to fully recover the τ_{eff} value at micro-cracked areas. It could be seen the τ_{eff} degradation and regeneration behavior at the micro-cracked positions is a good correlation with the solar module performance behavior of the micro-cracked module before and after the PID stress and recovery processes. It is supposed that the μ-PCD response and the τ_{eff} value act as indicators to examine the electrical characteristics of solar modules before and after PID stress and recovery processes for solar modules with and without micro-cracks.

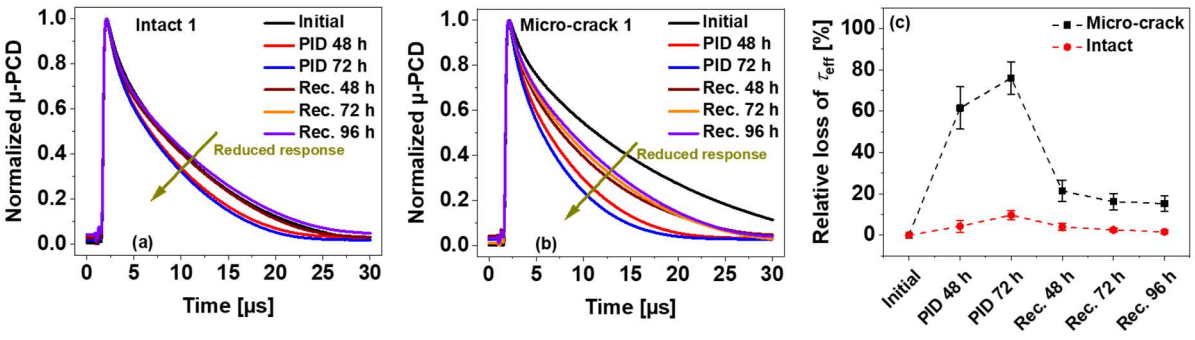

Figure 3. 11. Normalized μ-PCD responses of the intact and micro-cracked solar modules (a, b), and τ_{eff} relative losses at the intact and micro-cracked areas (c) before and after the PID stress and recovery processes.

3.3.3. The degradation and regeneration behavior of micro-cracked mini-modules due to the PID effect after PID stress/recovery cycles

Biasing high negative potential will result in the performance loss, whereas applying high positive potential will regenerate the module performances partially. The PID stress/recovery cycles are an essential first step to examine the cyclic PID behavior of the solar modules and to choose the best scenario for degradation and recovery. Three principle rate scenarios for solar modules after the PID stress/recovery cycles could be conducted by Pingel [107], as illustrated in Figure 3. 12.

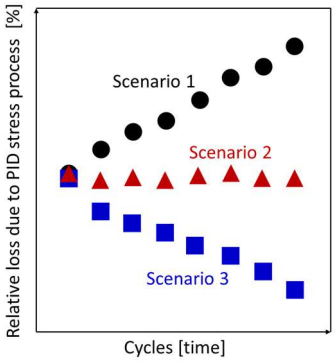

Figure 3. 12. Three scenarios resulting from the PID stress/recovery cycles.

Firstly, the regeneration rate of the PID recovery process is slower than the degradation rate of the PID stress process, i.e. the relative loss of electrical characteristics due to the PID stress process tends to increase after cyclic PID stress/recovery tests. In this scenario, the solar modules are susceptible to PID. Secondly, the regeneration rate of the PID recovery process is similar to the degradation rate of the PID stress process, i.e. the relative loss of electrical characteristics due to the PID stress process tends to be stable after cyclic PID stress/recovery tests. Herein, the PID effect is stable over PID stress/recovery cycles. Thirdly, the regeneration rate of the PID recovery process is faster than the degradation rate of the PID stress process,

i.e. the relative loss of electrical characteristics due to the PID stress process tends to decrease after cyclic PID stress/recovery tests. In this case, the performance of the PID-affected solar module will increase over time, which is the best scenario for the solar modules to control the PID effect.

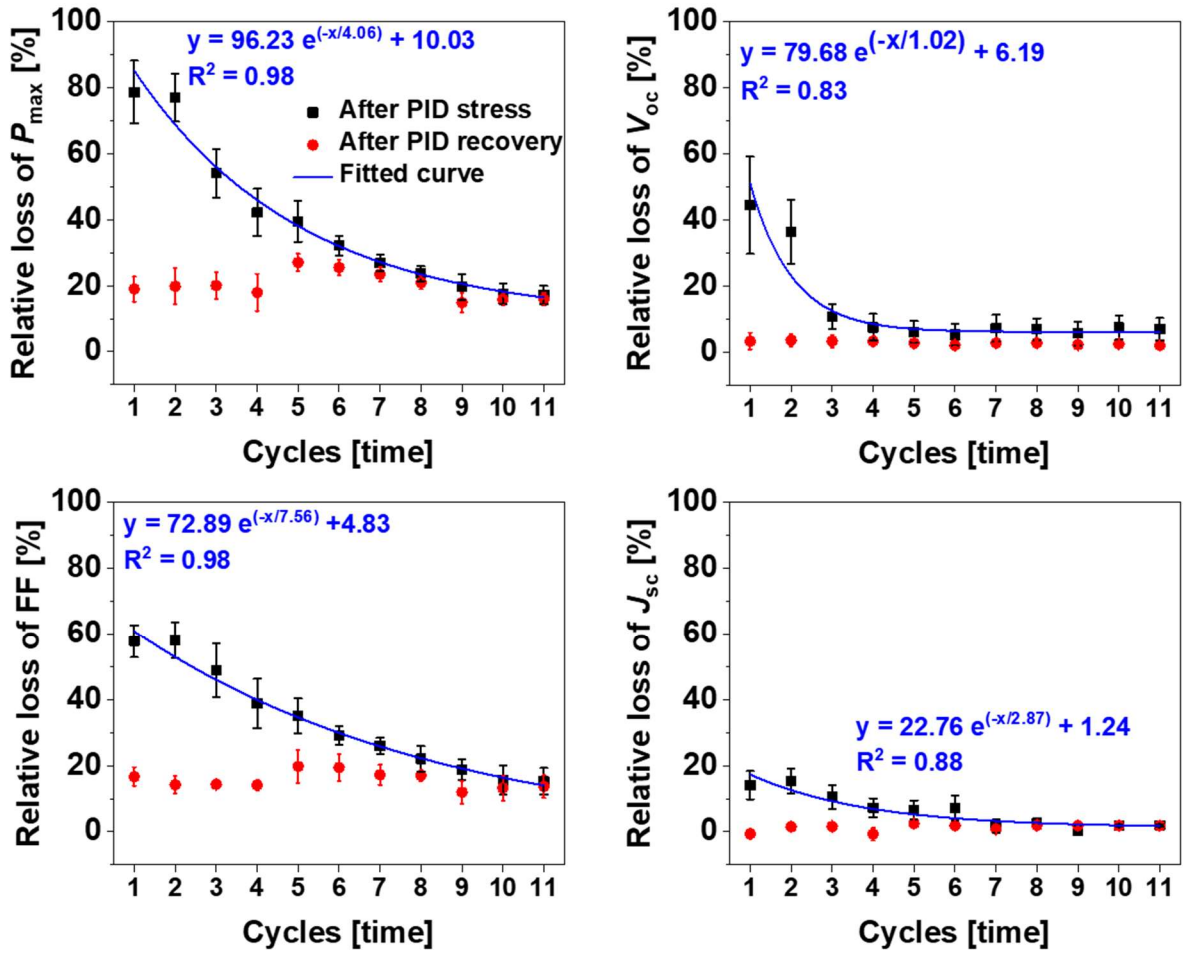

Figure 3. 13. The degradation and regeneration behavior of electrical characteristics for the micro-cracked solar module over eleven PID stress and recovery cycles.

Figure 3. 13 shows the degradation and regeneration behavior due to the PID effect for the micro-cracked solar modules over eleven PID stress/recovery cycles. The values of electrical characteristics were averaged in three modules. Herein, the relative losses of the average electrical characteristics were calculated by their initial values (before PID stress). Although the deterioration caused by the PID effect related to micro-cracks is severe, the relative losses

of P_{max}, V_{oc}, FF, and J_{sc} due to the PID stress process tends to decrease gradually and stable after stress/recovery cycles. The stable relative losses of P_{max}, V_{oc}, FF, and J_{sc} due to the PID stress process after nine PID stress/recovery cycles are 19.65%, 5.77%, 18.87%, and 0.44%, respectively. The above findings are likely because of the following reason. With an appropriate PID recovery duration, the penetration of Na ions into the cell active layer and then crystal defects (micro-cracks…) due to the PID test process is reduced gradually after each test cycle. This eliminates the PID effect gradually after each test cycle. However, its detailed mechanism needs further investigations.

Meanwhile, the regeneration of P_{max}, V_{oc}, FF, and J_{sc} due to the PID recovery process is incomplete but relatively stable after each stress/recovery cycle. Also, the stable relative losses of P_{max}, V_{oc}, FF, and J_{sc} due to the PID recovery process after nine PID stress/recovery cycles are 14.89%, 2.31%, 11.95%, and 1.86%, respectively. In this work, the PID stress and recovery processes have a similar duration; the performance loss of tested solar modules tends to subside after the PID stress/recovery cycles. This result coincides with the third scenario and then the second scenario above. It is evidence to believe that the performance degradation of intact or micro-cracked solar modules due to PID could be controlled after PID stress/recovery cycles. It is noted that this scenario was activated by the electrical recovery method but not triggered by temperature even for intact modules [108].

It was observed that the relative losses of P_{max}, V_{oc}, FF, and J_{sc} due to the PID stress process decreases with increasing the number of PID stress/recovery cycles. However, the correlation between the relative losses of P_{max}, V_{oc}, FF, and J_{sc} due to the PID stress process and the number of PID stress/recovery cycles has not been revealed. In this work, the authors investigated the correlation based on an exponential decreasing model:

$$y = A_0 e^{(-x/\tau)} + y_0 \tag{3.1}$$

where A_0, x, y, and τ parameters are amplitude, cycle number, the relative loss of electrical characteristics, and exponential time constant, respectively. The fitted curves of the relative losses of P_{max}, V_{oc}, FF, and J_{sc} due to the PID stress process versus the number of the PID stress/recovery cycles, as illustrated in the fitted curves of Figure 3. 13. As listed in Table 3. 2, although the fitted coefficients (R^2) of determination in the cases of V_{oc} and J_{sc} are lower than that in the cases of P_{max}, FF, generally, R^2 for each case is relatively highly correlated.

Table 3. 2. Fitted parameters for the exponential decreasing model of relative losses.

$y = A_0e^{(-x/\tau)} + y_0$					
Relative loss (%)	**A_0 (%)**	**τ**	**y_0 (%)**	**Decreasing rate ($\lambda = 1/\tau$)**	**Fitted coefficient (R^2)**
P_{max}	96.23	4.06	10.03	0.25	0.98
V_{oc}	79.68	1.02	6.19	0.98	0.83
FF	72.89	7.56	4.83	0.13	0.98
J_{sc}	22.76	2.87	1.24	0.35	0.88

This finding verifies that the relationship of the relative losses of P_{max}, V_{oc}, FF, and J_{sc} due to the PID stress process and the number of the PID stress/recovery cycles actively complies with an exponentially decreasing function. According to the exponential model, the relative losses of P_{max}, V_{oc}, FF, and J_{sc} due to the PID stress process could reach to the critical points of 10.03 %, 6.19 %, 4.83 %, and 1.24 % after a certain number of the PID stress/recovery cycles, respectively. The critical point (10.03 %) of the P_{max} relative losses coincides with the experimental result in the literature [107], which reported power regeneration to over 90% after PID stress/recovery cycles in a time frame of several years. Thus, the cyclic PID test could

prevent solar modules from the PID effect significantly. Remarkably, the decreasing rate (0.98) of the V_{oc} relative loss is the highest, i.e., the V_{oc} regeneration rate is the fastest. Whether the cyclic PID test method is a feasible solution for minimizing the PID effect, it depends on relevant factors such as PID duration, PID recovery duration, the number of PID stress/recovery cycles, temperature, humidity, etc. Further investigations of the cyclic PID test will realize a more stable performance, even receiving PID conditions.

3.4. Conclusions

This work demonstrated that the PID shunting path due to the decoration of Na^+ ions at the micro-cracked areas acts as the primary PID mechanism causing the losses of V_{oc} and FF for p-type c-Si solar modules. The micro-cracked regions are also supposed as the additional recombination centers, leading to the reduction of J_{sc} and V_{oc} of solar modules after PID stresses. Furthermore, the PID recovery possibility is difficult to achieve by biasing a high reverse voltage for un-laminated solar cells regardless of with or without micro-cracks, even the more significant degradation due to the high voltage stress. However, the PID recovery has been made significantly but incompletely for both laminated intact and micro-cracked solar cells by the same PID recovery method above. The average loss of P_{max} is about 78.68 % after a PID stress duration of 72 h, but it is 18.97% and 18.63% after a PID recovery duration of 72 h and 96 h, respectively. The authors supposed that the PID recovery behavior occurs quickly at an early stage then subsides after time and eventually saturates regardless of increasing PID recovery duration. The incomplete recovery behavior of PID-affected solar cells is attributed to the incomplete recovery of R_{sh} and FF. The degradation and regeneration of the τ_{eff} value are a function of the PID stress and recovery processes. The μ-PCD response also plays a critical role in indicating the PID effect due to micro-cracks of solar cells. Finally, this work also performed the cyclic PID tests for 11 cycles with the same stress/recovery duration of 72 h. The achieved results showed the decreasing tendency of the loss of electrical characteristics

due to the PID stress process after PID degradation/recovery cycles. Notably, the correlation between the relative losses of P_{max}, V_{oc}, FF, and J_{sc} due to the PID stress process and the number of the PID stress/recovery cycles was modeled by the exponential decreasing function. This model revealed that the cyclic PID test method could maintain P_{max} of solar cells up to 90% (as shown in Table 3. 2) in solar cells after a long time of several years. Thus, the cyclic PID test method can suppress/reduce PID behavior effectively. Therefore, we suggest that the cyclic PID test with suitable conditions might be an easy and cost-effective way to control the PID effect.

Chapter 4 | The PID delay effect of UV light

4.1. Introduction

Outdoor-installed solar modules are subjected to harsh conditions such as high temperature, moisture, electrical and mechanical stress, and UV light radiation during their lifetime. Therein, the UV light is one of the critical candidates, which causes the aging of solar cells, resulting in the degradation of solar modules. This is because the UV light gradually deteriorates the quality of the encapsulating layer of solar modules made from polymeric materials over time. Notably, the UV light with wavelength ranges of 320-400 nm (UVA) and 280-320 nm (UVB) existing in the sunlight is responsible for the deterioration [16]. Furthermore, UV light irradiation, along with a high temperature of more than 50 ^{o}C, resulted in the EVA discoloration degradation [17]. Also, UV light irradiation combined with damp-heat (DH) conditions induced acetic acid in solar modules, which causes the corrosion effect on Ag electrodes, leading to the acceleration of the PV power degradation [24].

As well known, PID causes the reduction of PV reliability and stability. Currently, the conventional indoor PID stress tests with conditions, such as high temperature, humidity, and voltage, have been conducted to examine the PV performance due to the PID behavior. However, the actual PID effect occurring in outdoor installed modules should be affected by not only high temperature, humidity, and high voltage but also the UV light radiation. So far, few works utilized the UV light irradiation in the conventional indoor PID tests combined with the DH tests. Notably, several publications reported that light radiation could slow down the PID effect [109][56][110]. Therein, Masuda and Hara, furthermore, highlighted that only UV light irradiation of wavelengths shorter than 400 nm during PID stress tests could induce the PID delay effect. Inversely, Koentopp *et al*. reported that light radiation on solar cells before the PID test could accelerate the PID susceptibility of the solar cells. However, the PID

recovery rate is not affected [60]. As such, conclusions of previous works on the UV light effect for different PID phenomena are still contentious. Therefore, further research on the influence of UV light irradiation on PID as well as its mechanism need to be conducted.

This work presents and discusses the PID delay effect by UV light irradiation during the PID test for p-type c-Si solar modules in detail. EL images and *J–V* characteristics were utilized to confirm these findings. The μ-PCD technique was used to estimate τ_{eff} values as well as rapid (τ_1) and slow (τ_2) decay time constants, and to monitor performance deterioration induced by PID test. Besides, the conductivity measurements of the SiN_x thin films in the cases of light irradiation with various wavelengths and no-light irradiation were also conducted to prove the conductivity increase of the SiN_x thin films with UV light irradiation during PID tests, which relates to the mechanism causing the PID delay effect for p-type c-Si solar cells.

4.2. Experimental procedure

4.2.1. PID tests and characteristics measurements of solar modules before and after PID tests

To examine the PID delay effect during the PID test, commercial square p-type single c-Si solar cells with a size of 30 mm × 30 mm and a thickness of 200 μm were utilized in this work. The top-to-bottom structure of single-solar module as shown in Figure 4. 1a consists of the following: a semi-tempered cover glass with the size of 60 mm × 60 mm and the thickness of 3.2 mm, two sheets of a fast-cure-type EVA encapsulant of 450-μm thickness, one aforementioned solar cell between two EVA sheets, and a back sheet composed of PVF of 38 μm/PET of 250 μm/ PVF of 38 μm. Lamination was carried out at 135 °C for 20 min using a vacuum laminator. The edges of the solar module were covered by aluminum (Al) foil, which

acts as an Al frame, as illustrated in Figure 4. 1b.

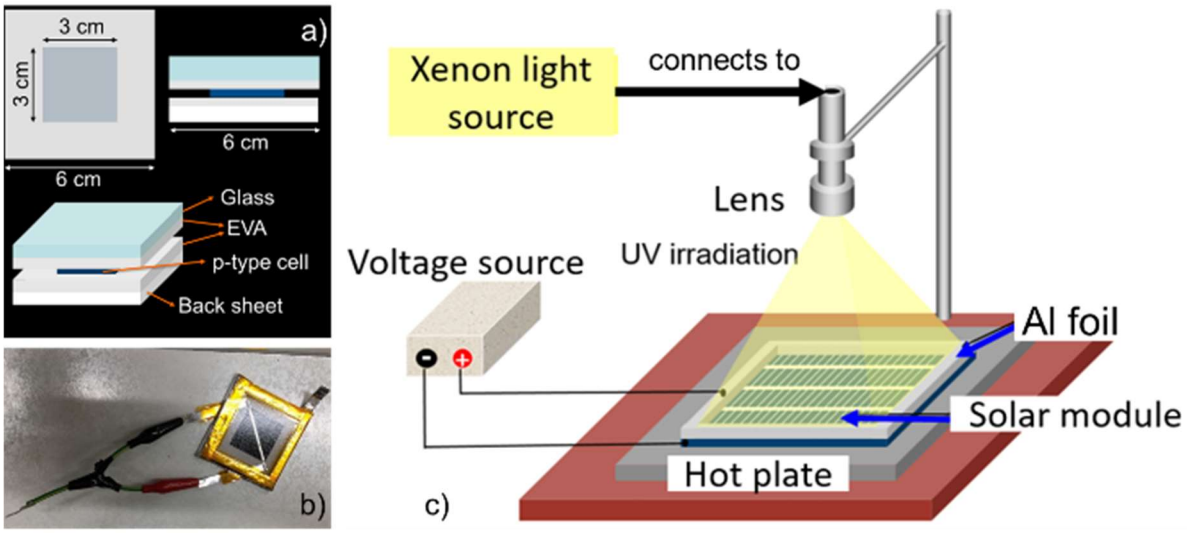

Figure 4. 1. a) The structure of the solar module, b) the solar module with edge covered by an Al foil, c) the light-PID test system.

Meanwhile, Figure 4. 1c shows a light-PID test system by which PID tests with light irradiation were performed. A high negative voltage of -1000 V was applied between shorted electrodes of the solar module and the grounded Al frame. PID test temperature was controlled at 85 ºC by a hot plate. Relative humidity (RH) during the PID test was controlled below 60 % in all experiments. Monochromatic UV and visible lights irradiated by a xenon lamp with the aid of band-pass filters through the lens were divided into two groups: group 1 (UV-light) including wavelengths of 300 nm, 320 nm, 370 nm, and 390 nm, and group 2 (visible light) including wavelengths of 460 nm and 500 nm. The full width at half maximum (FWHM) of the transmission for each filter was 10 nm. Because our purpose is to investigate the correlation between the PID delay effect level and the wavelength of UV light irradiation, so we utilized different wavelengths and fixed the same photon flux in every wavelength. The similar photon flux of 9.26×10^{14} $cm^{-2}s^{-1}$ for the irradiated UV and visible lights, which corresponds to power densities of 613 $\mu W/cm^2$ (0.8 SUN), 575 $\mu W/cm^2$ (0.65 SUN), 497 $\mu W/cm^2$ (0.4 SUN), 472 $\mu W/cm^2$ (0.32 SUN), 400 $\mu W/cm^2$ (0.31 SUN) and 368 $\mu W/cm^2$ (0.31 SUN) for wavelengths

of 300 nm, 320 nm, 370 nm, 390 nm, 460 nm and 500 nm, were subjected, respectively. As discussed in the literature [110], they addressed that the PID delay occurred when the UV light intensity more than 0.3 SUN was irradiated, but 0.3 SUN case has almost similar delay effect with the 1.0 SUN case. So, the photon flux of 9.26×10^{14} $cm^{-2}s^{-1}$ for the irradiated UV and visible lights is suitable to induce the PID delay effect.

Each PID test with and without light irradiation of different wavelengths was carried out twice in two different samples, so fourteen solar modules were prepared for all PID stress tests with the whole test duration up to 24 h (7 modules/experiment chain). A solar simulator measured *J–V* curve characteristics before and after the PID tests under standard test conditions (1 sun, AM 1.5, 25°C). EL images were also taken by a THEMOS-1100L (Hamamatsu Photonics K. K.) measurement system before and after the PID tests with the applied current density of 10 mA/cm^2. In particular, τ_{eff} values, lifetime constants τ_1 and τ_2 were extracted from the μ-PCD signal curves before and after the PID tests, which were characterized by a commercially available μ-PCD measurement system from Semilab (WT-1000B). The components of the μ-PCD signal curves can be utilized as an indicator of PID for p-and n-type c-Si solar cells, as reported in the works of Islam *et al.* [111] and Ishikawa *et al.* [112].

4.2.2. Conductivity measurement of SiN_x thin films under UV and visible light irradiation

A SiN_x layer known as an ARC has a significant influence on the PID resistance of p-type c-Si solar cells. This could be obtained by increasing the refractive index (i.e., increase Si/N ratio) during the deposition process [43] [113] [62]. It could be explained that decreasing resistivity or increasing conductivity of the SiN_x layer causes a low electric field across SiN_x, leading smaller Na ions to drift across SiN_x, and then avoiding PID [114]. Investigating the influence of UV light on the change in the SiN_x properties is necessary for this work. To clarify

the mechanism of the PID delay effect by UV light irradiation during the PID test, research on conductivity change in SiN_x thin films under the UV light was carried out. In this work, three SiN_x thin film samples with different refractive indexes (*n*) were deposited by a plasma-enhanced chemical vapor deposition (PE-CVD) method. These samples were fabricated in Toyota Technology Institute, Japan, by Prof. Kyotaro Nakamura. The specific deposition conditions, electrical and optical characteristics of the SiN_x thin films are shown in Table 1.

Table 1. Deposition conditions, electrical and optical characteristics of SiN_x thin films.

Refractive index, *n*	**SiH_4 (sccm)**	**NH_3 (sccm)**	**N_2 (sccm)**	**Deposition time (s)**	**Thickness (nm)**	**Band gap (eV)**	**Dark conductivity (pS/cm)**
1.95	20	140	135	285	91.8	3.56	0.37
2.12	39	120	135	285	86.6	3.18	0.23
2.20	44	110	135	285	85.7	2.97	0.48

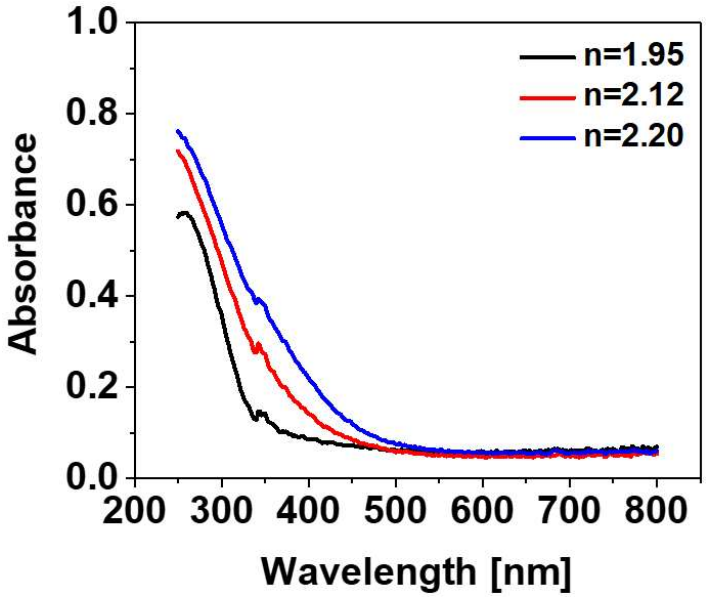

Figure 4. 2. The absorption spectra of SiN_x thin films with various refractive indexes.

The Si/N ratio (not shown here) of the utilized SiN_x thin films was controlled by SiH_4 and NH_3 flow rates. Herein, the refractive index estimated at a 600-nm wavelength (λ) was measured by a spectroscopic ellipsometer (Horiba Jobin Yvon Uvisel, HORIBA, Ltd.; 190 nm < λ < 2100 nm) for all samples. The absorption spectra of the SiN_x thin films were measured by optical spectroscopy (V-570, Jasco Corp.). The bandgap of the SiN_x thin films with different refractive indexes was estimated based on the absorption edge, as shown in Figure 4. 2.

The conductivity of the SiN_x thin films with and without light irradiation was estimated by a two-probe measurement with the applied voltage of 40 V, which allows evaluating SiN_x to act as conductive materials. The utilized UV and visible light wavelengths were 300 nm, 320 nm, 370 nm, 390 nm, 460 nm, and 500 nm with 10-nm FWHM. The photon flux was controlled to be a similar value around 9.26×10^{14} $cm^{-2}s^{-1}$. During the conductivity measurement at room temperature, SiN_x thin films were placed in a vacuum chamber with a pressure of 2.3×10^{-2} Pa, which avoids the conductivity change in SiN_x owing to possible current leak through the adsorbed moisture on the surface.

4.2.3. The rapid and slow time constant decay components

In this chapter, the μ-PCD signal curves were also measured by a commercially available μ-PCD measurement system (WT-1000B, Semilab Inc.). So far, it has been shown that the μ-PCD signal curves in various semiconductor materials can be described with several components [115][116][117][118]. A standard μ-PCD signal curve consists of two following primary components, including rapid and slow time constant decay components. In this work, the μ-PCD signal curve, as shown in Figure 4. 3, was normalized by the peak value with the aim of comparison of the rapid and slow decay components before and after PID tests. The μ-PCD signal curve is expressed by the double-exponential function below:

$$\Delta A = A_1 \exp(-t/\tau_1) + A_2 \exp(-t/\tau_2), \quad (4.1)$$

where A_1 and A_2 are the numbers of the excited carrier for the rapid decay and the slow decay, respectively, τ_1 and τ_2 are rapid and slow decay time constants, respectively. The rapid decay usually includes surface recombination and rapid trapping of carries at defects, while the slow decay is governed by bulk recombination. The slow decay is also influenced by the rapid decay behavior, suggesting induced deterioration that can affect carrier transportation is detected by the time constants τ_1 and τ_2.

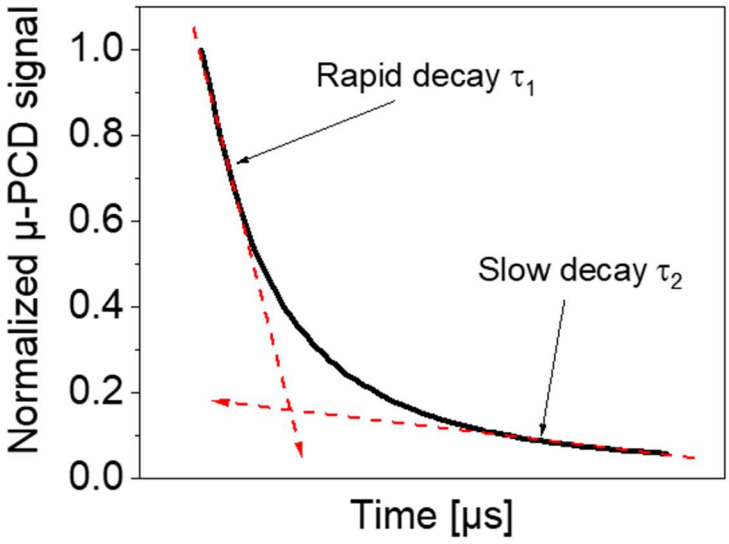

Figure 4. 3. The rapid and slow time constant decay components extracted from the normalized µ-PCD signal curve.

4.3. Results and discussion

4.3.1. PID behavior in the cases with and without light irradiation

Figure 4. 4 shows EL images for the tested solar modules before and after PID stress duration up to 24 h with and without light irradiation of wavelengths above and comparison of their normalized EL intensities, which were averaged in two experiment chains. The behavior of the EL intensity reduction can be observed after the PID tests, and the EL intensity reduction is likely as a function of the PID stress duration. However, the EL intensity reduction rate in the case of UV light irradiation in the 300-390 nm wavelength range is slower than that in the cases

of no-light irradiation (in the dark) and visible light irradiation (460 nm and 500 nm). Meanwhile, the EL intensity reduction rate in the cases of no-light irradiation and visible light irradiation (460 nm and 500 nm) are similar to each other.

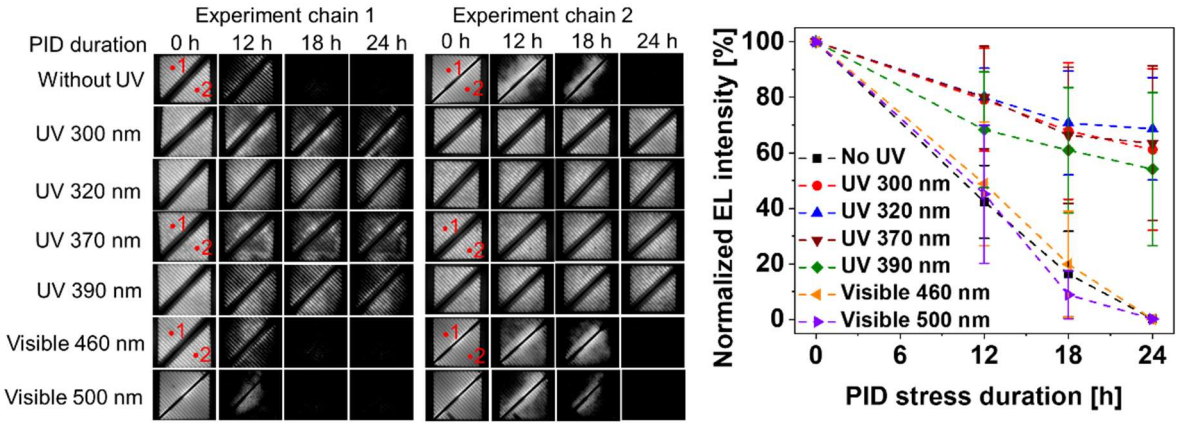

Figure 4. 4. EL images (experiment chain 1 and 2) of the tested solar modules before and after PID tests up to 24 h in the cases of light irradiation with different wavelengths and no-light irradiation (left), and the comparison of their normalized average EL intensity (right). Note that points 1 and 2 marked in the left picture are the locations at which the effective lifetime of solar cells would be measured, as described in Section 3.3 below.

Moreover, it seems that the reduction rate of the EL intensity depends on the UV light irradiation in the 300-390 nm wavelength range. It could be observed that the reduction rate of the EL intensity is slower by UV light irradiation with a shorter wavelength. The EL intensity can predict some performances of solar cells since the EL intensity correlates with V_{oc} [119]. Our results show that the degradation rate of EL intensity in the case of irradiating UV light in the 300-390 nm wavelength range is slower than that in the other cases after the PID stress duration, suggesting similar degradation trends, especially in V_{oc} presented below.

J–V characteristics under one-sun illumination (100 mW/cm^2, AM 1.5) for the tested solar modules before and after PID tests up to 24 h were performed. The behavior of *J–V* curves in two experiment chains is similar to each other, so *J–V* characteristics in experiment chain 1

(representative) are shown in Figure 4. 5. It is observed that the PID-based deterioration level in terms of electrical characteristics became apparent gradually with increasing the duration time in all cases. Still, the deterioration level in the cases of UV light irradiation in the 300-390 nm wavelength range has relatively slowed down. The deterioration level of the electrical characteristics needs to assess quantitatively by normalizing by the initial values.

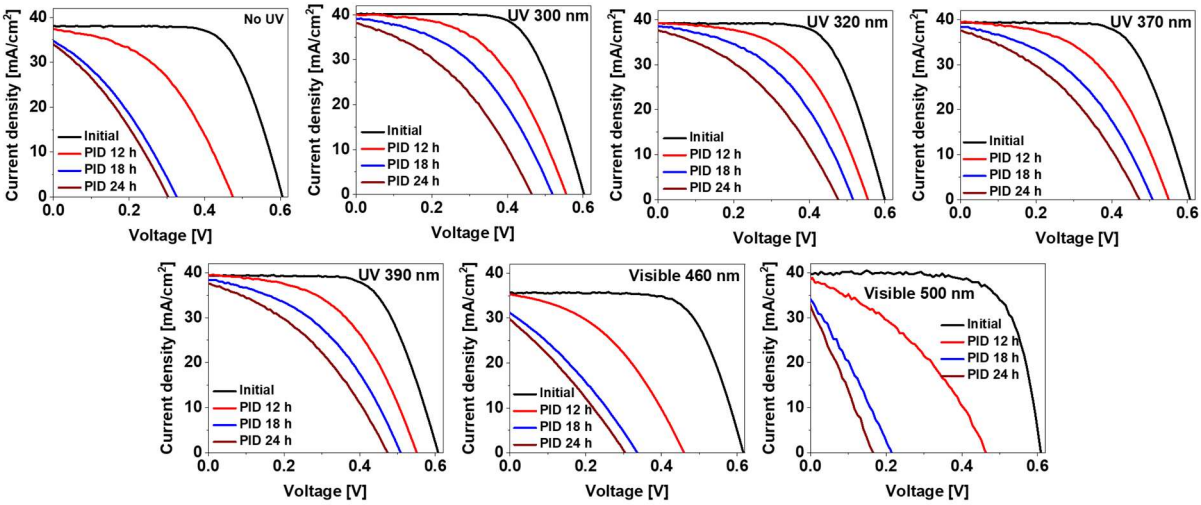

Figure 4. 5. One-sun illumination J–V characteristics of the tested solar modules before and after PID tests up to 24 h for various light irradiation conditions in experiment chain 1.

Figure 4. 6 indicates the normalized average electrical characteristics of the tested solar modules in both experiment chains, composed of P_{max}, V_{oc}, FF, and R_{sh} before and after the PID tests. Therein, R_{sh} was determined from the slope of the illumination *J–V* curve at J = J_{sc} at V = 0 based on the equivalent circuit of the double diode model for the solar cell [106] [120] [121]. Generally, the degradation rate of P_{max}, V_{oc}, FF, and R_{sh} in the case of UV light irradiation in the 300−390 nm wavelength range is significantly slower in comparison with that in the other cases, which is in agreement compared with the normalized average EL intensity as shown in Figure 4. 4. Thus, this suggests that the PID delay effect occurred during the irradiation of UV light in the 300−390 nm wavelength range during the PID test. It coincides with the suggestion, as shown in the work of Masuda and Hara [110], that the PID delay effect

only occurs in the case of irradiating UV light with the wavelengths below 400 nm. Furthermore, the PID delay effect might be more effective under the shorter wavelength UV light. The delay rate of the solar cell performances' deterioration might be investigated in further PID experiments with a longer duration.

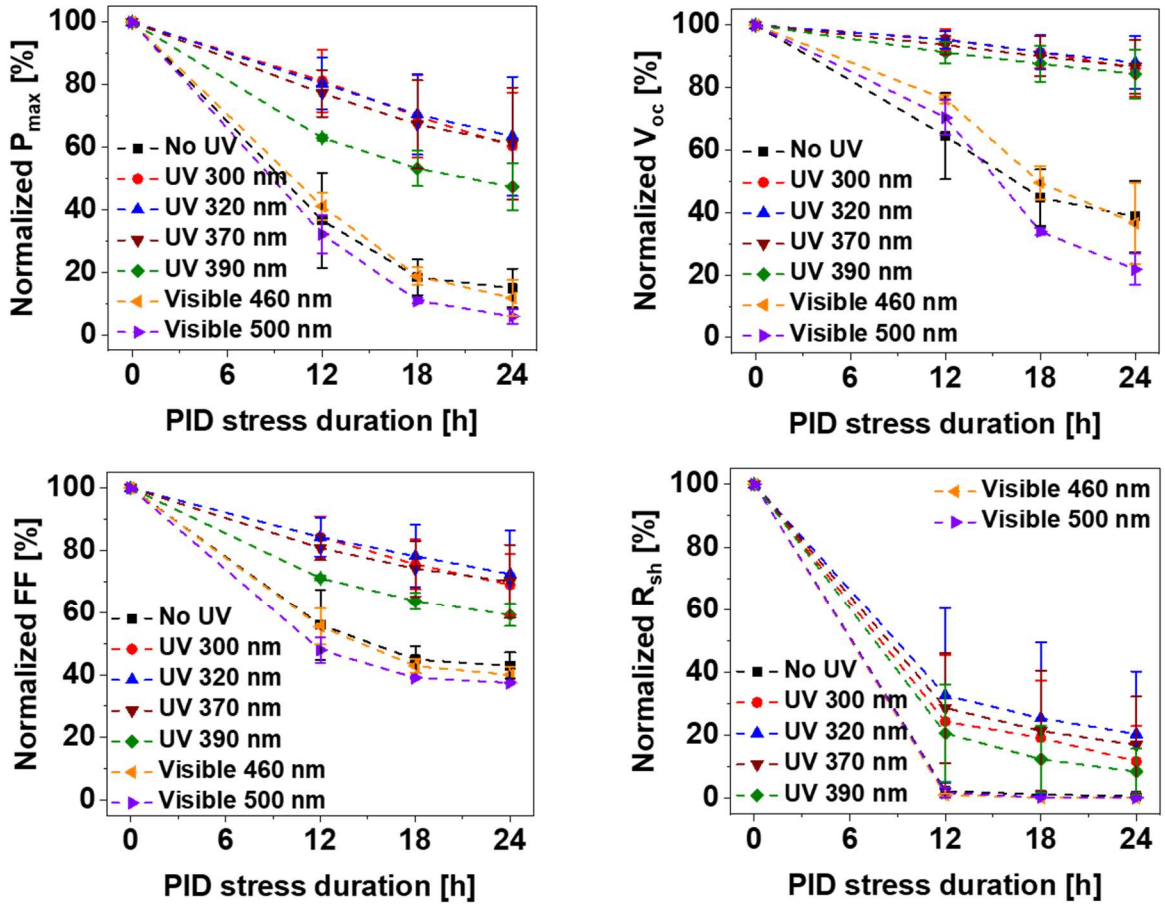

Figure 4. 6. Degradation behavior of normalized P_{max}, V_{oc}, FF, and R_{sh} in the cases with and without irradiating light of different wavelengths.

4.3.2. The proposed mechanism of the PID delay effect by UV light irradiation during PID test

As shown in Figure 4. 7, in comparison with no light irradiation (in dark case), the conductivity of SiN_x thin films increases due to UV light irradiation with the case of a wavelength range of 300−320 nm for SiN_x with n = 1.95 (SiN_x bandgap 3.56 eV) and with the

case of a wavelength range of 300−390 nm for SiN_x with n = 2.12 (SiN_x bandgap 3.18 eV).

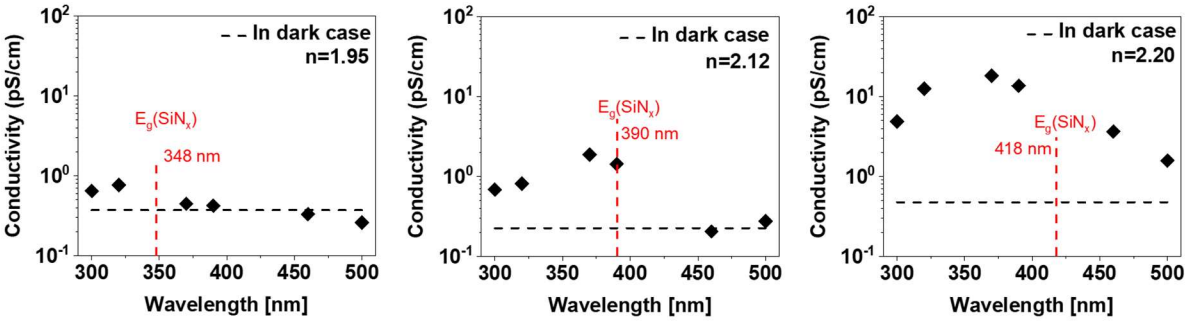

Figure 4. 7. The conductivity change in SiN_x thin films with different refractive indexes at different wavelength light irradiation.

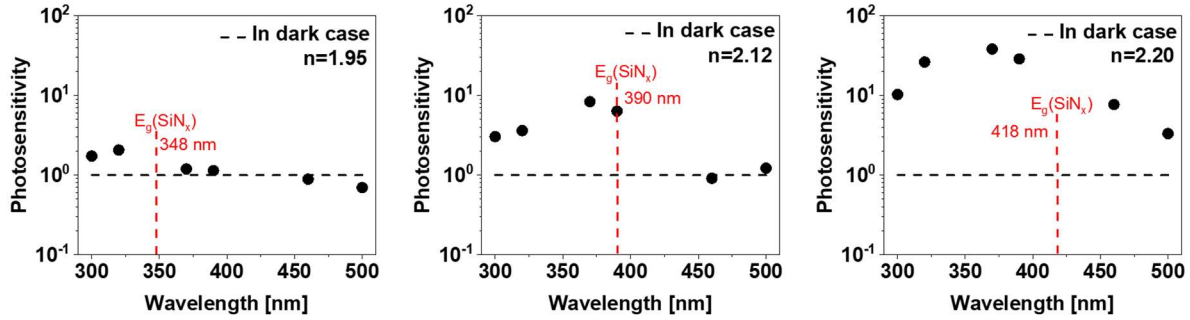

Figure 4. 8. The photosensitivity change in SiN_x thin films with different refractive indexes at different wavelength light irradiation.

The same behavior of photosensitivity (photoconductivity/dark-conductivity) was also indicated in Figure 4. 8. Thus, the conductivity and photosensitivity increase of SiN_x thin films under UV light irradiation depend on their refractive indexes and are limited by their bandgap. With n = 2.20, the conductivity and photosensitivity increase strongly under visible light radiation with wavelength up to 500 nm, since the light absorption in that range happens in the SiN_x with such high refractive index. Also shown in Figure 4. 8, the increased level of photosensitivity is proportional to the increased level of refractive index. This revealed that a SiN_x thin film with a higher refractive index has higher light absorption. Therefore, SiN_x thin films used in solar cells with higher refractive indexes (but limited by 2.2) could suppress PID

more significantly. These results are in good agreement with previous results using SiN_x thin films prepared by catalytic chemical vapor deposition (Cat-CVD) method reported by our group [122]. The SiN_x conductivity increases under UV light irradiation regardless of SiN_x thin films prepared by Cat-CVD or PE-CVD method. Thus, PID delay effects could be observed independent of preparation methods of ARC SiN_x, that is, PE-CVD or Cat-CVD. As a result, the UV light with the wavelength range of 300–390 nm is very useful to delay or suppress PID for p-type c-Si solar cells.

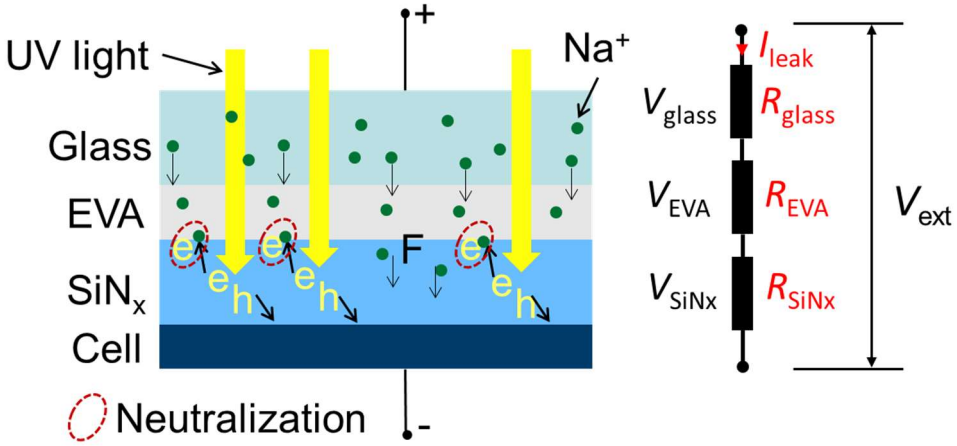

Figure 4. 9. A schematic diagram for the mechanism of the PID delay effect by irradiating UV light during the PID test.

The mechanism of the PID delay effect by UV light irradiation during PID tests in p-type c-Si solar cells is proposed in Figure 4. 9. Under UV light irradiation, the SiN_x ARC layer of the solar cell is attributed to prevent or restrict the penetration of Na ions into the solar active layer, leading to slow down the PID effect. The mechanism has two following critical points. Firstly, after absorbing the UV light in the 300−390 nm wavelength range, the SiN_x ARC layer generates charge carriers (electrons and holes), increasing the SiN_x conductivity, i.e. decreasing the SiN_x resistance (R_{SiNx}). Note that a high voltage is applied between the glass and the active cell layer in the structure of the solar module during the PID test. Then, there are corresponding voltages across the glass (V_{glass}), the EVA layer (V_{EVA}), and the SiN_x layer (V_{SiNx}), as illustrated

in Figure 4. 9. Herein, V_{SiNx} is estimated by the following formula [123]:

$$V_{SiNx} = \frac{R_{SiNx}}{R_{glass} + R_{EVA} + R_{SiNx}} V_{ext} \quad (4.2)$$

Most reports highlighted the degradation of c-Si solar modules caused by EVA discoloration degradation related to UV irradiation exposure with a high power intensity in the long term around several hundred even thousands of days [9][19][20][21]. So, the properties of the glass and the EVA layer are considered to be constant within this work. According to the above formula, the voltage across the SiN_x layer is proportional to the SiN_x resistance. Thus, the SiN_x resistance is decreased by UV light irradiation, leading to reduced V_{SiNx}, i.e. the reduction of the electrical field across the SiN_x layer. The reduced electrical field will cause the drop of the electromotive force (F), which pushes positive ions like Na ions (mainly from the cover glass) towards the active Si layer of the p-type c-Si solar cells [114][124][56]. A well-known mechanism of PID in p-type c-Si solar cells is that the penetration of Na ions into the p-n junction of the solar cell causes leakage current. Therefore, less Na^+ ions can drift across the SiN_x layer, restricting the PID effect. Although Swanson et al. discussed a model that is related to the UV effect on the conductivity increase of the SiN_x layer, the model is still not clear and detailed. It has not been supported by the measurement of the conductivity increase of SiN_x by UV light.

Secondly, charge carriers (electrons and holes) induced by UV light is separated by the electromotive force. The electrons are pulled towards the EVA/SiN_x interface while the holes are pushed towards the SiN_x/Si interface. Then, the electrons can neutralize Na^+ ions on the EVA/SiN_x interface, which might contain a large number of Na^+ ions up to 10^{21} cm^{-3} [125]. As a result, the neutralization could reduce a lot of free Na^+ ions before they drift across the SiN_x layer into the active cell layer. This results in the restriction of the PID effect.

Furthermore, based on the proposed mechanism of the PID delay effect by UV light, the

more strongly the SiN_x conductivity increases the higher the ability to avoid the PID effect is. As shown in Figure 4. 7, the SiN_x thin film has a higher refractive index, its conductivity increase under UV light is stronger. Therefore, the ability to avoid the PID effect is proportional to the SiN_x refractive index. This coincides with the works of literature [62] [123]. However, the SiN_x refractive index employed in solar cells should be less than 2.2 to avoid their power loss due to the parasitic light absorption in the SiN_x layer.

4.3.3. µ-PCD signal analysis in the cases with and without light irradiation during PID test

The µ-PCD signals for the samples without light irradiation, with light radiation of 460-nm wavelength (representing a wavelength's group 2), and with UV light irradiation of 370-nm wavelength (representing a wavelength's group 1) were analyzed. Figure 4. 10 illustrates the normalized µ-PCD signals in experiment chain 1 (representative) for the tested solar modules before and after PID tests in the above-mentioned light irradiation cases.

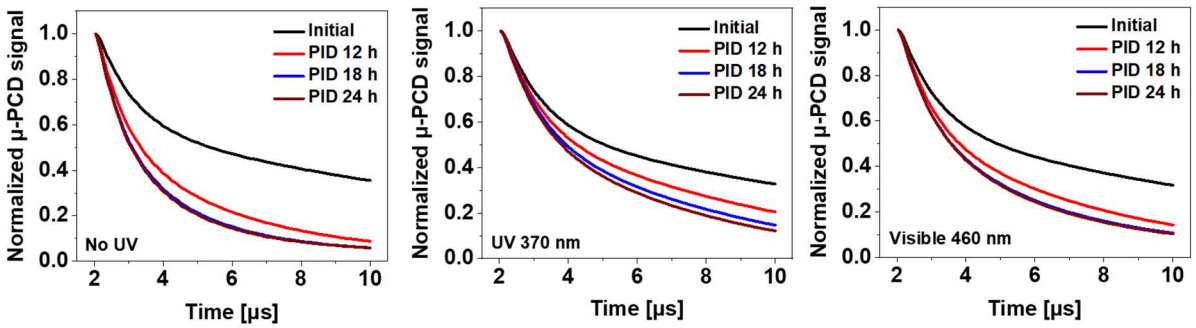

Figure 4. 10. Normalized µ-PCD signals for the tested solar modules before and after PID tests in the cases of no-light irradiation, UV light irradiation of 370 nm, and visible light irradiation of 460 nm.

It could be seen that the µ-PCD signals in three cases show a reduced tendency over the PID test duration. The reduction rate of the µ-PCD signals in the cases of no-UV light irradiation and visible light irradiation with 460-nm wavelength presented faster than that in the case of

UV light irradiation with 370-nm-wavelength. These behaviors are very similar to the behavior of the degradation of solar cell performances over PID stress duration in the above three cases. To analyze the correlation between the reduction of the components of the μ-PCD signal and the degradation of the solar cell performances after the PID test, the μ-PCD signals were fitted with Eq. (4.1) to estimate the τ_1, τ_2 constants while the τ_{eff} value was also estimated from the decay profile, for the solar cells before and after PID tests at two points 1 and 2 as shown in EL images in Figure 4. 4. The τ_1, τ_2 constants, and the τ_{eff} values listed in Table 2 were averaged at both points 1 and 2 in two experiment chain 2. Meanwhile, the normalized τ_1, τ_2, and τ_{eff} values were calculated according to the initial values before the PID stress test at each point in each experiment chain, and then they were averaged. Therefore, the deviation of the normalized τ_1, τ_2, and τ_{eff} values before PID stress tests has not seen, as illustrated in Figure 4. 11.

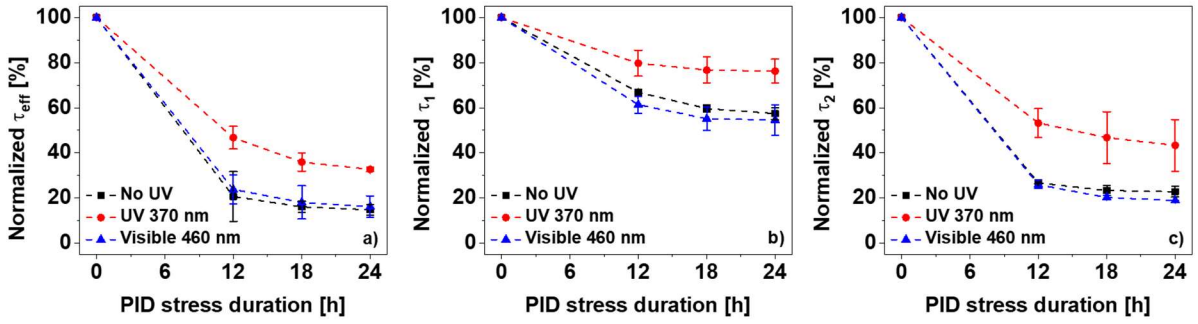

Figure 4. 11. The comparison of the normalized average values before and after PID tests in the cases of no-irradiating and irradiating light of different wavelengths for an effective lifetime a), rapid decay constant τ_1 b), and slow decay constant τ_2 c).

The normalized τ_1, τ_2, and τ_{eff} values after the PID test in three cases decreased as increasing of PID stress duration time. Furthermore, the reduction rates of the τ_1, τ_2, and τ_{eff} values have the same behavior in two cases without and with irradiating light of 460-nm wavelength. In contrast, the case of UV light irradiation with 370-nm wavelength recorded the suppressed behavior. These reveal that the reduction behavior of the τ_1, τ_2, and τ_{eff} values is a good correlation with the performance degradation of p-type c-Si solar modules in the PID tests. It

is noted that the τ_{eff} values of solar cells measured by the μ-PCD technique depend on many factors such as surface recombination, recombination in the emitter layer and bulk, and the effect of charge separation field due to the p–n junction. The τ_{eff} values might not be absolute values, but they are considered as relative values to understand the cell performance deterioration after PID tests.

Table 2. The average effective lifetime and the average rapid and slow decay time constants before and after PID tests.

PID stress duration	**Average τ_{eff} values (μs)**			**Average τ_1 and τ_2 constants (μs)**					
	No UV	**UV 370 nm**	**Visible 460 nm**	**No UV**		**UV 370 nm**		**Visible 460 nm**	
				τ_1	**τ_2**	**τ_1**	**τ_2**	**τ_1**	**τ_2**
Initial	12.87 ±1.26	12.15 ±0.36	13.43 ±1.05	0.94 ±0.01	11.70 ±0.56	0.99 ±0.00	11.96 ±0.28	0.92 ±0.00	11.29 ±0.87
PID 12 h	2.69 ±1.54	5.67 ±0.50	3.18 ±0.61	0.63 ±0.02	3.13 ±0.11	0.79 ±0.06	6.39 ±0.91	0.56 ±0.03	2.91 ±0.03
PID 18 h	2.07 ±0.50	4.37 ±0.41	2.41 ±0.80	0.56 ±0.02	2.72 ±0.14	0.76 ±0.06	5.63 ±1.51	0.51 ±0.05	2.29 ±0.28
PID 24 h	1.91 ±0.43	3.97 ±0.12	2.16 ±0.47	0.54 ±0.03	2.66 ±0.16	0.76 ±0.06	5.22 ±1.50	0.50 ±0.06	2.14 ±0.18

As a mechanism of PID for p-type c-Si solar cells, Na ions drift through the SiN_x ARC layer towards the interface between the Si solar cell surface and the SiN_x ARC layer. Na ions could

penetrate crystal defects such as micro-cracks, stacking faults, and so on, leading to the generation of electrically active surface and defect levels, thus reducing the effective carrier lifetime becomes gradually apparent. The τ_{eff} reduction rate in the case of irradiating UV light of 370-nm wavelength during the PID test is slower than that in the other cases because fewer Na ions penetrate crystal defects of the active cell layer owing to the UV light irradiation in the 300-390 nm wavelength range as mentioned in Section 4.3.2.

Crystal defects as dislocations, which are formed/grown through the penetration of Na ions into the active Si layer, act as defect nuclei as well as recombination centers [71][126]. The Na ion decoration of the crystal defects creates a sub-band of defect states which act as deep level states within the original bandgap. The defect level by Na is somewhat deep around 0.35 eV above the valence band in Si [127]. We assume that the recombination centers appear more at the deep energy level states after the PID test, so the SRH recombination processes take place more at the deep energy level states after PID test. It is known that the rapid decay component is related to the recombination processes that involve defects at the surface [126]. Therefore, the τ_1 constant decreases gradually after the PID test in three cases. Notably, the reduction rate of the τ_1 constant in the case of irradiating UV light of 370 nm is the slowest in three cases after PID tests. This could be interpreted as such because possibly, the Na ion number, which penetrates the c-Si solar cell due to the 300-390 nm-wavelength UV light effect, is the least in three cases after the PID test. Consequently, the deep energy level states are the least formed in the case of irradiating UV light of 370 nm.

In μ-PCD measurement progress, the photoconductivity of solar cells rapidly increases due to the irradiation of laser light and then saturates by trapping the carriers at defects [128]. It is observed that carrier traps do not lead to rapid carrier recombination and prevent carriers from reaching recombination centers as well as extends carrier lifetime. After the active laser light turns off, the rapid decay occurs through the surface states and deep energy level states, and

then the slow decay occurs. The τ_2 constant is mainly dominated by the remission rate of the trapped carriers [129][130][131][132][133]. Nevertheless, if the number of the trapped carriers increases, recombination in bulk occurs at a higher rate, leading to the shorter τ_2 constant. As indicated in Figure 4. 11c, the normalized τ_2 constant in the case of irradiating UV light of 370 nm is highest at the same time after PID tests. In other words, the reduction rate of the τ_2 constant in the case of irradiating UV light of 370 nm is slowest in three cases. This might be assumed that UV light irradiation in the 300−390 nm wavelength range contributes to reducing or suppressing the formation of carrier traps after PID tests, leading to postponing the performance degradation of solar cells after PID tests. However, this proposal needs more detailed researches in terms of defect level, the defect density in the future.

4.4. Conclusion

This chapter presented that irradiating UV light in the 300−390 nm wavelength range on p-type c-Si solar cells during the PID test can delay the degradation of the solar cell performance caused by PID. The mechanism of the PID delay effect by UV light irradiation during PID test in p-type c-Si solar cells is proposed that the conductivity increase of the SiN_x ARC layer under the 300−390 nm-wavelength UV light, which prevents or reduces many Na ions from penetrating the c-Si solar cell, slows down the degradation rate of the solar cell performance. The μ-PCD technique was also utilized to analyze the PID delay mechanism of UV light irradiation during the PID test for p-type c-Si solar cells in detail. The reduction of the τ_1, τ_2 and τ_{eff} components of the μ-PCD signal in the cases of no-irradiating and irradiating UV and visible light, which is a good correlation with the performance degradation of p-type Si solar cells, acts as a function of PID stress duration. The reduction rate of the τ_1 constant in the case of irradiating the 300−390 nm-wavelength UV light is slowest because of the formation of deep-level states owing to the penetration of Na ions into the active Si layer under UV light, in

that case, is lowest. The reduction rate of the τ_2 constant in the case of irradiating the 300−390 nm-wavelength UV light is also slowest because the number of such defects acting as traps is lowest by UV light irradiation. Na ions could penetrate crystal defects, which lead to the generation of electrically active surface and defect levels, gradually reducing τ_{eff} over time.

Chapter 5 | Summary

5.1. Conclusion

This study has focused on three crucial issues as follows: Understanding and proposing a model of PID mechanism related to micro-cracks, presenting and discussing recovery possibility and method for PID-affected micro-cracked solar cells, clarifying the effect of UV light for solar cells within PID stress tests and utilizing it to control PID behavior.

Chapter 1 briefly outlined the relevant issues of PV reliability, including failure types such as discoloration, delamination, corrosion, and breakage & cracks. Notably, PID was introduced in detail. This chapter presented the status of current research and development for PID. Therein, the background of PID covered definition, main factors affecting and elevating PID, techniques testing PID, and some PID mechanisms for c-Si solar cells/modules. Besides, this chapter also showed several PID recovery methods used in both the laboratory and industry. Finally, this chapter highlighted limited issues for PID investigation, leading to perform this study.

Chapter 2 shows the PID shunts at micro-cracked regions observed by EL, look-in thermal images, and confirmed by EQE responses before and after PID stress tests. At micro-cracked areas, local electrical characteristics composed of P_{max}, V_{oc}, FF, and J_{sc} deteriorated after PID stress tests. It is hypothesized that the degradation of typical R_{sh} at local micro-cracked regions is a root cause leading to PID. This chapter suggests that the micro-crack related shunt area depends not only on the length but also on other factors such as width, and depth of micro-cracks in solar cells. Furthermore, this chapter also proposes the decoration of sodium (Na) ions in micro-cracks as the primary mechanism resulting in PID for p-type c-Si solar cells. The micro-cracked region with the degradation of Na ions become recombination centers, and act

as local defects, leading to ohmic conductivity across the p-n junction. This PID mechanism was confirmed by the EDX mapping on the surface of an intact region, the surface, and the cross-section site of micro-cracked areas.

Chapter 3 demonstrates that micro-cracks act as the additional recombination center, which reduces J_{sc}, and τ_{eff} of solar modules after PID stress processes. Besides, micro-cracks also act as shunting defects, resulting in the reduction of R_{sh}, which is the root cause of the degradation of V_{oc}, FF. Thus, PID becomes more severe for solar cells with micro-cracks compared to intact solar cells. The performance degradation of solar cells caused by PID at micro-cracked regions could be regenerated effectively but incompletely by applying a reverse bias voltage. The behavior of the PID degradation and recovery was observed by EL images, confirmed by EQE responses before and after PID stress tests. The incomplete recovery of solar cell performance is attributed to be due to the incomplete recovery of R_{sh} and FF. The degradation and regeneration of the τ_{eff} value are a function of the PID stress and recovery processes. The μ-PCD response plays a critical role in indicating PID behavior induced by micro-cracks of solar cells. Finally, this chapter assesses and models the dependence of the PID behavior after degradation/regeneration cycles on the duration of PID stress and recovery processes. The results show the decreasing tendency of the loss of electrical characteristics caused by PID after PID degradation/regeneration cycles. This trend, which is favorable for minimizing the PID effect, needs to be investigated further.

Chapter 4 shows that irradiating UV light in the 300–390 nm wavelength range on p-type c-Si solar cells during the PID test can delay the degradation of the solar cell performance caused by PID. Also, in this chapter, the author proposes a mechanism of the PID delay effect by UV light irradiation during the PID test in p-type c-Si solar cells. Therein, the conductivity increase of the SiN_x ARC layer under the 300–390 nm-wavelength UV light, which prevents or reduces many Na ions from penetrating the c-Si solar cell, slows down the degradation rate

of the solar cell performance. The μ-PCD technique was also utilized to analyze the PID delay mechanism of UV light irradiation during the PID test for p-type c-Si solar cells in detail. The reduction of the τ_1, τ_2 and τ_{eff} components of the μ-PCD signal in the cases of no-irradiating and irradiating UV and visible light, which is a good correlation with the performance degradation of p-type Si solar cells, acts as a function of PID stress duration. The reduction rate of the τ_1 constant in the case of irradiating the 300–390 nm-wavelength UV light is slowest because of the formation of deep-level states owing to the penetration of Na ions into the active Si layer under UV light, in that case, is lowest. The reduction rate of the τ_2 constant in the case of irradiating the 300–390 nm-wavelength UV light is also slowest because the number of such defects acting as traps is lowest by UV light irradiation. Na ions could penetrate crystal defects, which lead to the generation of electrically active surface and defect levels, gradually reducing τ_{eff} over time.

Thus, this work suggested the more realistic and accurate PID mechanism with the combination of factors, including high potential, mechanical, and damp-heat stresses and UV light irradiation for solar modules installed in the field. Apart from stacking-fault, micro-crack is also a critical candidate, leading to the severe PID-s phenomenon for p-type c-Si solar cells. This work recommends micro-cracks must be inspected and controlled strictly, and micro-cracked solar cells should be removed to minimize the PID effect for commercial solar panels. Furthermore, this dissertation proposed a cyclic PID stress/recovery test method as a long-term solution to minimizes/ eliminates the PID effect over time. By using this method, a model was built to predict the PV performance after a long time of operation. Possibly, this model allows determining the warranty period of commercial solar panels, at least in terms of performance deterioration caused by the PID effect. Finally, this dissertation also showed the critical influence of UV light on PID behavior. Therefore, UV light should be added in the conventional PID tests as an essential factor to achieve more precise experimental results.

5.2. Research directions in the future

The research plan, including three important issues, need to be addressed in the next five years as follows:

1. Model development for potential stress in the free field

Correlation of environmental conditions and high voltage stress of the solar cells with PID behavior.

The data from the free field are continuously evaluated and analyzed to provide a basis for understanding when there is a stress load between the module surface and solar cells. In particular, the data from a surface potential measuring system and climate data are assessed. The evaluation shows systematic relationships, from which the model development is derived.

Model development for the simulation of the high voltage stress for the environmental conditions.

For the development of test procedures, a parameterized model is required based on the above data. The model can map the stress state for the various environmental conditions from the free field measurements. The variables, including temperature, humidity, UV/light irradiation intensity, soil, and dirt, are inserted into the modeling process in different methods. Another possibility is to use a neural network as a model basis. Since the influence of partly unknown parameters, such as degree of contamination and airflow direction over the module surface are not known or incomplete, this type of modeling offers flexible customization options.

Review of the developed model.

The model review should be based on independent data. A part of the modules performing free-field measurements is used to build the model. Other modules are used for validation.

Furthermore, the model is applied using measurements in climatic chambers and adjusted if necessary.

2. Dependence of PID behavior with cyclic degradation and regeneration on the material characteristics

Cell level PID tests with cyclic degradation and regeneration.

In the module layer stack, consisting of glass, encapsulation film, and cell, the electrical potentials are measured as a function of polarity (degradation/regeneration) and time sequence. For this purpose, the PID test series with mini-modules (single-cell solar module networks) as well as with non-encapsulated solar cells (PID cell tests) are carried out.

Ratios of degradation and regeneration rates are determined for various combinations of cells and encapsulant sheets.

Dependencies are modeled and correlated with the material characteristics (e.g., the resistivity of the encapsulant films) based on the findings of the two above steps.

3. Model development for degradation/regeneration behavior

Development of a cross-scale model.

First, a set-up model allows the PID test results to be correlated at the cell, module, and system level. Particular attention is paid to the simulation of power loss depending on the specific potential stress.

Implementation of the model in a calculation program.

The developed model will be transferred to a program for calculating the yield forecast as a function of the cyclic stress load. The input data for the program are, on the one hand, weather data prevailing at the respective location and, on the other hand, the reaction of the type of module considered to degradation/regeneration cycles.

Review of the model

The established calculation model is checked by comparing the simulated/calculated yield curves with the real measured ones without countermeasures and with applied countermeasures. If necessary, adjustments to the model or program are made.

Reference

[1] "The future of solar photovoltaic." [Online]. Available: https://www.irena.org/-/media/Files/IRENA/Agency/Publication/2019/Nov/IRENA_Future_of_Solar_PV_2019.pdf.

[2] A. E. Becquerel, "Mémoire sur les effets électriques produits sous l'influence des rayons solaires," *Comptes Rendus*, vol. 9, pp. 561–567, 1839.

[3] "Photovoltaic report." [Online]. Available: https://www.ise.fraunhofer.de/content/dam/ise/de/documents/publications/studies/Photovoltaics-Report.pdf.

[4] D. Chung, C. Davidson, R. Fu, K. Ardani, and R. Margolis, *U.S. Photovoltaic prices and cost breakdowns: Q1 2015 benchmarks for residential, commercial, and utility-scale systems*. Naional Renewable Energy Laboratory NREL/TP- 6A20-64746, 2015.

[5] J. H. Wohlgemuth, D. W. Cunningham, P. Monus, J. Miller, and A. Nguyen, "Long term reliability of photovoltaic modules," in *Conference Record of the 2006 IEEE 4th World Conference on Photovoltaic Energy Conversion, WCPEC-4*, 2006, pp. 2050–2053.

[6] C. R. Osterwald and T. J. McMahon, "History of accelerated and qualification testing of terrestrial photovoltaic modules: A literature review," *Prog. Photovoltaics Res. Appl.*, vol. 17, pp. 11–33, 2009.

[7] M. A. Munoz, M. C. Alonso-García, N. Vela, and F. Chenlo, "Early degradation of silicon PV modules and guaranty conditions," *Sol. Energy*, vol. 85, pp. 2264–2274, 2011.

[8] M. D. Kempe, "Control of moisture ingress into photovoltaic modules," in *Conference Record of the IEEE Photovoltaic Specialists Conference*, 2005, pp. 503–506.

[9] J. H. Wohlgemuth and S. Kurtz, "Reliability testing beyond qualification as a key component in photovoltaic's progress toward grid parity," in *IEEE International Reliability Physics Symposium Proceedings*, 2011.

[10] D. E. Carlson, R. Romero, F. Willing, D. Meakin, L. Gonzalez, R. Murphy, H. R. Moutinho, and M. Al-Jassim, "Corrosion Effects in Thin-Film Photovoltaic Modules," *Prog. Photovoltaics Res. Appl.*, vol. 11, pp. 377–386, 2003.

[11] A. Jentsch, K. J. Eichhorn, and B. Voit, "Influence of typical stabilizers on the aging behavior of EVA foils for photovoltaic applications during artificial UV-weathering," *Polym. Test.*, vol. 44, pp. 242–247, 2015.

[12] A. Skoczek, T. Sample, E. D. Dunlop, and H. A. Ossenbrink, "Electrical performance results from physical stress testing of commercial PV modules to the IEC 61215 test sequence," *Sol. Energy Mater. Sol. Cells*, vol. 92, pp. 1593–1604, 2008.

[13] A. Ndiaye, A. Charki, A. Kobi, C. M. F. Kébé, P. A. Ndiaye, and V. Sambou, "Degradations of silicon photovoltaic modules: A literature review," *Sol. Energy*, vol. 96, pp. 140–151, 2013.

[14] K. W. Jansen and A. E. Delahoy, "A laboratory technique for the evaluation of

electrochemical transparent conductive oxide delamination from glass substrates," *Thin Solid Films*, vol. 423, pp. 153–160, 2003.

[15] M. A. Quintana, D. L. King, T. J. McMahon, and C. R. Osterwald, "Commonly observed degradation in field-aged photovoltaic modules," in *Conference Record of the IEEE Photovoltaic Specialists Conference*, 2002, pp. 1436–1439.

[16] Z. Jiang, M. Bliss, T. R. Betts, and R. Gottschalg, "Ageing of amorphous silicon devices in dependence of irradiance dose," in *the 21st International Photovoltaic Science and Engineering Conference*, 2011.

[17] G. Oreski and G. M. Wallner, "Evaluation of the aging behavior of ethylene copolymer films for solar applications under accelerated weathering conditions," *Sol. Energy*, vol. 83, pp. 1040–1047, 2009.

[18] T. Kojima and T. Yanagisawa, "The evaluation of accelerated test for degradation a stacked a-Si solar cell and EVA films," *Sol. Energy Mater. Sol. Cells*, vol. 81, pp. 119–123, 2004.

[19] M. D. Kempe, "Modeling of rates of moisture ingress into photovoltaic modules," *Sol. Energy Mater. Sol. Cells*, vol. 90, pp. 2720–2738, 2006.

[20] M. D. Kempe, G. J. Jorgensen, K. M. Terwilliger, T. J. McMahon, C. E. Kennedy, and T. T. Borek, "Acetic acid production and glass transition concerns with ethylene-vinyl acetate used in photovoltaic devices," *Sol. Energy Mater. Sol. Cells*, vol. 91, pp. 315–329, 2007.

[21] M. D. Kempe, "Ultraviolet light test and evaluation methods for encapsulants of photovoltaic modules," *Sol. Energy Mater. Sol. Cells*, vol. 94, pp. 246–253, 2010.

[22] A. Realini, "MTBF - PVm Mean Time Before Failure of Photovoltaic modules," *Abacus A J. Account. Financ. Bus. Stud.*, no. 1–58, 2003.

[23] H. E. Yang, R. French, and L. Bruckman, *Durability and reliability of polymers and other materials in photovoltaic modules*, 1st ed. William Andrew, 2019.

[24] T. Ngo, Y. Heta, T. Doi, and A. Masuda, "Effects of UV on power degradation of photovoltaic modulesin combined acceleration tests," *Jpn. J. Appl. Phys.*, vol. 55, pp. 052301:1–8, 2016.

[25] A. W. Czanderna and F. J. Pern, "Encapsulation of PV modules using ethylene vinyl acetate copolymer as a pottant: A critical review," *Sol. Energy Mater. Sol. Cells*, vol. 43, pp. 101–181, 1996.

[26] A. Masuda, S. Suzuki, Y. Hara, S. Sakamoto, and T. Doi, "Possible Measure of Reliability for Crystalline-Si Photovoltaic Modules," in *29th European Photovoltaic Solar Energy Conference and Exhibition*, 2014, pp. 2566–2569.

[27] A. Masuda, N. Uchiyama, and Y. Hara, "Degradation by acetic acid for crystalline Si photovoltaic modules," *Jpn. J. Appl. Phys.*, vol. 54, pp. 04DR04: 1-5, 2015.

[28] R. Pérez and P. Gumbsch, "Ab initio study of the cleavage anisotropy in silicon," *Acta Mater.*, vol. 48, pp. 4517–4530, 2000.

[29] M. Köntges, I. Kunze, S. Kajari-Schröder, X. Breitenmoser, and B. Bjørneklett, "The risk of power loss in crystalline silicon based photovoltaic modules due to micro-

cracks," *Sol. Energy Mater. Sol. Cells*, vol. 95, pp. 1131–1137, 2011.

[30] T. K. Wen and C. C. Yin, "Crack detection in photovoltaic cells by interferometric analysis of electronic speckle patterns," *Sol. Energy Mater. Sol. Cells*, vol. 98, pp. 216–223, 2012.

[31] S. Kajari-Schröder, I. Kunze, U. Eitner, and M. Köntges, "Spatial and orientational distribution of cracks in crystalline photovoltaic modules generated by mechanical load tests," *Sol. Energy Mater. Sol. Cells*, vol. 95, pp. 3054–3059, 2011.

[32] V. Gade, N. Shiradkar, M. Paggi, and J. Opalewski, "Predicting the long term power loss from cell cracks in PV modules," in *2015 IEEE 42nd Photovoltaic Specialist Conference, PVSC 2015*, 2015, pp. 1–6.

[33] S. Würzner, A. Falke, R. Buchwald, and H. J. Möller, "Determination of the impact of the wire velocity on the surface damage of diamond wire sawn silicon wafers," *Energy Procedia*, vol. 77, pp. 881–890, 2015.

[34] A. Grün, A. Lawerenz, R. Porytskyy, and O. Anspach, "Investigation of Wafer Surfaces with Space-Resolved Breaking Strength Tests and Corresponding Analysis of the Crack Depth," in *26th European Photovoltaic Solar Energy Conference and Exhibition*, 2011, pp. 961–965.

[35] W. J. R. Song, S. K. Tippabhotla, A. A. O. Tay, and A. S. Budiman, "Effect of interconnect geometry on the evolution of stresses in a solar photovoltaic laminate during and after lamination," *Sol. Energy Mater. Sol. Cells*, vol. 187, pp. 241–248, 2018.

[36] M. Köntges, M. Siebert, A. Morlier, R. Illing, N. Bessing, and F. Wegert, "Impact of transportation on silicon wafer-based photovoltaic modules," *Prog. Photovoltaics Res. Appl.*, vol. 24, pp. 1085–1095, 2016.

[37] H. Schulte-Huxel, S. Kajari-Schröder, and R. Brendel, "Analysis of Thermal Processes Driving Laser Welding of Aluminum Deposited on Glass Substrates for Module Interconnection of Silicon Solar Cells," *IEEE J. Photovoltaics*, vol. 5, pp. 1606–1612, 2015.

[38] R. Khatri, S. Agarwal, I. Saha, S. K. Singh, and B. Kumar, "Study on long term reliability of photo-voltaic modules and analysis of power degradation using accelerated aging tests and electroluminescence technique," *Energy Procedia*, vol. 8, pp. 396–401, 2011.

[39] G. Mon, L. Wen, R. G. Ross, and D. Adent, "Effects of temperature and moisture on module leakage current," in *18th IEEE Photovoltaic Specialists Conference*, 1985, pp. 1179–1185.

[40] C. R. Osterwald, T. J. McMahon, and J. A. Del Cueto, "Electrochemical corrosion of SnO2:F transparent conducting layers in thin-film photovoltaic modules," *Sol. Energy Mater. Sol. Cells*, vol. 79, pp. 21–33, 2003.

[41] J. A. Del Cueto and T. J. McMahon, "Analysis of leakage currents in photovoltaic modules under high-voltage bias in the field," *Prog. Photovoltaics Res. Appl.*, vol. 10, pp. 15–28, 2002.

[42] R. Swanson, M. Cudzinovic, D. DeCeuster, V. Desai, J. Jürgens, N. Kaminar, W. Mulligan, L. Rodrigues-Barbosa, D. Rose, D. Smith, A. Terao, and K. Wilson, "The

surface polarization effect in high-efficiency silicon solar cells," in *15th International Photovoltaic Science & Engineering Conference*, 2005, pp. 410–411.

[43] S. Pingel, O. Frank, M. Winkler, S. Oaryan, T. Geipel, H. Hoehne, and J. Berghold, "Potential induced degradation of solar cells and panels," in *35th IEEE Photovoltaic Specialists Conference*, 2010, pp. 2817–2822.

[44] N. G. Dhere, N. S. Shiradkar, and E. Schneller, "Evolution of leakage current paths in MC-Si PV modules from leading manufacturers undergoing high-voltage bias testing," *IEEE J. Photovoltaics*, vol. 4, pp. 654–658, 2014.

[45] J. Berghold, O. Frank, H. Hoehne, S. Pingel, S. Richardson, and M. Winkler, "Potential induced degradation of solar cells and panels," in *25th European Photovoltaic Solar Energy Conference and Exhibition/5th World Conference on Photovoltaic Energy Conversion*, 2010, pp. 3753–3759.

[46] S. Hoffmann and M. Koehl, "Effect of humidity and temperature on the potential-induced degradation," *Prog. Photovoltaics Res. Appl.*, vol. 22, pp. 173–179, 2014.

[47] H. Mehrer, *Diffusion in solids: fundamentals, methods, materials, diffusion-controlled processes*. Springer Science & Business Media, 2007.

[48] P. Hacke, M. Kempe, K. Terwilliger, S. Glick, N. Call, S. Johnston, S. Kurtz, and Bennett, "Characterization of multicrystalline silicon modules with system bias voltage applied in damp heat," in *25th European Photovoltaic Solar Energy Conference and Exhibition/5th World Conference on Photovoltaic Energy Conversion*, 2010, pp. 3760–3765.

[49] A. Raykov, H. Nagel, D. Amankwah, and W. Bergholz, "Climate Model for Potential-Induced Degradation of Crystalline Silicon Photovoltaic Modules," in *the 27th European Photovoltaic Solar Energy Conference and Exhibition*, 2012, pp. 3399–3404.

[50] P. Hacke, K. Terwilliger, R. Smith, S. Glick, J. Pankow, M. Kempe, S. K. I. Bennett, and M. Kloos, "System voltage potential-induced degradation mechanisms in PV modules and methods for test," in *37th IEEE Photovoltaic Specialists Conference*, 2011, pp. 000814–000820.

[51] J. A. del Cueto and S. R. Rummel, "Degradation of photovoltaic modules under high voltage stress in the field," *Reliab. Photovolt. Cells, Modul. Components, Syst. III*, vol. 10, p. 77730J, 2010.

[52] S. Koch, C. Seidel, P. Grunow, S. Krauter, and M. Schoppa, "Polarization effects and test for crystalline silicon cells," in *the 26th European Photovoltaic Solar Energy Conference and Exhibition*, 2011, pp. 1726–1731.

[53] Z. Xiong, T. M. Walsh, and A. G. Aberle, "PV module durability testing under high voltage biased damp heat conditions," *Energy Procedia*, vol. 8, pp. 384–389, 2011.

[54] T. M. Walsh, Z. Xiong, Y. S. Khoo, A. A. O. Tay, and A. G. Aberle, "Singapore modules-optimised PV modules for the tropics," *Energy Procedia*, vol. 15, pp. 388–395, 2012.

[55] J. Hattendorf, R. Loew, W.-M. Gnehr, L. Wulff, M. C. Koekten, D. Koshnicharov, a Blauaermel, and J. a Esquivel, "Potential induced degradation in mono-crystalline silicon based modules: An acceleration model," in *27th European Photovoltaic Solar*

Energy Conference and Exhibition, 2012, pp. 3405–3410.

[56] P. Hacke, K. Terwilliger, S. Glick, G. Tamizhmani, S. Tatapudi, C. Stark, S. Koch, T. Weber, J. Berghold, S. Hoffmann, M. Koehl, S. Dietrich, M. Ebert, and G. Mathiak, "Interlaboratory study to determine repeatability of the damp-heat test method for potential-induced degradation and polarization in crystalline silicon photovoltaic modules," *IEEE J. Photovoltaics*, vol. 5, no. 1, pp. 94–101, 2015.

[57] P. Hacke, K. Terwilliger, S. Koch, T. Weber, J. Berghold, S. Hoffmann, M. Koehl, S. Dietrich, M. Ebert, and G. Mathiak, "Results of IEC 62804 draft round robin testing," 2013. [Online]. Available: https://www.nrel.gov/docs/fy13osti/60493.pdf.

[58] F. Ebneali, S. Tatapudi, and G. Tamizhmani, "Potential induced degradation of pre-stressed photovoltaic modules: Influence of polarity, surface conductivity and temperature," in *the 39th IEEE Photovoltaic Specialists Conference*, 2013, pp. 1548–1553.

[59] IEC TS 62804-1, *Photovoltaic (Pv) modules - Test methods for the detection of potential-induced degradation - part 1: Crystalline silicon*, 1.0. International Electrotechnical Committee, 2015.

[60] M. B. Koentopp, M. Kröber, and C. Taubitz, "Toward a PID test standard: Understanding and modeling of laboratory tests and field progression," *IEEE J. Photovoltaics*, vol. 6, no. 1, pp. 252–257, 2016.

[61] W. Luo, Y. S. Khoo, P. Hacke, V. Naumann, D. Lausch, S. P. Harvey, J. P. Singh, J. Chai, Y. Wang, A. G. Aberle, and S. Ramakrishna, "Potential-induced degradation in photovoltaic modules: A critical review," *Energy Environ. Sci.*, vol. 10, pp. 43–68, 2017.

[62] H. Nagel, A. Metz, and K. Wangemann, "Crystalline Si solar cells and modules featuring excellent stability against potential-induced degradation," in *26th European Photovoltaic Solar Energy Conference and Exhibition*, 2011, pp. 3107–3112.

[63] H. Mehlich, D. Decker, U. Scheit, M. Uhlig, S. Frigge, M. Runge, B. Heinze, H.-P. Sperrlich, J. Mai, H. Schlemm, E. Vetter, J. Höhne, S. Reichel, and W. Stein, "A new method for high resistance against potential induced degradation," in *27th European Photovoltaic Solar Energy Conference and Exhibition*, 2012, pp. 3411–3413.

[64] D. Lausch, V. Naumann, O. Breitenstein, J. Bauer, A. Graff, J. Bagdahn, and C. Hagendorf, "Potential-Induced Degradation (PID): Introduction of a Novel Test Approach and Explanation of Increased Depletion Region Recombination," *IEEE J. Photovoltaics*, vol. 4, pp. 834–840, 2014.

[65] C. Taubitz, M. Schütze, and M. B. Koentopp, "Towards a kinetic model of potential-induced shunting," in *27th European Photovoltaic Solar Energy Conference and Exhibition*, 2012, pp. 3172–3176.

[66] V. Naumann, C. Hagendorf, S. Grosser, M. Werner, and J. Bagdahn, "Micro structural root cause analysis of potential induced degradation in c-Si solar cells," *Energy Procedia*, vol. 27, pp. 1–6, 2012.

[67] V. Naumann, D. Lausch, S. Großer, M. Werner, S. Swatek, C. Hagendorf, and J. Bagdahn, "Microstructural analysis of crystal defects leading to potential-induced degradation (PID) of Si solar cells," *Energy Procedia*, vol. 33, pp. 76–83, 2013.

[68] J. Bauer, V. Naumann, S. Großer, C. Hagendorf, M. Schütze, and O. Breitenstein, “On the mechanism of potential-induced degradation in crystalline silicon solar cells,” *Phys. Status Solidi - Rapid Res. Lett.*, vol. 6, pp. 331–333, 2012.

[69] V. Naumann, D. Lausch, A. Hähnel, J. Bauer, O. Breitenstein, A. Graff, M. Werner, S. Swatek, S. Großer, J. Bagdahn, and C. Hagendorf, “Explanation of potential-induced degradation of the shunting type by Na decoration of stacking faults in Si solar cells,” *Sol. Energy Mater. Sol. Cells*, vol. 120, Part A, pp. 383–389, 2014.

[70] A. Armigliato, M. Servidori, S. Solmi, and I. Vecchi, “On the growth of stacking faults and dislocations induced in silicon by phosphorus predeposition,” *J. Appl. Phys.*, vol. 48, pp. 1806–1812, 1977.

[71] V. Naumann, C. Brzuska, M. Werner, S. Großer, and C. Hagendorf, “Investigations on the formation of stacking fault-like PID-shunts,” *Energy Procedia*, vol. 92, pp. 569–575, 2016.

[72] K. Hara, S. Jonai, and A. Masuda, “Potential-induced degradation in photovoltaic modules based on n-type single crystalline Si solar cells,” *Sol. Energy Mater. Sol. Cells*, vol. 140, pp. 361–365, 2015.

[73] D. Lausch, V. Naumann, A. Graff, A. Hähnel, O. Breitenstein, C. Hagendorf, and J. Bagdahn, “Sodium outdiffusion from stacking faults as root cause for the recovery process of potential-induced degradation (PID),” *Energy Procedia*, vol. 55, pp. 486–493, 2014.

[74] E. Photovoltaic and S. Energy, “Potential-induced degradation and temperature-driven regeneration: a realistic simulation,” in *28th European Photovoltaic …*, 2012, pp. 3303–3308.

[75] J. Oh, S. Bowden, and G. S. TamizhMani, “Potential-Induced Degradation (PID): Incomplete Recovery of Shunt Resistance and Quantum Efficiency Losses,” *IEEE J. Photovoltaics*, vol. 5, pp. 1540–1548, 2015.

[76] K. Hara, K. Ogawa, Y. Okabayashi, H. Matsuzaki, and A. Masuda, “Influence of surface structure of n-type single-crystalline Si solar cells on potential-induced degradation,” *Sol. Energy Mater. Sol. Cells*, vol. 166, pp. 132–139, 2017.

[77] S. Yamaguchi, A. Masuda, and K. Ohdaira, “Progression of rapid potential-induced degradation of n-type single-crystalline silicon photovoltaic modules,” *Appl. Phys. Express*, vol. 9, pp. 112301:1–4, 2016.

[78] S. Bae, W. Oh, K. D. Lee, S. Kim, H. Kim, N. Park, S.-I. Chan, S. Park, Y. Kang, H.-S. Lee, and D. Kim, “Potential induced degradation of n-type crystalline silicon solar cells with p+ front junction,” *Energy Sci. Eng.*, vol. 5, pp. 30–37, 2017.

[79] S. Yamaguchi, A. Masuda, and K. Ohdaira, “Changes in the current density-voltage and external quantum efficiency characteristics of n-type single-crystalline silicon photovoltaic modules with a rear-side emitter undergoing potential-induced degradation,” *Sol. Energy Mater. Sol. Cells*, vol. 151, pp. 113–119, 2016.

[80] S. Yamaguchi, A. Masuda, and K. Ohdaira, “Potential-induced degradation behavior of n-type single-crystalline silicon photovoltaic modules with a rear-side emitter,” in *43rd Photovoltaic Specialists Conference*, 2016, pp. 0938–0942.

[81] V. Naumann, T. Geppert, S. Großer, D. Wichmann, H.-J. Krokoszinski, M. Werner,

and C. Hagendorf, “Potential-induced degradation at interdigitated back contact solar cells,” *Energy Procedia*, vol. 55, pp. 498–503, 2014.

[82] A. Masuda and Y. Hara, “Potential-induced degradation of thin-film Si photovoltaic modules,” *Jpn. J. Appl. Phys.*, vol. 56, pp. 04CS04: 1-5, 2017.

[83] S. Yamaguchi, C. Yamamoto, K. Ohdaira, and A. Masuda, “Reduction in the short-circuit current density of silicon heterojunction photovoltaic modules subjected to potential-induced degradation tests,” *Sol. Energy Mater. Sol. Cells*, vol. 161, pp. 439–443, 2017.

[84] P. Hacke, K. Terwilliger, S. H. Glick, G. Perrin, J. Wohlgemuth, S. Kurtz, K. Showalter, J. Sherwin, E. Schneller, S. Barkaszi, and R. Smith, “Survey of potential-induced degradation in thin-film modules,” *J. Photonics Energy*, vol. 5, pp. 053083: 1–14, 2015.

[85] P. Hacke, S. Spataru, S. Johnston, K. Terwilliger, K. Vansant, M. Kempe, J. Wohlgemuth, S. Kurtz, A. Olsson, and M. Propst, “Elucidating PID degradation mechanisms and in situ dark I-V monitoring for modeling degradation rate in CdTe thin-film modules,” *IEEE J. Photovoltaics*, vol. 6, pp. 1635–1640, 2016.

[86] V. Fjällström, P. M. P. Salomé, A. Hultqvist, M. Edoff, T. Jarmar, B. G. Aitken, K. Zhang, K. Fuller, and C. K. Williams, “Potential-Induced Degradation of CuIn1-xGaxSe2 Thin Film Solar Cells,” *IEEE J. Photovoltaics*, vol. 3, pp. 1090–1094, 2013.

[87] S. Yamaguchi, S. Jonai, K. Hara, H. Komaki, Y. Shimizu-Kamikawa, H. Shibata, S. Niki, Y. Kawakami, and A. Masuda, “Potential-induced degradation of Cu(In,Ga)Se2 photovoltaic modules,” *Jpn. J. Appl. Phys.*, vol. 54, pp. 08KC13: 1–7, 2015.

[88] K. Sporleder, V. Naumann, J. Bauer, S. Richter, A. Hähnel, S. Großer, M. Turek, and C. Hagendorf, “Local Corrosion of Silicon as Root Cause for Potential-Induced Degradation at the Rear Side of Bifacial PERC Solar Cells,” *Phys. Status Solidi - Rapid Res. Lett.*, vol. 13, pp. 1900163: 1–4, 2019.

[89] K. Hara, H. Ichinose, T. N. Murakami, and A. Masuda, “Crystalline Si photovoltaic modules based on TiO2-coated cover glass against potential-induced degradation,” *RSC Adv.*, vol. 4, pp. 44291–44295, 2014.

[90] K. Hara, S. Jonai, and A. Masuda, “Crystalline Si photovoltaic modules functionalized by a thin polyethylene film against potential and damp-heat-induced degradation,” *RSC Adv.*, vol. 5, pp. 15017–15023, 2015.

[91] S. Jonai, K. Hara, Y. Tsutsui, H. Nakahama, and A. Masuda, “Relationship between cross-linking conditions of ethylene vinyl acetate and potential induced degradation for crystalline silicon photovoltaic modules,” *Jpn. J. Appl. Phys.*, vol. 54, pp. 08KG01: 1–5, 2015.

[92] F. Fruehauf and M. Turek, “Quantification of Electroluminescence Measurements on Modules,” *Energy Procedia*, vol. 77, pp. 63–68, 2015.

[93] O. Breitenstein, F. Fruhauf, D. Hinken, and K. Bothe, “Effective Diffusion Length and Bulk Saturation Current Density Imaging in Solar Cells by Spectrally Filtered Luminescence Imaging,” *IEEE J. Photovoltaics*, vol. 6, pp. 1243–1254, 2016.

[94] O. Breitenstein, J. P. Rakotoniaina, and M. H. Al Rifai, “Quantitative Evaluation of Shunts in Solar Cells by Lock-In Thermography,” *Prog. Photovoltaics Res. Appl.*, vol.

11, pp. 512–526, 2003.

[95] O. Breitenstein, J. P. Rakotoniaina, M. H. Al Rifai, and M. Werner, “Shunt types in crystalline silicon solar cells,” *Prog. Photovoltaics Res. Appl.*, vol. 12, pp. 529–538, 2004.

[96] O. Breitenstein, J. Bauer, P. P. Altermatt, and K. Ramspeck, “Influence of defects on solar cell characteristics,” *Solid State Phenom.*, vol. 156–158, pp. 1–10, 2010.

[97] X. Gou, X. Li, S. Wang, H. Zhuang, X. Huang, and L. Jiang, “The effect of microcrack length in silicon cells on the potential induced degradation behavior,” *Int. J. Photoenergy*, vol. 2018, pp. 1–6, 2018.

[98] J. Käsewieter, F. Haase, M. H. Larrodé, and M. Köntges, “Cracks in solar cell metallization leading to module power loss under mechanical loads,” *Energy Procedia*, vol. 55, pp. 469 – 477, 2014.

[99] S. Kajari-Schröder, I. Kunze, and M. Köntges, “Criticality of cracks in PV modules,” *Energy Procedia*, vol. 27, pp. 658–663, 2012.

[100] V. Naumann, D. Lausch, A. Graff, M. Werner, S. Swatek, J. Bauer, A. Hähnel, O. Breitenstein, S. Großer, J. Bagdahn, and C. Hagendorf, “The role of stacking faults for the formation of shunts during potential-induced degradation of crystalline Si solar cells,” *Phys. Status Solidi - Rapid Res. Lett.*, vol. 7, pp. 315–318, 2013.

[101] V. Naumann, D. Lausch, A. Hähnel, O. Breitenstein, and C. Hagendorf, “Nanoscopic studies of 2D-extended defects in silicon that cause shunting of Si-solar cells,” *Phys. Status Solidi Curr. Top. Solid State Phys.*, vol. 12, pp. 1103–1107, 2015.

[102] N. C. Dong, M. A. Islam, Y. Ishikawa, and Y. Uraoka, “The influence of sodium ions decorated micro-cracks on the evolution of potential induced degradation in p-type crystalline silicon solar cells,” *Sol. Energy*, vol. 174, pp. 1–6, 2018.

[103] M. A. Islam, C. D. Nguyen, and Y. Ishikawa, “Effective minority carrier lifetime as an indicator for potential-induced degradation in p-type single-crystalline silicon photovoltaic modules,” *Jpn. J. Appl. Phys.*, vol. 58, no. 10, pp. 106507: 1–10, 2019.

[104] D. C. Nguyen, Y. Ishikawa, S. Jonai, K. Nakamura, A. Masuda, and Y. Uraoka, “Elucidating the mechanism of potential induced degradation delay effect by ultraviolet light irradiation for p-type crystalline silicon solar cells,” *Sol. Energy*, vol. 199, pp. 55–62, 2020.

[105] K. Whitfield, A. Salomon, S. Yang, and I. Suez, “Damp heat versus field reliability for crystalline silicon,” in *38th IEEE Photovoltaic Specialists Conference*, 2012, pp. 1864–1870.

[106] K. Ishibashi, Y. Kimura, and M. Niwano, “An extensively valid and stable method for derivation of all parameters of a solar cell from a single current-voltage characteristic,” *J. Appl. Phys.*, vol. 103, pp. 094507-1–6, 2008.

[107] S. Pingel, “Recovery Methods for Modules Affected by Potential Induced Degradation (PID),” in *27th European Photovoltaic Solar Energy Conference*, 2012, pp. 3379–3383.

[108] H. Nagel, R. Pfeiffer, a Raykov, and K. Wangemann, “Lifetime warranty testing of crystalline silicon modules for potential-induced degradation,” in *27th European*

Photovoltaic Solar Energy Conference and Exhibition, 2012, pp. 3163–3166.

[109] S. Koch, J. Berghold, and P. Grunow, "Towards a predictive model for potential-induced degradation (PID) based on climate data," in *2014 NREL Photovoltaic Module Reliability Workshop 2014*, 2014, pp. 213–246.

[110] A. Masuda and Y. Hara, "Effect of light irradiation during potential-induced degradation tests for p-type crystalline Si photovoltaic modules," *Jpn. J. Appl. Phys.*, vol. 57, pp. 08RG13-1–4, 2018.

[111] M. A. Islam, T. Oshima, H. Nakahama, and Y. Ishikawa, "Study on potential-induced degradation and recovery of bifacial n-type single crystalline Si photovoltaic modules," in *33rd European Photovoltaic Solar Energy Conference and Exhibition*, 2017, pp. 1730–1733.

[112] Y. Ishikawa, M. A. Islam, Y. Takagi, H. Iida, and H. Nakahama, "Lifetime estimation of silicon photovoltaic module using laser-based diagnosis technology," in *27th International Photovoltaic Science and Engineering Conference*, 2017.

[113] W. Soppe, H. Rieffe, and A. Weeber, "Bulk and surface passivation of silicon solar cells accomplished by silicon nitride deposited on industrial scale by microwave PECVD," *Prog. Photovoltaics Res. Appl.*, vol. 13, no. 7, pp. 551–569, 2005.

[114] V. Naumann, D. Lausch, K. Ilse, O. Breitenstein, J. Bauer, S. Großer, J. Bagdahn, and C. Hagendorf, "PID-shunting: Understanding from nanoscale to module level," in *NREL Photovoltaic Module Reliability Workshop 2014*, 2014.

[115] M. Ichimura, N. Yamada, H. Tajiri, and E. Arai, "Slow photoconductivity decay in 3C-SiC on Si substrates," *J. Appl. Phys.*, vol. 84, no. 5, pp. 2727–2731, 1998.

[116] T. E. Murphy, K. Moazzami, and J. D. Phillips, "Trap-related photoconductivity in ZnO epilayers," *J. Electron. Mater.*, vol. 35, no. 4, pp. 543–549, 2006.

[117] B. Berger, N. Schüler, S. Anger, B. Gründig-Wendrock, J. R. Niklas, and K. Dornich, "Contactless electrical defect characterization in semiconductors by microwave detected photo induced current transient spectroscopy (MD-PICTS) and microwave detected photoconductivity (MDP)," *Phys. Status Solidi A*, vol. 208, no. 4, pp. 769–776, 2011.

[118] K. O. Hara, N. Usami, K. Toh, M. Baba, K. Toko, and T. Suemasu, "Investigation of the recombination mechanism of excess carriers in undoped BaSi2 films on silicon," *J. Appl. Phys.*, vol. 112, pp. 083108-1–6, 2012.

[119] T. Fuyuki, H. Kondo, Y. Kaji, A. Ogane, and Y. Takahashi, "Analytic findings in the electroluminescence characterization of crystalline silicon solar cells," *J. Appl. Phys.*, vol. 101, pp. 023711-1–5, 2007.

[120] A. Bag, S. Mallik, C. Mahata, and C. K. Maiti, "Polycrystalline p-β-FeSi2(Al) on n-Si(100): Heterojunction thin-film solar cells," in *10th IEEE International Conference on Semiconductor Electronics (ICSE)*, 2012, pp. 285–287.

[121] A. Bag, S. Mallik, and C. K. Maiti, "Interlayer thickness dependence of photovoltaic properties of polycrystalline p-β-FeSi2(Al)/n-Si(100) heterojunctions," *J. Renew. Sustain. Energy*, vol. 6, p. 023110, 2014.

[122] D. C. Nguyen, Y. Ishikawa, C. T. Nguyen, K. Ohdaira, A. Masuda, and Y. Uraoka,

"Influence of UV light on the increase of SiNx conductivity toward elucidation of potential induced degradation mechanism," in *46th IEEE Photovoltaic Specialists Conference*, 2019.

[123] V. Naumann, K. Ilse, and C. Hagendorf, "On the Discrepancy between Leakage Currents and Potential-Induced Degradation of Cristalline Silicon Modules," in *28th European Photovoltaic Solar Energy Conference and Exhibition*, 2013, pp. 2994–2997.

[124] R. M. Swanson, D. De Ceuster, V. Desai, D. H. Rose, D. D. Smith, and N. Kaminar, "Preventing harmful polarization of solar cells," U.S. Patent 7554031, 2009.

[125] M. A. Islam, T. Oshima, D. Kobayashi, H. Matsuzaki, H. Nakahama, and Y. Ishikawa, "Carrier dynamics in the potential-induced degradation in single-crystalline silicon photovoltaic modules," *Jpn. J. Appl. Phys.*, vol. 57, pp. 08RG14-1–8, 2018.

[126] S. Yasuno, T. Kita, S. Morita, T. Kugimiya, K. Hayashi, and S. Sumie, "Transient photoconductivity responses in amorphous In-Ga-Zn-O films," *J. Appl. Phys.*, vol. 112, pp. 053715-1–6, 2012.

[127] S. M. Sze, *Physics of Semiconductor Devices*, 2nd ed. p. 21, 1981.

[128] S. Yasuno, T. Kugimiya, S. Morita, A. Miki, F. Ojima, and S. Sumie, "Correlation of photoconductivity response of amorphous In-Ga-Zn-O films with transistor performance using microwave photoconductivity decay method," *Appl. Phys. Lett.*, vol. 98, pp. 102107-1–3, 2011.

[129] T. Pisarkiewicz, "Photodecay method in investigation of materials and photovoltaic structures," *Opto-Electronics Rev.*, vol. 12, no. 1, pp. 33–40, 2004.

[130] D. Macdonald and A. Cuevas, "Trapping of minority carriers in multicrystalline silicon," *Appl. Phys. Lett.*, vol. 74, no. 12, pp. 1710–1712, 1999.

[131] Y. Hu, H. Schøn, Ø. Nielsen, E. J. Øvrelid, and L. Arnberg, "Investigating minority carrier trapping in n-type Cz silicon by transient photoconductance measurements," *J. Appl. Phys.*, vol. 111, pp. 053101-1–6, 2012.

[132] Y.-F. Chen, "Stretched-exponential law for carrier capture kinetics of a trapping center in compensated amorphous silicon," *Phys. Rev. B*, vol. 40, no. 5, pp. 3437–3438, 1989.

[133] J. A. Hornbeck and J. R. Haynes, "Trapping of minority carriers in silicon. I. P-type Silicon," *Phys. Rev.*, vol. 97, no. 2, pp. 311–321, 1955.

List of publications

A. Journal articles

1. ***Dong C. Nguyen***, Yasuaki Ishikawa, and Yukiharu Uraoka, "Recover possibilities of potential induced degradation caused by the micro-cracked locations in p-type crystalline silicon solar cells," submitted to Progress in Photovoltaics: Research and Applications, June, 2020.

2. ***Dong C. Nguyen***, Yasuaki Ishikawa, Sachiko Jonai, Kyotaro Nakamura, Atsushi Masuda, and Yukiharu Uraoka, "Elucidating the mechanism of potential induced degradation delay effect by ultraviolet light irradiation for p-type crystalline silicon solar cells," Sol. Energy, vol. 199, pp. 55-62, 2020.

3. ***Dong C. Nguyen***, Mohammad Aminul Islam, Yasuaki Ishikawa, and Yukiharu Uraoka, "The influence of sodium ions decorated micro-cracks on the evolution of potential induced degradation in p-type crystalline silicon solar cells," Sol. Energy, vol. 174, pp. 1-6, 2018.

B. Presentations at international conferences

1. ***Dong C. Nguyen***, Yasuaki Ishikawa, Atsushi Masuda, and Yukiharu Uraoka, "Investigation of potential induced degradation delay effect of UV light for p-type crystalline Si solar cells," 8th Malaysia-Japan joint workshop on PV systems, Kuala Lumpur, Malaysia, 26 September 2019

2. ***Dong C. Nguyen***, Yasuaki Ishikawa, Cong Thanh Nguyen, K. Ohdaira, Atsushi Masuda, and Yukiharu Uraoka, "Influence of UV light on the increase of SiNx conductivity toward elucidation of potential induced degradation mechanism," 46th IEEE PV Specialist Conference, Chicago, USA, June 2019.

3. ***Dong C. Nguyen***, Yasuaki Ishikawa, Atsushi Masuda, and Yukiharu Uraoka, "Dependence of the PID delay effect on the UV light wavelength during PID stress tests for p-type crystalline Si solar cells," 3rd International Workshop on the Sustainable Actions for "Year by Year Aging" under Reliability Investigations in PV Modules, Ibaraki, Japan, 30 October 2018.

C. Presentations at domestic conferences

1. ***Dong C. Nguyen***, Yasuaki Ishikawa, Sachiko Jonai, Kyotaro Nakamura, Atsushi Masuda, Yukiharu Uraoka "The PID delay effect by UV light irradiation for p-type crystalline Si solar modules based on the different refractive indexes of silicon nitride layer," AIST 太陽光発電 成果報告会, Ibaraki, Japan, 17 November 2019.

2. ***Dong C. Nguyen***, Y. Ishikawa, S. Jonai, K. Nakamura, A. Masuda, and Y. Uraoka, "Investigation of correlation between the conductivity increasing of SiNx thin films by UV light and potential induced degradation," 80th JSAP Fall Meeting 2019, Hokkaido, Japan, 21 September 2019.

3. ***Dong C. Nguyen***, V. Naumann, Y. Ishikawa, and Y. Uraoka, "Dependence of power-loss caused by potential induced degradation on recovery duration after degradation/recovery cycles for p-type crystalline silicon solar cells," 学振第 175 委員会 第 16 回 「次世代の太陽光発電システム」シンポジウム, Miyazaki, Japan, 3 July 2019.

4. ***Dong C. Nguyen***, Y. Ishikawa, A. Masuda, and Y. Uraoka, "Analysis of suppression effect of UV irradiation during PID stress test for p-type crystalline Si solar cells," AIST 太陽光発電 成果報告会, Ibaraki, Japan, 13 November 2018.

5. ***Dong C. Nguyen***, Y. Ishikawa, and Y. Uraoka, "Elucidation of potential induced degradation at the micro-cracked regions for p-type crystalline Si solar cells using microwave photo-conductance decay technique," 79th JSAP Fall Meeting 2018, Nagoya, Japan, 21 September 2018.
6. ***Dong C. Nguyen***, Y. Ishikawa, and Y. Uraoka, "The influence of micro-cracks on the evolution of potential induced degradation in p-type crystalline silicon solar cells," 学振第175 委員会 第 15 回 「次世代の太陽光発電システム」シンポジウム, Hokkaido, Japan, 12 July 2018.

D. Relevant articles and presentations

1. Mohammad Aminul Islam, ***Dong C. Nguyen***, and Yasuaki Ishikawa, "Effective minority carrier lifetime as an indicator for potential-induced degradation in p-type single-crystalline silicon photovoltaic modules," Japanese Journal of Applied Physics, vol. 58, pp. 106507: 1-10, 2019.
2. Ishikawa Yasuaki, Islam Mohammad Aminul, **Dong C. Nguyen**, "Detail analysis of potential induced degradation (PID) in p-type crystalline Si photovoltaic module," 29th International Photovoltaic Science and Engineering Conference, Xi'an, China, 2019.

Awards

1. Ministry of Education, Culture, Sports, Science and Technology (MEXT), ***Top Global University Project Scholarship Recipient*** (October 2017 – September 2018).
2. Nara Institute of Science and Technology, Graduate School of Materials Science, ***2018 Grant-in-Aid for Ph.D. Students***.
3. Nara Institute of Science and Technology, Graduate School of Materials Science ***GSMS Scholarship*** (October 2018 – September 2020).